

WEARABLE SENSORS FOR BRAIN INJURY PREDICTION AND FRAILTY ASSESSMENT

by

Patricio Arrué Cornejo

---

Copyright © Patricio Arrué Cornejo 2023

A Dissertation Submitted to the Faculty of the

DEPARTMENT OF BIOMEDICAL ENGINEERING

In Partial Fulfillment of the Requirements

For the Degree of

DOCTOR OF PHILOSOPHY

In the Graduate College

THE UNIVERSITY OF ARIZONA

2023

THE UNIVERSITY OF ARIZONA  
GRADUATE COLLEGE

As members of the Dissertation Committee, we certify that we have read the dissertation prepared by: *Patricio A. Arrué Cornejo*, titled: *Wearable Sensors for Brain Injury Prediction and Frailty Assessment* and recommend that it be accepted as fulfilling the dissertation requirement for the Degree of Doctor of Philosophy.

**Kaveh Laksari**

*Kaveh Laksari, PhD*

Apr 12, 2023  
Date: \_\_\_\_\_

**Nima Toosizadeh**

*Nima Toosizadeh, PhD*

Apr 12, 2023  
Date: \_\_\_\_\_

**Ali Bilgin**

*Ali Bilgin, PhD*

Apr 12, 2023  
Date: \_\_\_\_\_

**Russell Witte**

*Russel Witte, PhD*

Apr 15, 2023  
Date: \_\_\_\_\_

Final approval and acceptance of this dissertation is contingent upon the candidate's submission of the final copies of the dissertation to the Graduate College.

We hereby certify that we have read this dissertation prepared under our direction and recommend that it be accepted as fulfilling the dissertation requirement.

**Kaveh Laksari**

*Kaveh Laksari, PhD*  
Dissertation Committee Co-Chair  
*Biomedical Engineering*

Apr 12, 2023  
Date: \_\_\_\_\_<sup>®</sup>

**Nima Toosizadeh**

*Nima Toosizadeh, PhD*  
Dissertation Committee Co-Chair  
*Biomedical Engineering*

Apr 12, 2023  
Date: \_\_\_\_\_

**Signature:** *Kaveh Laksari*

**Email:** klaksari@arizona.edu

**Signature:** *Nima Toosizadeh*

**Email:** ntoosizadeh@arizona.edu

**Signature:** *Ali Bilgin*

**Email:** bilgin@arizona.edu

**Signature:** *Russell Witte*  
Russell Witte (Apr 15, 2023 10:31 PDT)

**Email:** rwitte@arizona.edu

## Acknowledgments

I would like to express my gratitude to my advisors Dr. Kaveh Laksari and Dr. Nima Toosizadeh for their guidance, inspiration and all the support they brought to me during my PhD. They always were role models on how a scientist should be; extremely professionals and organized in all their tasks and meeting all I expect from ethical and human aspects of a mentor. I am really grateful for being their student and I will work hard after this to make you proud.

I would like to thank my committee members Dr. Ali Bilgin and Dr. Russell Witte for enthusiastic serving on my dissertation committee, as well as for the comprehensive exam. For both process they pushed me to be fully prepared for every aspect of my work, aspects that now I will be aware from now my entire career.

I am thankful to the University of Arizona for receiving me, trusting in me for all this process. I always felt a part of home here, and I will never forget all the kind and friendly people, all the supportive staff like Andrea Anduaga who was the best academic advisor I could ask! All the perfect places to work, and obviously the seminars that opened my horizons for what I would like to see, and contribute, in my homeland. Special thanks for my labmates, I felt them as my brothers and sisters in science and I hope them the best: Ali, Aditi, Carissa, Harrison, Danya, Jordan and Sohrab. I will miss you!

I probably could not make it but for my family, my loved sisters and 'Los viejos', you are the best inspiration, and I will work hard to make your life better. Thank you, my love Camila, for always being a support and bringing to me all the affection I need, even with thousands of km of distance, I always felt accompanied by you. Thanks to all my mentors I have had in my entire life: Sergio, Ana, Gabriel, Miguel Ángel, Patricio, tio Lalo and Roger. I will continue working for a better and equal future for everyone.

## Dedications

This work is dedicated to my family, and for all the people which deserves better healthcare.

# Table of Contents

List of Figures .....	8
List of Tables .....	9
<b>ABSTRACT.....</b>	<b>10</b>
<b>1. INTRODUCTION .....</b>	<b>12</b>
1.1. Wearable sensors in health system .....	12
1.2. Wearable sensors to improve brain injury prediction in head impacts in sports.....	13
1.3. Wearable sensors for assessing frailty.....	15
1.3.1. Cardiac-motor interconnection as a frailty assessment tool in older adults.....	15
1.3.2. Frailty assessment in aortic stenosis patients.....	16
1.4. Specific aims.....	17
1.4.1. Chapter 2: Low-rank representation of head impact kinematics: A data-driven emulator ...	17
1.4.2. Chapter 3: Associating frailty and dynamic dysregulation between motor and cardiac autonomic systems .....	17
1.4.3. Chapter 4: Frailty Assessment in Aortic Stenosis based on Dynamic Interconnection between Cardiac and Motor Systems .....	18
<b>2. LOW-RANK REPRESENTATION OF HEAD IMPACT KINEMATICS: A DATA-DRIVEN EMULATOR.....</b>	<b>19</b>
2.1. Introduction .....	19
2.2. Materials and method .....	21
2.2.1. Dimension reduction through principal component analysis.....	22
2.2.2. Data-driven emulator.....	23
2.2.3. Parametrizing biphasic impulse profiles .....	24
2.2.4. Accuracy of injury prediction metrics .....	25
2.2.4.1. Kinematics-based injury metrics.....	25
2.2.4.2. Brain angle injury metric.....	26
2.2.4.3. Tissue deformation-based injury metrics .....	26
2.2.4.4. Injury metric error analysis .....	27
2.3. Results.....	28
2.3.1. Dimension reduction through PCA .....	28

2.3.2.	Data-driven emulator.....	28
2.3.3.	Natural frequencies .....	30
2.3.4.	Parametrizing biphasic impulse profiles .....	31
2.3.5.	Accuracy for injury prediction metrics.....	31
2.3.5.1.	Kinematic-based injury metrics .....	31
2.3.5.2.	Brain angle injury metric.....	33
2.3.5.3.	Tissue deformation-based injury metrics .....	34
2.4.	Discussion.....	35
2.5.	Acknowledgment .....	37
<b>3.</b>	<b>ASSOCIATING FRAILITY AND DYNAMIC DYSREGULATION BETWEEN MOTOR AND CARDIAC AUTONOMIC SYSTEMS.....</b>	<b>38</b>
3.1.	Introduction .....	38
3.2.	Methods.....	39
3.2.1.	Participants .....	39
3.2.2.	Frailty assessment and clinical measures .....	40
3.2.3.	UEF test.....	40
3.2.4.	CCM analysis .....	42
3.2.5.	Statistical analysis .....	44
3.3.	Results.....	45
3.3.1.	Participants and clinical measures.....	45
3.3.2.	CCM analysis .....	45
3.4.	Discussion.....	48
3.4.1.	Effect of frailty on system interconnections.....	48
3.4.2.	Frailty identification using multimodal models .....	51
3.4.3.	Limitations and further work .....	52
3.4.4.	Conclusions and clinical implications.....	52
3.5.	Acknowledgements.....	53
<b>4.</b>	<b>FRAILITY ASSESSMENT IN AORTIC STENOSIS BASED ON DYNAMIC INTERCONNECTION BETWEEN CARDIAC AND MOTOR SYSTEMS .....</b>	<b>54</b>
4.1.	Introduction .....	54
4.2.	Methods.....	56

4.2.1.	Participants .....	56
4.2.2.	Frailty assessment and clinical measures .....	56
4.2.3.	Upper extremity function (UEF) motor test.....	57
4.2.4.	Heart rate (HR) outcomes .....	58
4.2.5.	Convergent cross mapping (CCM) analysis.....	58
4.2.6.	Statistical analysis .....	60
4.3.	Results.....	61
4.3.1.	Participants and clinical measures.....	61
4.3.2.	Effect of frailty.....	61
4.3.3.	Effect of AS condition.....	61
4.4.	Discussion.....	65
4.4.1.	Effect of frailty on HR dynamics and motor performance.....	65
4.4.2.	Effect of AS on HR dynamics and motor performance .....	66
4.4.3.	CCM parameters for identifying frailty .....	67
4.4.4.	Limitations and further work .....	68
4.4.5.	Conclusions and clinical implications.....	68
4.5.	Acknowledgements.....	69
<b>5.</b>	<b>CONCLUDING REMARKS.....</b>	<b>70</b>
5.1.	Low-rank representation of head impact kinematics: A data-driven emulator .....	70
5.2.	Associating frailty and dynamic dysregulation between motor and cardiac autonomic systems limitations .....	71
5.3.	Frailty assessment in aortic stenosis based on dynamic interconnection between cardiac and motor systems .....	71
5.4.	Limitations.....	72
5.5.	Conclusions .....	74
	<b>APPENDIX A – SUPPLEMENTARY MATERIALS (CHAPTER 2) .....</b>	<b>75</b>
<b>6.1.</b>	<b>REFERENCES .....</b>	<b>81</b>

## List of Figures

<b>Figure 2.1</b> Constructing triangular and half-sine biphasic impulses.....	<b>23</b>
<b>Figure 2.2</b> Representation of strain metrics with highlighted regions .....	<b>25</b>
<b>Figure 2.3</b> Low-rank reconstruction of angular velocity using PCA modes .....	<b>27</b>
<b>Figure 2.4</b> The three most energetic temporal modes for angular velocity.....	<b>29</b>
<b>Figure 2.5</b> Distribution graphs for second to fifth principal components .....	<b>30</b>
<b>Figure 2.6</b> Natural frequencies and their contribution to head motion kinematics .....	<b>30</b>
<b>Figure 2.7</b> Computed $HIC_{15}$ , $RIC_{36}$ and $BrIC$ comparison .....	<b>32</b>
<b>Figure 2.8</b> Computed brain angle metric comparison .....	<b>33</b>
<b>Figure 2.9</b> Simulated strain metrics comparison .....	<b>34</b>
<b>Figure 3.1</b> Overview of the CCM method to assess interconnection .....	<b>43</b>
<b>Figure 3.2</b> CCM parameters and NRMSE across frailty groups .....	<b>46</b>
<b>Figure 3.3</b> Convergence curves distribution for CCM predictions .....	<b>47</b>
<b>Figure 3.4</b> ROC curve for previous and current frailty multimodal tests .....	<b>47</b>
<b>Figure 4.1</b> Overview of the CCM method to assess interconnection .....	<b>59</b>
<b>Figure 4.2</b> UEF score, HR dynamics parameters and CCM parameters for frailty and aortic stenosis .....	<b>63</b>
<b>Figure 4.3</b> Heart rate distributions for frailty and aortic stenosis groups .....	<b>65</b>
<b>Figure SM.1</b> Representative reconstruction of the linear acceleration .....	<b>75</b>
<b>Figure SM.2</b> The three most relevant temporal modes for linear acceleration.....	<b>75</b>
<b>Figure SM.3</b> Representative reconstruction of the angular acceleration .....	<b>76</b>
<b>Figure SM.4</b> The three most relevant temporal modes for angular acceleration.....	<b>76</b>
<b>Figure SM.5</b> Peak distribution comparison between augmented data and ground truth .....	<b>77</b>
<b>Figure SM.6</b> Peak duration distribution comparison between augmented data and ground truth .....	<b>78</b>

**Figure SM.7** Statistical parameters per time point for ground truth and an augmented dataset..... 79

**Figure SM.8** Convergence analysis for required number of modes to satisfy Equation 2.1 ..... 80

## List of Tables

**Table 2.1** Mean and standard error of acceleration magnitude and duration ..... 31

**Table 2.2** Sensitivity and specificity of kinematics-based injury metrics for approximations..... 33

**Table 2.3** Sensitivity and specificity of strain metrics for approximations..... 34

**Table 3.1** Demographic information and clinical measures of participants..... 46

**Table 3.2** Differences in UEF, HRV, and CCM features across frailty groups..... 48

**Table 3.3** Logistic models for predicting frailty using UEF, HR dynamics, and CCM parameters ..... 50

**Table 4.1** Demographic information and clinical measures of participants ..... 62

**Table 4.2** Differences in UEF, HR dynamics and CCM features across frailty groups ..... 64

**Table SM.1** p-values for significant differences between ground truth and approximations ..... 77

## ABSTRACT

Advances in medical technology, accessibility to health care, healthier lifestyle, diet, and hygiene have allowed us to increase life expectancy from 46 years in 1950 to almost 74 in 2019. Worldwide, the population is becoming older, and new aging-related challenges have appeared, increasing the burden on a debilitated-in-workforce healthcare system. Wearable sensors and sensor-enhanced health information systems are regarded as one way to face the implications of the aforementioned demographic change. Indeed, continuously monitoring health time series would bring detailed aspects that could potentially enable early diagnosis and an informed prognosis of any disease or injury. This dissertation presents some efforts on developing methods for injury prediction and frailty assessment from real-time health signals obtained from wearable sensors. This work was divided into three consecutive studies.

In the first study, we studied an existing data set of 537 head impact kinematics in sports settings, consisting of 6 degrees of freedom measurements. We presented a principal component analysis-based method for building an accurate low-rank approximation of head impact kinematics. We found that only a few modes were sufficient for the accurate reconstruction of the entire data set. Then, we studied these representative modes in the frequency domain, which were primarily low frequency under 40Hz. We compared our approximation against existing impact parametrization methods and showed significantly better performance in injury prediction using a range of kinematic and brain tissue deformation-based metrics. In all cases, our representation reproduced similar results in injury prediction to the ground truth. Finally, we developed a data-driven emulator capable of generating new kinematic data sets of any size, being particularly useful for training machine learning algorithms that have been investigated for approximating brain deformation in real-time for early brain injury diagnosis.

In the second study, we focused on frailty syndrome, which is associated with a lack of physiological reserve and consequent adverse outcomes (treatment complications and death). Previous research has shown associations between heart rate (HR) dynamics (HR changes during physical activity) and frailty. We analyzed the effect of frailty on the interconnection between the motor and cardiac systems during a localized upper-extremity function (UEF) test. Fifty-six older adults aged 65 or older were recruited to perform a rapid elbow flexion-extension test for 20 seconds while we monitored motor performance and heart rate, utilizing wearable gyroscopes and electrocardiogram devices, respectively. Frailty was assessed

using the gold-standard Fried phenotype. We quantified the interconnection between motor (angular displacement) and cardiac (HR) performance using convergent cross-mapping (CCM). A significantly weaker interconnection was observed among pre-frail and frail participants compared to non-frail individuals. Findings suggested a strong association between cardiac-motor interconnection and frailty.

In the final study, we continued the development of an integral frailty assessment tool, now specifically for heart diseases. Aortic stenosis (AS) is the most commonly acquired valvar disease and is associated with an increased risk of frailty. The current work aimed to assess differences in motor and ANS performance as symptoms of frailty between community-dwelling older adults with and without AS. Older adults, 55 years and older, with and without AS were recruited. Frailty was assessed using the Fried phenotype. Participants performed an upper-extremity function (UEF) physical task – 20 seconds of rapid elbow flexion of the right arm. Arm motion was measured by gyroscopes and heart rate (HR) was measured using an electrocardiogram (ECG) sensor attached to the left side of the chest. Outcomes included UEF motor score (a validated score from 0: “not frail” to 1: “extremely frail” based on slowness, weakness, exhaustion, and flexibility), HR percentage increase due to physical activity and decrease due to rest, and ANS performance (scored from 0: “poor” to 1: “excellent”). ANS performance was measured using convergent cross mapping (CCM) representing the interconnection between HR and motor data. ANOVA models were used with the Fried frailty, AS condition, age, BMI, and sex as independent variables and UEF outcomes as dependent variables. There was a significant difference in UEF motor scores between older adults with and without AS and between the frailty groups. CCM parameters showed significant differences between the frailty groups; however, they were not found to be significantly different between the AS groups. No significant interaction was observed between frailty and AS condition. Our findings suggested that ANS measures may be highly associated with frailty regardless of AS condition. Combining motor and HR dynamics parameters in a multimodal model may provide a promising tool for frailty assessment.

The results presented in this work show ways in which data acquired from wearable sensors could be translated into injury prediction and frailty assessment. These are topics that seem to be deeply important and responsive to future demographic changes in healthcare systems, regarding frailty and aging.

# 1. INTRODUCTION

## 1.1. Wearable sensors in health system

Advances together with the improvement of quality of life have contributed to significant increases in the elderly population and average lifetime during the last decades (1). Although this fact is promising, new medical and logistic concerns appeared. These changes will not only lead to a rise in multimorbidity and aging-related prevalent diseases (2), but also to a deficit of the health workforce concerning the increased need for care. Even now is possible to observe that the potential support ratio (PSR), defined by the number of persons aged 15 to 64 years divided by the number of persons aged 65 and above (3), has alarmingly decreased worldwide from 11.7 in 1950 to an expected to be 2.7 in 2050. Indeed, while it is expected to have a healthier elderly population than years ago, the PSR changes may outweigh this effect. For solution, biomedical engineering has focused on developing new devices, software, and equipment for improving medicine.

Wearable sensors and devices have become a research topic of interest because they can potentially contribute to modern healthcare logistics, such as delivering part of care services, remote and ambulatory monitoring, assessment, patient therapy and rehabilitations, and prognosis. They basically are one potential key to solve the demographic issues we will face in some years, in addition to reducing healthcare costs by decreasing clinical visits and hospitalizations, through prevention or remote medical guidance.

Wearable devices involve a wide range of sensors that can be categorized into medical and peripheral sensors. The term “wearable” implies that the device is attached to the human body or in a piece of clothing, and its design allows prolonged use. They have become popular and widely used in their commercial versions, developed for non-clinical applications such as for sports (heart rate monitoring, pedometer, respiration rate, etc.). The evolution of wearable technology has led to numerous advances in models for assessment and prognosis. Multimodal methodologies use combinations of methodologies to reach reliable assessment (4). The methodologies for feature detection, assessment, and decision support can also involve the use of intelligent information processing, such as machine and deep learning. The

wearable technology allows real-time functionality assessment, and consequently more accurate assessments compared to subjective questionnaires.

In this thesis, we presented the main studies performed during the PhD, which are related to the development of models for brain injury prediction and frailty assessment using multimodal methodologies, in which wearable sensors are the data source. They represent an effort to show the value of wearable technology and data engineering use in prevalent medical scenarios that affect millions of people every day, to improve the health system and, in the future, contribute to less expensive and accurate solutions to counterweight the demographic imbalance that will affect the healthcare workforce.

## 1.2. Wearable sensors to improve brain injury prediction in head impacts in sports

Traumatic brain injury (TBI) is an injury that affects the brain functionality. It is a major cause of death by injury and one of the most debilitating health problems in the US, with nearly two million cases every year (5). Leading causes of TBI are falls, being struck by or against an object, and motor-vehicle crashes. Historically, the diagnosis standard for brain injury assessment has been a clinical task. Recently, several efforts for early injury and outcome predictions have been developed, including regression (6,7), traditional machine learning (ML)-based (8,9), and the more recent deep learning-based models (10–13).

Head impact kinematics is one of the most consequential metrics in predicting brain injury. Indeed, they are still widely used among researchers (14–18). With the advent of wearable sensor technology, several groups have been collecting on-field head kinematic measurements during contact sports events (19–22), since the sports related-TBI represents up to one-third of all causes of TBI (23). However, despite these efforts of data acquisition, on-field head kinematic measurements are not widely available. As a result, researchers have resorted to simplifying parameterizations of head collisions as idealized biphasic acceleration impulses (24–26). A potential disadvantage of these simplifications is overlooking valuable information that could be transcendental in the development of injury metrics. It is also important to characterize real-world head impact kinematics through simplifications that minimize the information lost.

Of note, kinematics describes the inertial response of the brain to head impacts; however, they are limited in the estimation of the dynamic brain response. Investigations have shown that strain, a metric of the tissue-level response of the brain based on its local deformation, is a better predictor of injury compared to kinematics (27,28). This finding has been validated through several cadaveric brain response, ultrasound techniques, and animal models. In order to estimate strain inside the brain, finite element models (FEM) of human head have been developed, including several structural features such as brain anisotropy, meninges, skull and cerebrospinal fluid (CSF) (29,30). Further, several brain tissue-level metrics based on strain have shown to be associated with brain injury, such as strain rate (deformation speed), fiber strain and cumulative strain damage measure CSDM (31), among others. There are some regions of the brain which are intimately related to one of the mechanisms of TBI, the Diffuse Axonal Injury (DAI). Axons are susceptible to damage due to rapid deformations by head impacts. Notably, one of the regions of the brain with denser population of axons is the corpus callosum, and consequently the fiber strain on the corpus callosum is one of the most accurate metrics for brain injury.

Furthermore, advances in computational methods, including deep learning algorithms, have provided new and exciting avenues for fast and accurate prediction and diagnosis of brain injury. Nevertheless, these techniques require a large number of kinematics data to train these algorithms (10,32). Currently, such a data set is not widely available. Thus, artificial augmentation of kinematic samples has been utilized as an alternative to satisfy the training data set requirements of such algorithms. In the following chapter, we presented a study in which a formal method is presented for extracting the most dominant features of on-field impact kinematics in sports. We subsequently used those features to construct an augmented data set that resembles the on-field measurements minimizing the information lost. Moreover, we present a modal reconstruction technique that, despite using relatively few modes, can emulate a desired number of augmented head impacts that are statistically similar to the ground truth impact measurements. This study represents an effort to improve brain injury prediction through the usage of wearable sensors.

### 1.3. Wearable sensors for assessing frailty

Older adult therapy strategies are not trivial due to the heterogeneity of the aging population (33,34). Subsequently, stratification of the status of older adults is required to manage personalized decisions in elderly healthcare. Frailty has been deemed as the way to fulfill this categorization need, which is an aging syndrome related to low physiological reserves in organs and systems and is associated with increased risk of hospitalization, adverse therapy outcomes, disability, and mortality (35). Frailty affects approximately 11% of community-dwelling older adults and as many as 30-70% of older surgical patients (36,37).

There are several efforts to develop multidimensional frailty assessment tools. The Fried frailty index and the Rockwood score are the most commonly used frailty measurements (35,38). However, practical issues such as the time requirement, partially objective measurements, multiple pieces of clinical information for the Rockwood score, and limitations in the applicability of these tools in clinical settings for the Fried test are the main concerns of these assessment instruments. In later chapters, two studies are presented that introduce a novel frailty assessment tool that solves many of the issues of its predecessors, in a simple, non-physically exhaustive, fast, and accurate arm test.

#### 1.3.1. Cardiac-motor interconnection as a frailty assessment tool in older adults

Wearable sensor technologies are already advanced in terms of their technical capabilities and are frequently used for cardio-vascular monitoring since the 1960s when the Holter monitor was introduced for the very first time (39). Nowadays, thanks to the miniaturization and refinement of sensors, using ECG wearable sensors allows us to record heart rate (HR) in real-time. Heart rate variability (HRV) and HR complexity during resting have been used as metrics for assessing autonomic nervous system (ANS) dysfunction. However, they are not directly associated with HR increase or recovery due to physical tasks, and there are between-subject and diurnal variabilities in HRV (40–43). Therefore, Toosizadeh et. al (44) previously introduced a combined motor and cardiac-based frailty assessment tool, in which HR dynamics are studied simultaneously with a motor frailty score during a 20-seconds flexion-extension arm test for

assessing cardiac and motor function and validating an accurate tool for frailty identification. The motor assessment was performed using wearable gyroscope sensors.

While that research showed alterations in cardiac and motor systems for frail participants, the association between frailty and dynamic interconnection between cardiac and motor systems is still unclear. The principle of network physiology states that the human body is a complex network of several physiological systems, where intricate dynamics exist between these systems to maintain homeostasis (45,46). Accurate identification of frailty requires a collection of information across multiple physiological systems (45–48), rather than only system-specific evaluations. Inspired by this fact, we propose a novel frailty predictor based on the interconnection between the cardiac and motor function through a multimodal model, being extensively detailed in chapter 3.

### 1.3.2. Frailty assessment in aortic stenosis patients

Noncommunicable diseases (NCDs) refers to a group of condition that are not mainly caused by an acute infection, resulting in long-term health consequences, and often creating a need for long-term treatment and care. According to the global burden of disease collaborative network, NCDs kill 41 million people each year, equivalent to 74% of all deaths globally (49). These data predict (for the year 2030) the highest world-wide mortality to be caused by heart disease (13.4%) (1). Morbidity, mortality, and economic burden of AS remain unacceptably high (51–53). Like other types of heart disease, AS is a disease of aging associated with the risk for frailty and is becoming more frequent as the population average age increases (54–57). Frailty assessment is not common in cardiology, especially for AS patients (58), because the Fried and Rockwood assessment tools are arduous, fully or partially subjective, require trained clinical staff to perform, or require walking for physical assessment (59,60). More importantly, no disease-specific tool is available to identify heart disease-related frailty that can be implemented for AS patients. In chapter 4, we presented a study in which we propose a frailty assessment tool on AS patients, combining motor score, HR dynamics, and cardiac-motor interconnection.

## 1.4. Specific aims

This research aimed to develop models to improve the prediction of head injury through data augmentation and accurately assess frailty. For these purposes, we used validated mathematical tools, including principal component analysis and convergent cross-mapping, on real transient data acquired by wearable sensors.

### 1.4.1. Chapter 2: Low-rank representation of head impact kinematics: A data-driven emulator

In this chapter, we present a method describing a data-driven head impact kinematics emulator. We analyzed a previously acquired 6 degrees-of-freedom kinematic data set of 537 head impacts measured during contact sports, using a mouthguard instrumented with a triaxial accelerometer and a triaxial gyroscope (19). Using principal component analysis we decreased the dimensionality of the measured head impact kinematics to construct a low-rank kinematics data set, and we contrasted this dataset with other kinematics approximations. We investigated the efficacy of each approximation by comparing its performance in detecting brain motion/deformation and injury prediction using three types of injury metrics. We compared the performance of each approximation against the ground truth (GT) data. We performed power spectral density analysis on the derived temporal modes to obtain their predominant frequencies. Finally, we present a modal reconstruction method for emulating augmented head impacts based on the normal distribution observed in the GT data.

### 1.4.2. Chapter 3: Associating frailty and dynamic dysregulation between motor and cardiac autonomic systems

This chapter covers a methodology for assessing cardiac-motor interconnection as an independent frailty predictor. Fifty-six older adult participants ( $\geq 65$  years) were recruited from community dwellings. First, we assessed frailty using the five-component Fried phenotype and participants were categorized into two frailty groups (non-frail and pre-frail/frail). We collected clinical measurements for adjusting physical

activity and cardiovascular performance based on cognitive status, comorbidity score, and depression. Then, participants performed the upper-extremity function (UEF) consisting of an extension-flexion arm test for 20 seconds, while we monitored the motor performance with wearable gyroscopes attached to the arm, and cardiac performance with a wearable electrocardiogram. We quantitatively assessed the directional nonlinear interactions between HR and motor data using the convergent cross-mapping technique (CCM). We compared the CCM parameters between frailty groups through a multivariable ANOVA model considering age, sex, and BMI as adjusting variables. Finally, we built a multimodal model including the proposed interconnection parameters.

### 1.4.3. Chapter 4: Frailty Assessment in Aortic Stenosis based on Dynamic Interconnection between Cardiac and Motor Systems

In chapter 4 we presented an investigation of frailty symptoms in aortic stenosis (AS) patients. We compared different parameters we found significantly associated with frailty, i.e. motor score, HR percentile changes, and CCM-based interconnection parameters, on 31 aortic stenosis and 55 non-aortic stenosis (NAS) participants. We considered age, sex, BMI, and comorbidity index score as adjusting variables. We previously assessed the frailty status of all the participants using the Fried frailty phenotype test. ANOVA analyses for comparing motor, cardiac, and CCM parameters across frailty groups and NAS/AS conditions were repeated with clinical measures with significant association with frailty as covariates. We tested our hypothesis of a weaker interconnection between motor and HR performance among pre-frail/frail participants, independent of AS condition.

## 2. LOW-RANK REPRESENTATION OF HEAD IMPACT KINEMATICS: A DATA-DRIVEN EMULATOR

### 2.1. Introduction

Traumatic brain injury (TBI) is one of the most debilitating health problems in our society today, with nearly two million new cases in the US every year (5). The majority of these cases are considered mild, also known as concussion (61). The substantial increase in reported concussions in contact sports (62), together with the recent findings of increased long-term pathological changes (63), has sparked a public discussion and raised awareness about TBI. An important requirement is an accurate and objective diagnosis of concussions, which in turn could inform better protective equipment design and safer activities (64–68).

Head motion kinematics, including the rate, frequency and direction of head's movement during collision, has been deemed as one of the most consequential metric in predicting brain injury. Historically, kinematic-based metrics such as head injury criterion (HIC) (14), rotational injury criterion (RIC) (15), and brain injury criterion (BRIC) (16) have been used to detect injury. These metrics are still widely used among researchers and are endorsed by safety regulating organizations such as the National Highway Traffic Safety Administration (NHTSA) (17) and the National Operating Committee on Standards for Athletic Equipment (NOCSAE) (18).

More recently, brain tissue deformation-based metrics have been introduced that use head kinematics as input to computational models that can approximate the effect of head motion on brain displacement and deformation. These metrics either use simple discrete mechanical elements in lumped-parameter models, i.e. mass-spring-damper combinations, to give a rigid-body estimate of brain's relative motion with respect to the skull (69–71), or more complex finite element (FE) models with detailed geometry of the brain anatomy, which can simulate the local brain deformation and interaction with the stiff bony or membranous structures (25,72,73).

In the case of lumped models, brain angle metric (BAM), developed based on a data set of concussive and sub-concussive head impacts (74), and in the case of FE models, maximum principal strain (MPS) and

axonal fiber strain (FS) along the white matter axon fibers have been proposed as effective injury diagnosis metrics (75).

Evidently, both for the kinematic-based and the brain deformation-based metrics, head impact kinematics play a major role. With the advent of wearable sensor technology, several groups have been collecting on-field head kinematic measurements during contact sports events (19,21,22,76,77). However, despite these pioneering efforts, on-field head kinematic measurements are not widely available. As a result, researchers have resorted to simplifying parameterizations of head collisions as idealized biphasic acceleration impulses (24,26,78). These biphasic impulses are commonly represented either by a triangle or half-sine and defined by two parameters: height and width constitute the magnitude and duration of a head impact impulse. The simplification of kinematic impulses serves the objective of emulating on-field kinematic data of a head impact with a few and manageable number of parameters to populate an otherwise infinite-dimensional loading space to investigate and establish a relation between head motion and brain injury. However, a potential disadvantage of these simplifications is overlooking valuable information that could prove detrimental in developing injury metrics. Therefore, it is paramount to understand the characteristics of real-world head impacts and whether we can accurately capture them through simplified approximations.

Furthermore, advances in computational methods, including machine learning algorithms, have provided new and exciting avenues . As a result, given the prohibitively high computational cost of current FE models, the biomechanics community has been trying to utilize such interpolative and machine learning techniques (10,75,78,79). However, a limitation of those techniques is the large number of kinematic data required to train these algorithms (in the order of thousands of head impacts (10)). Currently such a data set is not widely available. Thus, artificial augmentation of kinematic samples has been utilized as an alternative to satisfy the training data set requirements of such algorithms.

In this paper, we present a formal method to extract the most dominant features of on-field head impact kinematics from existing data in the context of contact sports. We subsequently use the extracted features in order to construct an augmented data set that resembles the on-field measurements.

We hypothesize that by using our method, based on principal component analysis (PCA), we will acquire more accurate injury predictions than current biphasic impulse approximations when compared against the ground truth measurements.

Furthermore, we present a modal reconstruction technique that, despite using relatively few modes, can emulate a desired number of augmented head impacts that are statistically similar to the ground truth impact measurements.

## 2.2. Materials and method

In order to study the characteristics of head impact kinematics and the efficacy of simplified approximations, we used a previously-collected data set of 537 head impact kinematics measured during contact sports, including American football, boxing, and mixed martial arts (19,20). For each impact, 6 degrees of freedom (DoF) kinematics -- linear acceleration and angular velocity in the three anatomical directions -- were collected at 1,000Hz for 100ms using a mouthguard instrumented with a triaxial accelerometer and a triaxial gyroscope (19). We construct three different reduced kinematics data sets to approximate the measured kinematics: 1) using principal component analysis (PCA), we decrease the dimensionality of the measured head impact kinematics to construct a low-rank kinematics data set, and 2-3) using previously proposed biphasic assumptions for acceleration impulses with acceleration magnitude and duration as the two variables, we construct biphasic data sets once for triangle (Tri) and once for half-sine (HS) approximations.

We investigate the efficacy of each approximation by comparing its performance in detecting brain motion/deformation and injury prediction using three types of metrics: 1) kinematics-based injury metrics, including HIC, RIC and BrIC, 2) brain angle metric (BAM), and 3) tissue deformation-based finite element injury metrics, including maximum principal strain (MPS) and axonal fiber strain (FS) in the whole brain (WB) and corpus callosum (CC).

We compare the performance of each approximation against the ground truth (GT) data described above. We perform power spectral density (PSD) analysis on the derived temporal modes to obtain their

predominant frequencies. These values are given by the maximum power spectral density (PSD) values of each mode.

Finally, we present a modal reconstruction method for emulating augmented head impacts.

### 2.2.1. Dimension reduction through principal component analysis

Our goal is to exploit the correlations between different measurements and find a reduced representation for three quantities of interest (QoIs), including: linear acceleration, angular velocity and angular acceleration in each anatomical direction. In the case of linear kinematics, anterior-posterior, inferior-superior, and lateral directions are considered and in the case of angular kinematics, axial, coronal and sagittal directions are considered as separate QoIs. To this end, we apply principal component analysis (PCA) to our data set. For each QoI, we form a data matrix  $\mathbf{X}_{m \times n}$ , where  $n=537$  is the number of measured head impacts and  $m=100$  is the number of time steps, and  $\mathbf{X} = [\mathbf{x}_1 | \mathbf{x}_2 | \dots | \mathbf{x}_n]$ , where each column represents the measured QoI for a particular head impact and each row represents the time instance of the measurement. To perform PCA, we compute the singular value decomposition (SVD) of the data matrix:  $\mathbf{X} = \mathbf{U}\mathbf{\Sigma}\mathbf{Y}^T$ , where  $\mathbf{U} = [\mathbf{u}_1 | \mathbf{u}_2 | \dots | \mathbf{u}_n]$  are a set of orthonormal modes, i.e.  $\mathbf{u}_i^T \mathbf{u}_j = \delta_{ij}$ ,  $\mathbf{\Sigma} = \text{diag}(\sigma_1, \sigma_2, \dots, \sigma_n)$  is a diagonal matrix, where  $\sigma_1 \geq \sigma_2 \geq \dots \geq \sigma_n$  are the singular values, and  $\mathbf{Y} = [\mathbf{y}_1 | \mathbf{y}_2 | \dots | \mathbf{y}_n]$  are the uncorrelated linear components, i.e.  $\mathbf{y}_i^T \mathbf{y}_j = \delta_{ij}$  with the joint probability distribution function (PDF) of  $p(y_1, y_2, \dots, y_n)$ . This gives an ordered array of the modal contributions inherent to head impacts response. Finally, we perform power spectral density (PSD) analysis on the derived modes  $\mathbf{u}_i$  to obtain their predominant frequencies. These values are given by the maximum PSD values of each mode.

A reduced representation of the impact data is obtained by:  $\mathbf{X} \simeq \sum_{i=1}^k \sigma_i \mathbf{u}_i \mathbf{y}_i^T$ . To quantify the performance of the reduction, we introduce:

$$\eta(k) = \frac{\sum_{i=1}^k \sigma_i}{\sum_{i=1}^n \sigma_i}, \quad (2.1)$$

## 2.2.2. Data-driven emulator

Once we extract the modal characteristics of the head impact data set, a reduced emulator of the head impact kinematics is obtained by truncating to  $k$  PCA modes:

$$\mathbf{x}^* = \sum_{i=1}^k \sigma_i y_i^* \mathbf{u}_i, \quad (2.2)$$

where  $(y_1^*, y_2^*, \dots, y_k^*)$  is a random point with  $k$  components drawn from the marginal PDF of  $p(y_1, y_2, \dots, y_n)$ . Equation (2.1) can be used as an emulator for producing new time series ( $\mathbf{x}^*$ ) for each of the QoIs that are nearly indistinguishable from the ground truth head impact kinematics measurements. Our approach can be interpreted as a stochastic dimension reduction technique and it is a special case of dimension reduction with time-dependent modes (80–84), in which the loading is a random input and the QoIs are random output. In order to ensure high quality augmented data, we establish features to statistically compare new time series with the GT, including parameters such as impact time, peak and duration of impacts, and orthonormal projections of PCA modes.

We will provide this emulator as a stand-alone program that allow users to build low-rank head kinematics data sets with various approximation levels ( $k$ ) and emulate a pre-defined number of impacts.

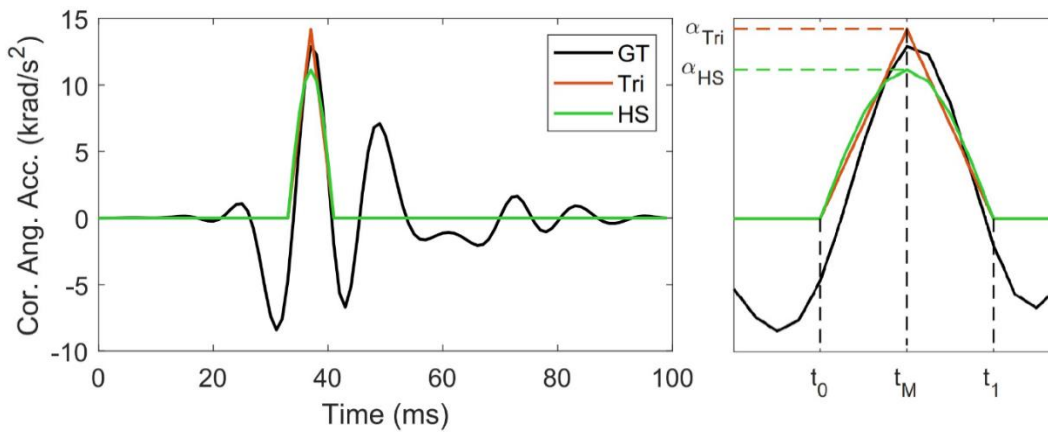


**Figure 2.1:** Constructing triangular and half-sine biphasic impulses (26,78): a representative angular acceleration trace in the coronal plane, magnified to better represent initiation time ( $t_0$ ), completion time ( $t_1$ ), time of peak ( $t_M$ ), and peak acceleration ( $\alpha_{Tri}$  and  $\alpha_{HS}$ ).

### 2.2.3. Parametrizing biphasic impulse profiles

In order to compare the performance of previously proposed biphasic models for angular and linear acceleration impulses (26,78) against our low-rank PCA approximation, we reconstruct biphasic triangle (tri) and half-sine (hs) representations of the 537 head impacts described above. First, the maximum absolute value of the angular acceleration profile ( $\alpha_M$ ) -- computed by differentiating angular velocity measurements using a first order forward divided difference method (two points) -- was identified, including the time of peak ( $t_M$ ). The impact duration ( $\Delta t$ ) is defined as the time interval on either side of  $t_M$ . The boundary of this interval is defined as where the sign or the convexity of the acceleration profile (whichever comes first) changes. Convexity changes are computed based on the second derivative test using a common three-point stencil central finite difference derivative. This process is described in Figure 2.1, where the impact duration ( $\Delta t = t_1 - t_0$ ) is the time elapsed between the initiation time ( $t_0 < t_M$ ) and the completion time ( $t_1 > t_M$ ) of impact. In the cases where  $t_M \rightarrow 0ms$  or  $t_M \rightarrow 100ms$ , since it is not possible to define  $t_0$  or  $t_1$  correctly, only half of the simplified pulse was created. Finally, the change in velocity ( $\Delta\omega$ ) was computed as the area under the acceleration impulse ( $\Delta\omega = \int_{t_0}^{t_1} \alpha(t)dt$ ), and the corresponding acceleration magnitudes for the triangle ( $\alpha_{Tri}$ ) and half-sine ( $\alpha_{HS}$ ) approximations were calculated through:

$$\alpha_{Tri} = 2 \frac{\Delta\omega}{\Delta t}, \quad \alpha_{HS} = \pi \frac{\Delta\omega}{2\Delta t}, \quad (2.3)$$

Angular velocity pulses were then computed through direct temporal integration of low-rank angular acceleration pulses.

## 2.2.4. Accuracy of injury prediction metrics

### 2.2.4.1. Kinematics-based injury metrics

We used  $HIC_{15}$ ,  $RIC_{36}$  and  $BrIC$  to compare the performance of our proposed PCA reduction against the triangle and half-sine biphasic signals, i.e. triangle and half-sine approximations. To this end, we used previously published injury threshold values: 1) for  $HIC_{15}$ , values of 240 and 667 have been reported as 50% risk of concussion (85) and skull fracture (86), respectively; 2) for  $RIC_{36}$ , a value of  $10.3 \times 10^6$  is reported as 50% risk of concussion (15); and 3) for  $BrIC$ , a value of 0.5 constitutes a 50% concussion risk (16). We used these thresholds to assess the performance of each reduction approach in providing injury predictions in terms of sensitivity and specificity with respect to the ground truth measurements.

Injury thresholds were used as indicators, defining true positives (above the threshold) and negatives (below the threshold), while the predictive value of each impulse approximation was compared against the GT measurement.

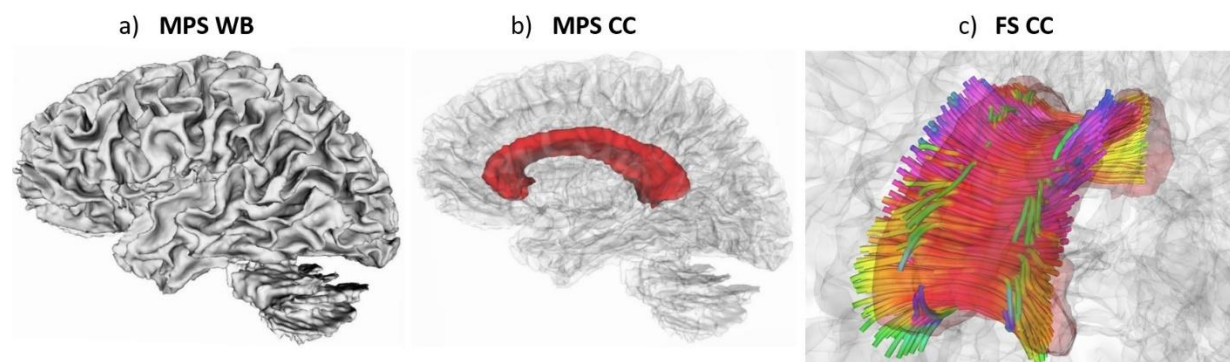


**Figure 2.2:** Representation of strains metrics with highlighted regions: a) maximum principal strain (MPS) in the whole brain (WB), b) maximum principal strain (MPS) in the corpus callosum (CC), c) fiber strain (FS) in the corpus callosum (CC). Fiber colors represents directions: inferior-superior (blue), lateral (red) and

anterior-posterior (green). Images were generated using 3DSlicer from ATLAS-based anatomical representation in FreeSurfer (87).

#### 2.2.4.2. Brain angle injury metric

We further compared the performance of each approximation using injury criterion based on lumped-parameter models of the head.

These models generally consider simplifying assumptions: skull and brain are considered rigid bodies and relative motion between the two represents a form of deformation and injury, and the compliance of the brain-skull interface such as the effect of bridging veins, dura and pia mater is represented by linear spring and damper elements (71,88,89). Given the head kinematics as the base excitation input, these models can estimate the relative motion of brain and skull, particularly the angular motion since that has been seen as the more consequential type of motion (90). Recently, brain angle metric (BAM) was developed based on the characteristics of human brain and skull in finite element simulations, and validated against observed concussive and sub-concussive head impacts (74). We compute BAM for each kinematic approximation (PCA, triangle and half-sine).

#### 2.2.4.3. Tissue deformation-based injury metrics

As a final step in studying the efficacy of the different kinematic approximations, we compared the performance of each approximation in predicting the tissue-level deformation metrics using finite element simulations, including maximum principal strain (MPS) in the whole brain (WB) and in the corpus callosum (CC) region, as well as axonal fiber strains (FS) in the corpus callosum region, which have all been proposed as predictive tissue-level metrics for injury classification (27,76,91) (Figure 2.2). Recently a convolutional neural network (CNN) was developed based on pre-trained FE simulations based on the Worcester Head Injury Model (WHIM) (92). This CNN method uses angular velocity data as input to approximate the regional brain deformations, i.e. maximum principal and axonal fiber strain (10).

#### 2.2.4.4. Injury metric error analysis

Having simulated the injury metrics for each head impact measurement, we calculated the corresponding injury metric ( $metric_{GT}$ ) and the injury metric estimated by the kinematics approximation ( $metric_{approx}$ ) using the equation below:

$$error = \left| \frac{metric_{approx} - metric_{GT}}{metric_{GT}} \right| \times 100. \quad (2.4)$$

Subsequently, we performed Friedman test (93) with a p value of 0.01 (MATLAB, `friedman`) to show significant differences between each approximated impulse and the ground truth. We also performed sensitivity and specificity analysis to provide an estimate for the efficacy of approximating the metrics for injury diagnosis. For this purpose, we used previously published values for 50% risk of concussion, including  $MPS_{WB} = 0.2$  (94),  $MPS_{CC} = 0.2$  (27), and  $FS_{CC} = 0.074$  (95).

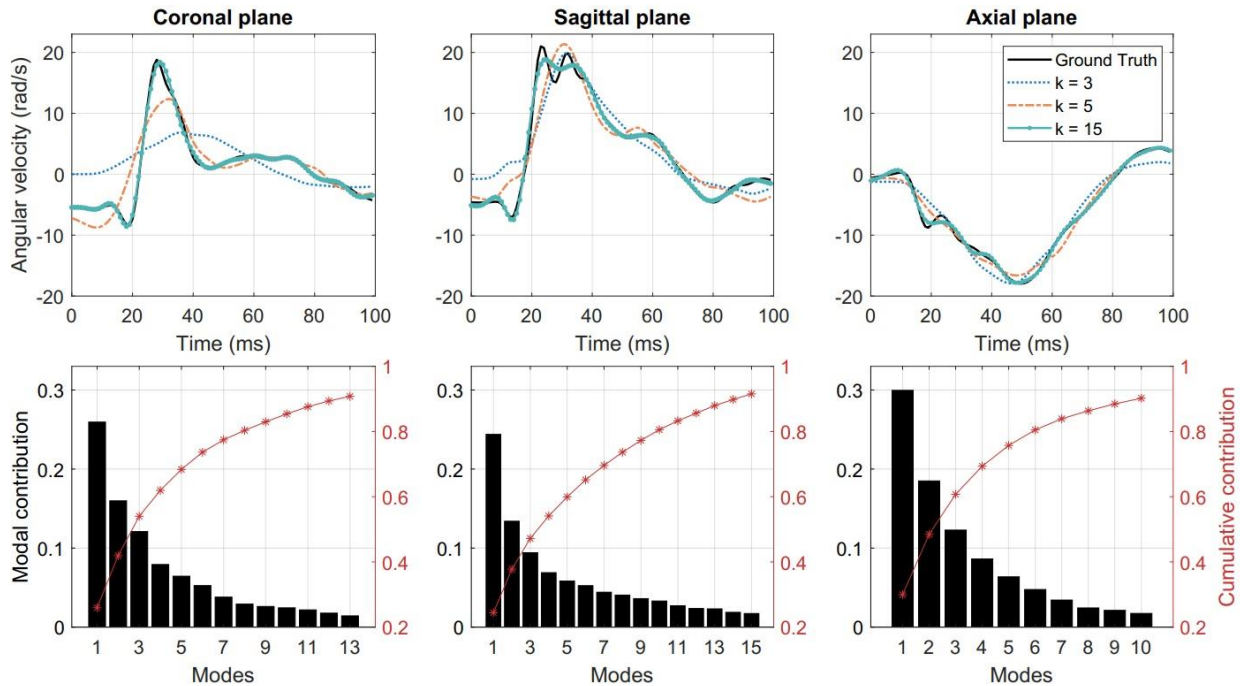


**Figure 2.3:** Low-rank reconstruction of angular velocity using  $k=3, 5, 15$  PCA modes. *Bottom:* Individual and cumulative contribution of PCA modes for angular velocity reconstruction. Columns from left to right show results for coronal, sagittal and axial directions, respectively.

## 2.3. Results

### 2.3.1. Dimension reduction through PCA

We performed PCA on the measured kinematics data for the QoIs, i.e. linear acceleration, angular velocity and angular acceleration in each anatomical direction. We used the reduction criterion of  $\eta = 0.90$ , as defined in Equation 2.1, for all these cases. In the case of angular velocity, the minimum number of modes that satisfies this reduction criterion is  $k=13, 15$  and  $10$  modes for coronal, sagittal and axial directions, respectively.

In Figure 2.3 (top row), the PCA reconstruction of angular velocity in three anatomical directions for a sample case is shown. The sample case was chosen randomly from the 537 cases and it is represented by a column of the data matrix  $\mathbf{X}$ . The ground truth measurement for the sample case as well as the reconstructed impulses with different levels of reduction are shown. It is clear that the 15-mode reduction yields a satisfactory reconstruction. In Figure 2.3 (bottom row) the individual and cumulative contribution of PCA modes are shown for the entire kinematics data set. These results demonstrate that with a relatively small number of PCA modes an accurate approximation of the head kinematic measurements can be achieved. As an additional analysis, in order to determine the convergence of this method, we performed PCA with several randomly selected subsets of the 537 ground truth measurements (with 100, 200, 300, 400, and 500 samples) and investigated the number of modes required to satisfy the  $\eta > 0.90$  criterion. The results show that the minimum number of modes slightly grows with subsets size but levels off below 500 cases, indicating that our data set of 537 could be sufficient to reliably reconstruct a head impact data set (See SM.8).

### 2.3.2. Data-driven emulator

The first three temporal modes show a classic modal behavior with 1, 2, and 3 peaks in all three anatomical directions (Figure 2.4).

Together, these first three modes capture nearly half of the total angular velocity response, and with each additional mode, we can reconstruct a closer approximation with the ground truth. For more analysis of the modes, see Supplementary Materials Figures SM.2 and SM.4.

To further study the distribution of these modal approximations, we show the orthonormal projection of the first five PCA modes ( $y_2, \dots, y_5$ ) against the first and most energetic mode ( $y_1$ ) of the PCA data (black circles and bars in Figure 2.5). It is clear that the modes follow a Gaussian distribution, which would be an important consideration for emulating more data points.

To show the performance of our data-driven emulator, we reproduced an additional  $k=537$  head impact cases by randomizing the  $y_k^*$  columns each with the same mean and variance as the original  $Y$  matrix (Equation 2.2). Projection of the orthonormal vectors  $y_i^*$  on  $y_1^*$  for an augmented data set (red circles and bars in Figure 2.5) shows similar distribution as the ground truth data. In addition, features of the augmented data generated on our emulator, such as duration and peak distributions, have not significant differences with respect those of GT (See figures SM.5, SM.6 and SM.7).

Thus, our emulator is able to successfully generate reliable kinematics sets of data based on real on-field measurements. A copy of the head impact kinematics emulator will be available on our website (96).

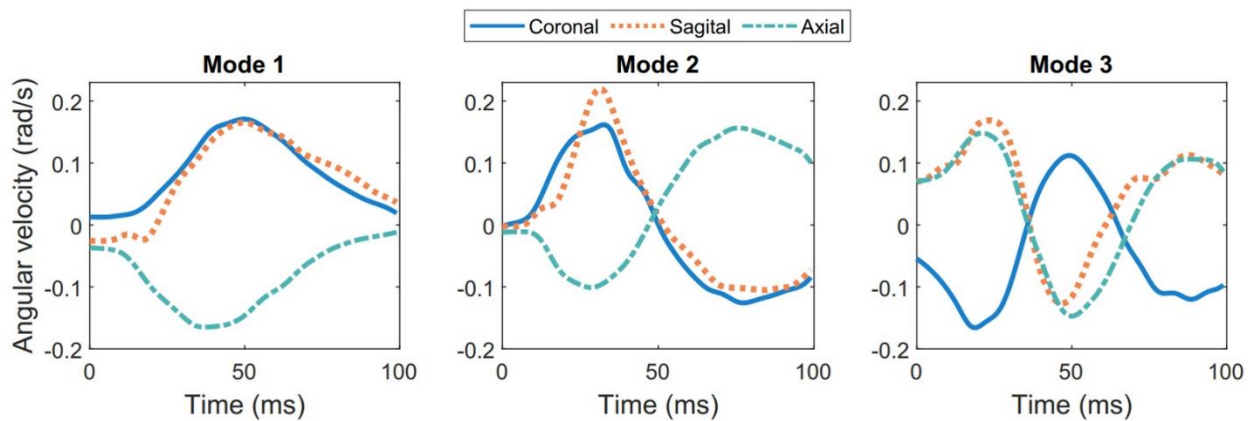


**Figure 2.4:** The three most energetic temporal modes for angular velocity for the entire 537 head impact data set.

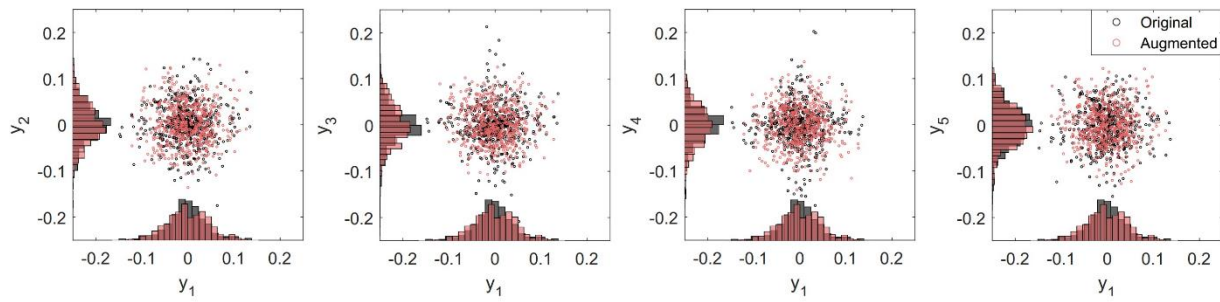


**Figure 2.5:** Distribution graphs for second to fifth principal components ( $y_2, \dots, y_5$ ) projected on to the first principal component ( $y_1$ ) for angular velocity in the sagittal direction. PCA data (in black) follows a Gaussian distribution. Emulated data (red) is generated performing a Gaussian random number generator based on mean and variances from the PCA modes.

### 2.3.3. Natural frequencies

The contribution of the most dominant frequencies, obtained through PSD criterion, are displayed in Figure 2.6. In general, low frequencies interval such from 10 to 40Hz have the highest predominance for each parameter. Notably, the cumulative contribution for rotational velocity is progressively decreasing with increasing frequency.

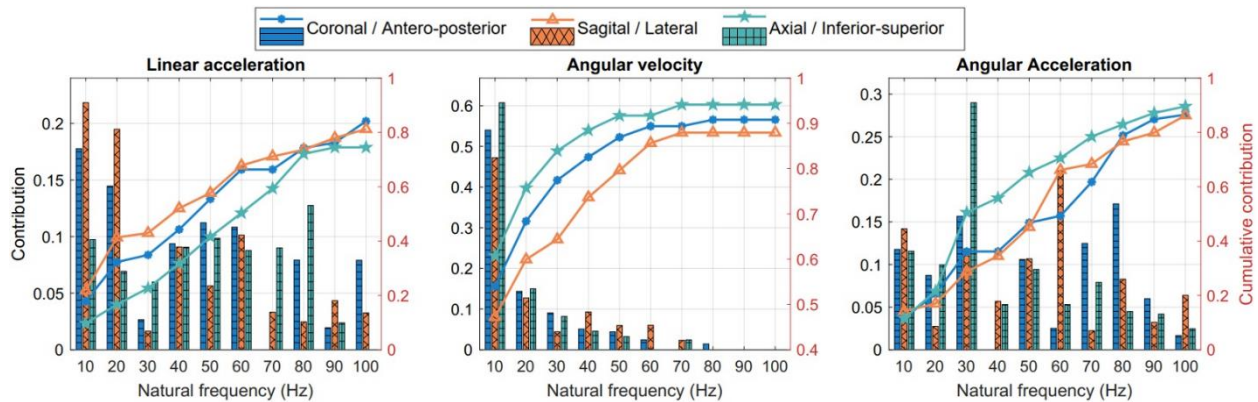


**Figure 2.6:** Natural frequencies and their contribution to head motion kinematics.

### 2.3.4. Parametrizing biphasic impulse profiles

Using the criteria described above, we fitted triangle and half-sine analog pulses to the ground truth kinematics measurements in order to parametrize the rotational acceleration magnitude and duration for each head impact. As a result, we derived 537 analog impulses in the three anatomical directions for both triangle and half-sine approximations. The results are presented in Table 2.1, where the rotational acceleration magnitude and duration average and standard errors of the mean are given for the ground truth and the impulses approximations.

**Table 2.1:** Mean and standard error of acceleration magnitude and duration for ground truth and three approximations (PCA, triangle, half-sine). The PCA magnitudes were obtained by decomposing the ground truth angular accelerations for the criterion  $\eta = 0.90$ , which constituted of 21 modes for coronal and sagittal directions and 20 modes for axial direction (See Figure SM.3).

	Coronal direction	Sagittal direction	Axial direction
Ground truth magnitude ( $rad/s^2$ )	818.89 $\pm$ 937.12	1,498.10 $\pm$ 1,753.40	655.16 $\pm$ 535.03
PCA magnitude ( $rad/s^2$ )	801.41 $\pm$ 922.08	1,460.50 $\pm$ 1,736.10	641.52 $\pm$ 523.06
Triangle magnitude ( $rad/s^2$ )	871.53 $\pm$ 1,011.8	1,625.40 $\pm$ 1,923.20	697.04 $\pm$ 553.95
Half-sine magnitude ( $rad/s^2$ )	681.25 $\pm$ 790.38	1,269.30 $\pm$ 1,500.40	545.64 $\pm$ 433.40
Duration ( $ms$ )	15.20 $\pm$ 6.75	15.00 $\pm$ 8.03	17.90 $\pm$ 8.45

### 2.3.5. Accuracy for injury prediction metrics

#### 2.3.5.1. Kinematic-based injury metrics

The injury metrics  $HIC_{15}$ ,  $RIC_{36}$  and  $BrIC$  were computed for every model and the ground truth. Figure 2.7 shows the distribution of all samples and the corresponding concussion and skull fracture thresholds.

The PCA predictions showed similar mean and standard deviations for HIC and RIC ( $38.20 \pm 139.55$  and  $1.89 \times 10^6 \pm 7.66 \times 10^6$  respectively) as the ground truth ( $38.49 \pm 140.13$  and  $2.26 \times 10^6 \pm 9.04 \times 10^6$ ); however, there is a significant difference between the ground truth predictions and the triangle ( $15.74 \pm 41.71$  and  $3.98 \times 10^5 \pm 1.06 \times 10^7$ ) and half-sine ( $14.80 \pm 39.31$  and  $3.86 \times 10^5 \pm 1.02 \times 10^6$ ) impulses.

Additionally, whereas the PCA-based impulses showed accurate predictions compared to the ground truth, we observed that the biphasic approximations either under-predicted injury (higher number of false negatives) in terms of HIC and RIC, or over-predicted injury (higher number of false positives) in terms of BrIC (Figure 2.7).

To better illustrate this, we performed sensitivity and specificity analysis for injury classification with respect to the ground truth, where the PCA-based signals showed high predictive performance compared to the biphasic impulses (Table 2.2).

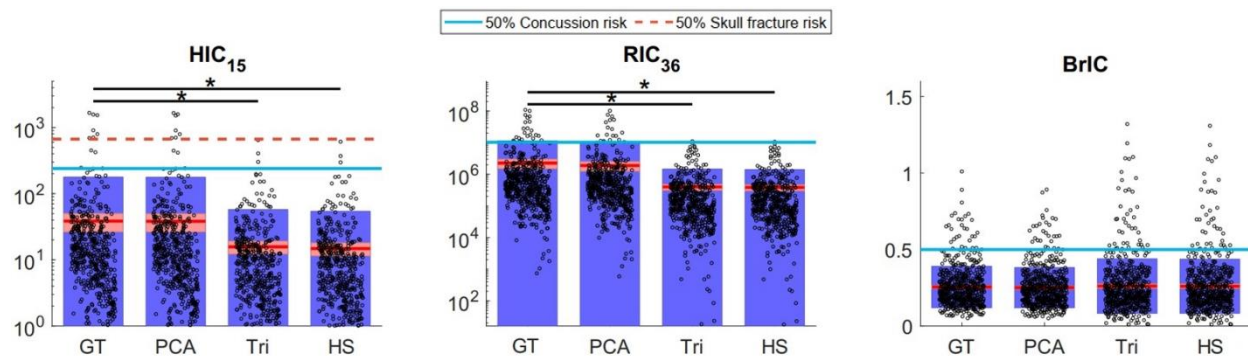


**Figure 2.7:** Computed  $HIC_{15}$ ,  $RIC_{36}$  and  $BrIC$  for each of the ground truth (GT) and the three approximated data sets: PCA, triangle (Tri), and half-sine (HS). The circles represent each sample, the solid red line represents the mean, and the blue and red regions show the standard deviation and standard error, respectively. The solid blue and dashed red lines represent 50% risk of concussion and skull fracture, respectively. Significant differences are indicated for  $p < 0.01$ . HIC and RIC graphs are on log-scale.

**Table 2.2:** Sensitivity and specificity of kinematics-based injury metrics for  $HIC_{15}$ ,  $RIC_{36}$  and  $BrIC$  for the three approximations: PCA-based method, triangles (Tri) and half-sine (HS) compared to the ground truth, considering thresholds of 50% risk of injuries.

	HIC (50% risk – skull fracture)			HIC (50% risk – concussion)			RIC (50% risk – concussion)			BrIC (50% risk – concussion)		
	PCA	Tri	HS	PCA	Tri	HS	PCA	Tri	HS	PCA	Tri	HS
	Sensitivity	1.00	0.00	0.00	0.91	0.27	0.27	0.79	0.04	0.04	0.9	0.77
Specificity	1.00	1.00	1.00	1.00	1.00	1.00	1.00	1.00	1.00	1.00	0.97	0.97

### 2.3.5.2. Brain angle injury metric

We computed 3DoF relative brain angles using the lumped model proposed in (74) to obtain the maximum resultant relative brain angle as a result of each head impact based on the ground truth kinematics and each of the three approximations. In coronal and axial directions, triangular and half-sine approximations gave significantly lower predictions for the brain angle metric, whereas the PCA modes showed no statistically significant difference from the ground truth (Figure 2.8). We observed substantially smaller approximation errors (Equation 2.4) for the PCA approach ( $\sim 3\%$ ) compared to the two biphasic approximations ( $\sim 25\%$ ) (Figure 2.8).

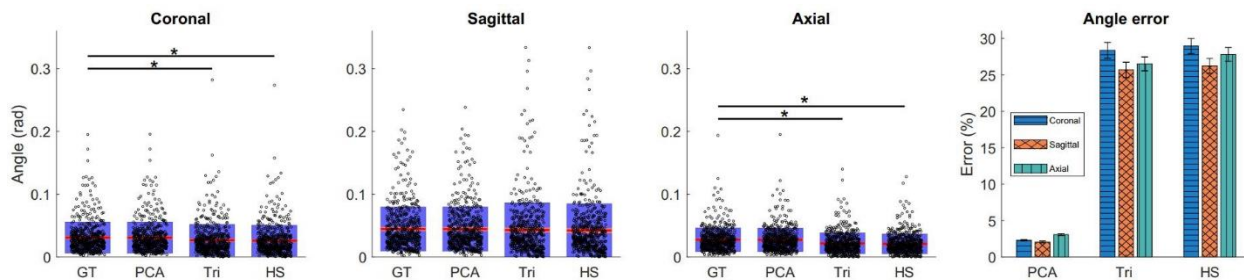


**Figure 2.8:** Computed brain angle metric (BAM) values for each impact case based on ground truth and the corresponding PCA and biphasic approximations. The significant differences are indicated for  $p < 0.01$ . The error comparison between models with means and SEM of each data set is shown on the right.

### 2.3.5.3. Tissue deformation-based injury metrics

Similar to brain angle metric, we calculated the errors between the ground truth strain metrics and those of low-rank approximations.

As can be seen in Figure 2.9, the PCA approach closely follows the ground truth simulation results in all three strain metrics: maximum principal strain (MPS) in the whole brain (WB) and corpus callosum (CC), as well as axonal fiber strain (FS) in the corpus callosum. The strains computed for the biphasic impulses significantly differ from the ground truth values and successively provide higher errors as we include region-specific and morphological information. Furthermore, based on the 50% concussion risk thresholds mentioned above, the PCA approach provides substantially higher sensitivity and specificity for injury classification (Table 2.3).

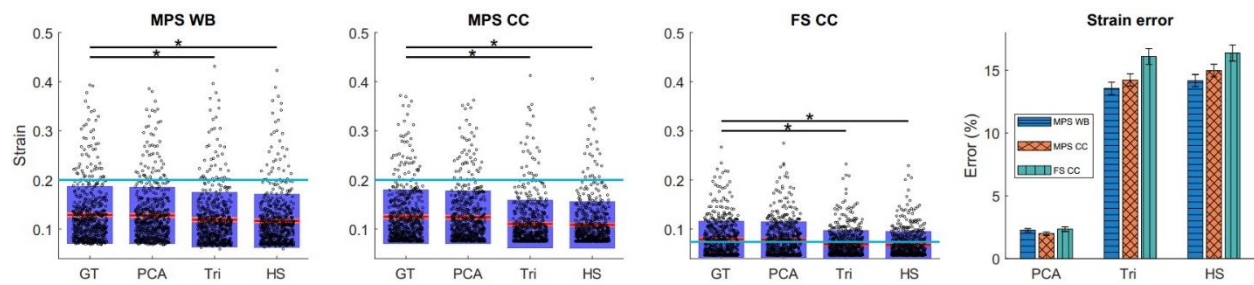


**Figure 2.9:** Simulated strain metrics for ground truth head impact measurements and the corresponding PCA and biphasic approximations. The blue line shows the 50% risk of concussion for each metric. The significant differences are indicated for  $p < 0.01$ . Also the mean and standard error of the mean are shown on the right for strain estimation errors.

**Table 2.3:** Sensitivity and specificity of strain metrics for maximum principal strain (MPS) for whole brain (WB) and corpus callosum (CC), as well as fiber strain (FS) for CC compared to the ground truth, with respect the threshold of 50% risk of concussion.

	MPS WB			MPS CC			FS CC		
	PCA	Tri.	H.S.	PCA	Tri.	H.S.	PCA	Tri.	H.S.
Sensitivity	0.93	0.74	0.63	0.98	0.55	0.53	0.97	0.63	0.62
Specificity	0.99	0.99	0.99	0.99	0.99	0.99	0.99	0.94	0.95

## 2.4. Discussion

In this study we provide a formal approach for reducing the dimensionality of head impact kinematics in contact sports settings. We first derived the most important modes contributing to the head kinematics through principal component analysis and then compared those to existing methods that approximate head kinematics with simple biphasic impulses. We show that the modal decomposition approach can capture the kinematic behavior of the head with better accuracy and provide better approximations of brain deformation and injury classification. This analysis confirms that although head kinematics during head collisions span a wide range of magnitudes and frequencies (76), we can accurately capture the impact head kinematics by using only a relatively small number of modes. The low-rank database constructed based on PCA analysis require only 15 modes to build the ground truth angular velocity kinematics with over 90% accuracy as well as accurately capture the predictive value of head impact kinematics using a variety of injury metrics.

A major advantage of our approach is that with the acquired modes above, we are able to emulate a head impact data set with any given number of cases without needing access to the ground truth measurements. This emulated data set would closely replicate head impacts measured by on-field wearable sensors that constitute current state of the art.

The advantage of this low-rank emulator, in addition to its computational efficiency, is that it avoids simplifying assumptions for the shape of acceleration impulses and only uses empirical measurements. In contrast, the conventional biphasic assumption for head impacts as simple impulses with only two variables, i.e. acceleration magnitude and duration, falls short in providing accurate estimates. This effect is more pronounced for acceleration impulses that are more variable due to the time derivative but is true for velocity profiles as well.

This apparent lack of accuracy in injury prediction in the biphasic approximations might be due to the fact that the biphasic triangle and half-sine signals are built using acceleration signals and then integrated to give the corresponding velocity profiles. Since there is no restitutive deceleration for these impulses, angular velocity eventually becomes constant after the acceleration returns to zero, contrary to the actual measured impulses (24). In the case of kinematics-based injury metrics, the discrepancies in misidentifying

concussive and subconcussive cases by HIC and RIC could be explained by these metrics' dependence on the shape of the acceleration impulse. In contrast, BrIC is only a function of peak angular velocity, and therefore exhibits less sensitivity to the shape of the impulse and the biphasic impulse's lack of restitutive deceleration (Figure 2.7).

In the case of brain angle metric, the biphasic impulse approximations show over five-fold errors compared to PCA-based impulses. This difference could be attributed to the simplification of the biphasic models that influences the solution of the mechanical lumped-parameter models. This discrepancy seems to affect the coronal direction the most and the sagittal direction the least for the biphasic approximations.

Similar to the brain angle results, brain finite element strains showed superior performance by our PCA-based approach. In previous publications, it has been shown that the closer the model is to the correct anatomical and morphological attributes of the brain, the more accurate the injury predictions become (97,98). Similarly, we see a decline in performance for the biphasic models as we include more region-specific and morphological details: from maximum principal strains (MPS) in the whole brain to MPS in corpus callosum and on to axonal fiber strains (Table 2.3).

Several other points are worth noting based on our analysis. Relative with time domain, we observe differences in kinematics profiles in the three anatomical directions. It seems that the head experiences higher linear accelerations in the anterior-posterior direction ( $3.54 \pm 2.97m/s^2$ ) compared to lateral ( $2.62 \pm 2.25m/s^2$ ) and inferior-superior ( $3.01 \pm 3.44m/s^2$ ) directions, and higher angular accelerations in the sagittal direction ( $190.53 \pm 177.34rad/s^2$ ) compared to coronal ( $314.50 \pm 401.53 rad/s^2$ ) and axial ( $177.34 \pm 128.16 rad/s^2$ ) directions. This observation might be attributed to the type and direction of loading in the specific activity, e.g. direction of tackling in football, as well as anatomical features such as the neck constraint in those directions (99). In the frequency domain, there is a dominant low-frequency response (10 to 40 Hz) in the head kinematics, expressed by  $\sim 90\%$  of the total angular velocity response in the axial plane,  $\sim 83\%$  in the coronal plane and  $\sim 74\%$  in the sagittal plane, confirming previous findings on frequency dependence of head impacts (76,100). These results could prove useful for designing better helmets and other safety devices to avoid brain injury by targeting specific low-frequency range of motion.

In summary, our proposed PCA decomposition approach not only provides a deeper understanding of the head's response during impacts, but also provides a formal basis for reconstructing and augmenting head impact kinematics data. Our current emulator is built upon the 537 measured on-field head impacts described above and successfully generates new kinematic data, whose features such peak or duration are nearly indistinguishable (see figure SM.7). It is expected that with more on-field measurements, we would be able to improve the performance of the emulator even further, but our convergence analysis showed the available 537 cases to be sufficient (Figure SM.8). This type of approach might prove necessary given the increased need for larger training data sets in modern machine learning algorithms.

## 2.5. Acknowledgment

We thank Prof. David Camarillo of Stanford University for providing the head kinematics. PA thanks the Fulbright and CONICYT project Equal Opportunities Scholarship 56170002, and also Carissa Grijalva of the University of Arizona, for helping with the visualizations. KL thanks BIO5 Institute at the University of Arizona for partial support for this study under award number 1119000-KL2. We also thank the National Institutes of Health for partial support of this study under grant number R03NS108167

### 3. ASSOCIATING FRAILITY AND DYNAMIC DYSREGULATION BETWEEN MOTOR AND CARDIAC AUTONOMIC SYSTEMS

#### 3.1. Introduction

Frailty is an aging syndrome related to low physiological reserves in organs and systems and is associated with increased risk of hospitalization, adverse therapy outcomes, disability, and mortality (35). Muscle loss (sarcopenia), and weakness (dynapenia) are the main symptoms of frailty (101), which are triggered by metabolic and hormonal derangements (102–105), and the so called “heightened inflammatory state” (106), caused by excessive levels of C-reactive protein (CRP), proinflammatory cytokines interleukin 6 (IL-6), and white blood cells and tumor necrosis factor-alpha (TNFalpha) (106–108). Consequently, frailty is highly associated with a decrease in motor function performance (109). Furthermore, frailty is associated with an impaired cardiac autonomic nervous system (ANS) because of alterations in the action potential on the sinoatrial node myocytes, which impacts the cardiac function and the heart rate variability (HRV) (110). While research showed alterations in several physiological systems, the association between frailty and dynamic interconnection between cardiac and motor systems is still unclear. Indeed, the human body is a complex network of several physiological systems, where intricate dynamics exist between these systems to maintain homeostasis (45,46). Accurate identification of the level of physiological reserve requires a collection of information across multiple physiological systems (45–48), rather than only system-specific evaluations. To explore the extent of dynamic behaviors within and across physiological systems, principles of network physiology has been introduced. The concept of network physiology claims that dysregulation of interactions between physiological systems leads to loss of resilience and the ability to recover from stressors (47), which is inherent to the concept of frailty.

We have previously developed a methodology for assessing frailty that incorporates an upper-extremity function (UEF) and corresponding heart rate (HR) response to physical activity. The UEF test consists of repetitive and rapid elbow flexion and extension (111), during which several kinematics features

representing dynapenia are measured using motion sensors (35). Since UEF involves upper-extremity motion, it is feasible to perform for bedbound patients and where walking tests are difficult for frail older adults. In our recent research we showed that HR dynamics, measured by changes in HR due to the UEF physical function (i.e., HR dynamics), were significantly associated with frailty (112). Combining UEF motor and cardiac functions, we were able to identify frailty with higher accuracy compared to models including each of the motor or HR dynamics parameters separately (113). Nevertheless, it is unclear whether frailty can influence the interconnection between motor and HR dynamics, and whether applying interconnection measures improve frailty identification.

The goal of the current study was to determine the effect of frailty on the interconnection between motor and cardiac systems. Build upon our previous research, the main hypothesis was that due to frailty, a weaker interconnection would exist between motor and HR performance. Recently, the concept of interconnection assessment within different physiological systems has gained attention (114–119). Granger causality is a classical approach that identifies causality between variables based on the removal of one to determine the predictability of the other variable (120), but its usage is limited to linear systems that have stationary behaviors, or for those in which variables are strongly coupled (121). In contrast, convergent cross-mapping (CCM) assesses the non-linear directional interactions of variables in a complex dynamic system, based on state-space reconstruction of time series collected from each system (122). The secondary hypothesis was that the accuracy of frailty identification would be improved using additional CCM interconnection parameters compared to models incorporating each of motor and HR parameters individually.

## 3.2. Methods

### 3.2.1. Participants

Older adult participants ( $\geq 65$  years) were recruited between October 2016 and March 2018. Participants were recruited from primary, secondary, and tertiary health care settings such as primary and community care providers, assisted living facilities, retirement homes, and aging service organizations. The inclusion criteria were 1) being 65 years or older; 2) the ability to walk a minimum distance of 4.57 m (15 ft) for

frailty assessment; and 3) the ability to read and sign an informed consent. The exclusion criteria were: 1) severe motor disorders (Parkinson's disease, multiple sclerosis, or recent stroke); 2) severe upper-extremity disorders (e.g., elbow bilateral fractures or rheumatoid arthritis); 3) cognitive impairment identified by a Mini Mental State Examination (MMSE) score  $\leq 23$  (123); 4) terminal illness; 5) diseases/treatments that can bias the HR measurements (including arrhythmia and use of pacemaker); and 6) usage of  $\beta$ -blockers or similar medications that can influence HR. Written informed consent was obtained from all participants. The study was approved by the University of Arizona Institutional Review Board. All research was performed in accordance with the relevant guidelines and regulations, according to the principles expressed in the Declaration of Helsinki (124).

### 3.2.2. Frailty assessment and clinical measures

The frailty assessment was executed using the five-component Fried phenotype as the gold standard (35). The Fried phenotype considers five criteria: 1) unintentional weight loss of 4.54 kg (10 pounds) or more in the previous year; 2) grip strength weakness (adjusted with body mass index (BMI) and sex); 3) slowness based on the required time to walk 4.57 m (15 ft) (adjusted with height and sex); 4) self-reported exhaustion based on a short two-question version of Center for Epidemiological Studies Depression (CES-D); and 5) self-reported low energy expenditure based on a short version of Minnesota Leisure Time Activity Questionnaire (125). Participants were categorized into three frailty groups, which were non-frail if they met none of the criteria, pre-frail if they met one or two criteria, and frail if they met three or more criteria. Clinical measures collected included: 1) MMSE and Montreal Cognitive Assessment (MoCA) for cognition (123,126); 2) comorbidity based on Charlson Comorbidity Score (CCI) (127); and 3) depression using Patient Health Questionnaire (PHQ-9) (128). These measures were considered as adjusting variables in the statistical analysis because they could potentially influence physical activity and the cardiovascular system performance.

### 3.2.3. UEF test

After frailty assessment and clinical measures, participants were asked to sit on a chair and rest for two minutes to regain normal resting status. Participants then performed the UEF task of elbow flexion-

extension as quickly as possible for 20 seconds with the right arm. After the UEF task, participants rested on the chair for another two minutes. We have shown that UEF results are similar on both left and right hands (129). Before the test, participants practiced the UEF test with their non-dominant arm to become familiar with the protocol. The protocol was explained to participants and using exact same verbal instruction they were encouraged only once, before elbow flexion, to do the task as fast as possible. Wearable motion sensors (triaxial gyroscope sensors, BioSensics LLC, Cambridge, MA, sampling frequency=100 Hz; Figure 1A) were used to measure forearm and upper arm motion, and ultimately the elbow angular velocity. Angular velocity data from gyroscopes were filtered using first-order high pass butter-worth filter with a cutoff of 2.5 Hz. Maximums and minimums of the angular velocity signal were detected, and subsequently, elbow flexion cycles were identified. Motor performance was assessed to represent: 1) slowness based on speed of elbow flexion; 2) flexibility based on range of motion, 3) weakness based on strength of upper-extremity muscles; 4) speed variability and motor accuracy; 5) fatigue based on reduction in speed during the 20-second task, and 6) number of flexion cycles. A sub-score was assigned for each of those features, determined previously based on multivariable ordinal logistic models, with the Fried frailty categories as the dependent variable and UEF parameters plus demographic information as independent variables (112). The normalized UEF motor score from zero (resiliency) to one (extreme frailty) was computed as the sum of sub-scores corresponding to performance results and demographic information (i.e., BMI) (111). More details about UEF validation, repeatability, and the normalized score are explained in previous research (111,129,130).

HR was recorded using a wearable ECG device with two electrodes and one built-in accelerometer (360° eMotion Faros, Mega Electronics, Kuopio, Finland; ECG sampling frequency=1000 Hz and accelerometer sampling frequency=100 Hz; Figure 1A). One ECG electrode was placed on the upper mid-thorax and the other one inferior to the left rib cage. The placement of the electrodes on the left chest would minimize the movement artifacts due to UEF test with the right arm. ECG data was analyzed for 20 seconds of baseline, 20-second UEF, and 30 seconds of recovery. RR intervals (successive R peaks of the QRS signal) were computed using the Pan-Tompkins algorithm (131). The automated peak detection process was manually inspected by two researchers (PA and NT). Previously two types of HR parameters were extracted, one representing baseline HR and HR variability (HRV), and one representing HR dynamics (changes in HR during UEF and HR recovery after the task) (44). Briefly, HR dynamics included time to reach

maximum and minimum HR, as well as percent increase and decrease in HR during activity and recovery periods, respectively. In addition to previously developed parameters, in the current study, the interconnection between motor and HR data were assessed using CCM.

### 3.2.4. CCM analysis

We quantitatively assessed the directional nonlinear interactions between HR and motor data using CCM. An overview of the method is summarized in Figure 3.1. CCM tests whether a historical trace of HR can predict motor performance (or inversely, whether a historical trace motor performance can predict HR). To calculate the CCM, we first created evenly sampled data of synchronized HR and motor function with a sampling frequency of 10Hz, using spline interpolation (Figure 3.1B). Each HR data point represents average HR values over 0.1 seconds. Corresponding motor data represent the angular displacement travelled during each 0.1 second of UEF. For calculating motor performance, motor function  $M_f$  was defined by:

$$M_{f_i} = \int_{t_i}^{t_i+0.1} \omega_e dt, \quad (3.1)$$

where  $\omega_e$  represents the angular velocity of the elbow.

Taken's embedding theorem generally guarantees that the space state of a dynamic system could be represented from a single-observed time series  $X$  as an  $E$ -dimensional manifold (132). The shadow or reconstructed manifold, denoted by  $M_X$ , consists of an  $E$ -dimensional data with lagged coordinates ( $\tau$ ) of the variable:

$$M_X = \langle X(t), X(t - \tau), X(t - 2\tau) \dots X(t - (E - 1)\tau) \rangle. \quad (3.2)$$

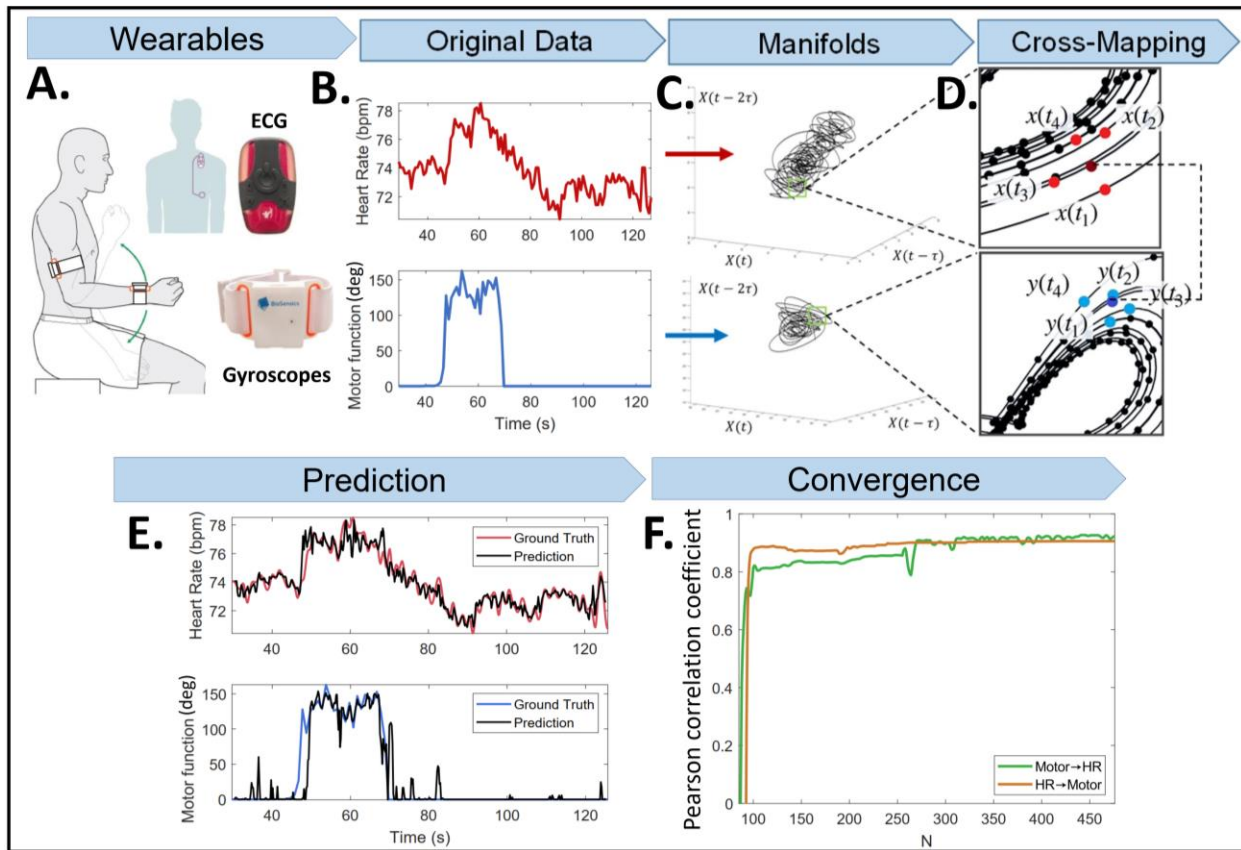


**Figure 3.1:** Overview of the CCM method to assess interconnection between motor and HR data: A) Wearable devices (gyroscopes) to obtain angular velocity and ECG during the UEF physical task; B) Motor performance and HR extraction; C) CCM shadow attractor manifolds on time-lagged coordinate systems; D) Prediction of HR from motor function and vice-versa in a time point (dark red and dark blue dots, respectively) using a distance-based weighted average of neighbors (bright red and bright blue dots); E) Comparison between predicted motor (or HR) data and ground truth; and F) Convergence curves of Pearson correlation coefficient between predicted and ground truth as a function of library length (data points used for developing manifolds).

Subsequently, we reconstructed  $E$ -dimensional manifolds from each of these two time series (132) (Figure 3.1C). Dimension ( $E$ ) of four was selected based on the average false nearest neighbor approach (133). A time lag ( $\tau$ ) of 1 second was used for analysis based on the delayed mutual information method (134). We

predicted one time series (e.g., motor function) by historical records of the other signal (e.g., shadow manifold of HR) using a k-nearest neighbor technique. For a dimension  $E$ , we determined  $E + 1$  nearest neighbors and identified indices of each data points in manifolds ( $M_X$ ). Using these indices for one manifold (e.g., motor data  $X(t)$ ), we found corresponding neighbors in the second manifold (e.g., HR data  $Y(t)$ ) (Figure 3.1D), and then predicted  $X(t)$  to  $\hat{Y}(t)$  as the weighted mean of  $E + 1$  points in the second manifold (135):

$$\hat{Y}(t) = \sum_{i=1}^{E+1} w_i Y(t_i), \quad (3.3)$$

where  $w_i$  weights are calculated based on the Euclidean distances between  $M_Y$  and its  $i^{th}$  nearest neighbor on  $X(t)$ .

The Pearson correlation coefficient and the normalized root-mean-square-error (NRMSE) between the predicted and original time series were calculated to assess the strength of interconnections (Figure 3.1E). NRMSE was calculated by normalizing the RMSE between the predicted and the ground truth with respect to the standard deviation of observations. As documented in previous studies, the correlation coefficient is expected to increase with increasing the time-series length (i.e., library length, Figure 3.1F). For the current study, the correlation and NRMSE values were calculated at the maximum library length (Figure 3.1F).

### 3.2.5. Statistical analysis

Analysis of variance (ANOVA) models were used to evaluate the differences in demographic information between the frailty groups, except for sex. Instead, the chi-square ( $\chi^2$ ) test was used to assess the difference in sex categories among frailty groups. CCM parameters were compared between frailty groups using multivariable ANOVA models; age, sex, and BMI were considered as adjusting variables since they have been previously associated with motor and cardiac performance and frailty (111,136–138). Cohen's effect size ( $d$ ) was estimated. ANOVA analyses for comparing CCM parameters across frailty groups were repeated with clinical measures with significant association with frailty as covariates. To assess the additional value of interconnection measures compared to previous models with individual motor and HR

parameters, logistic regression models were implemented with frailty as the dependent variable and HR, motor, and CCM parameters as independent parameters. A stepwise parameter selection based on Akaike information criterion (AIC) values was implemented to identify independent predictive variables. The area under the curve (AUC) with 95% confidence interval (CI) was calculated using receiver operator characteristics (ROC) curves for each predicting model. Statistical analyses were done using JMP (Version 16, SAS Institute Inc., Cary, NC, USA), and statistical significance was concluded when  $p < 0.05$ .

### 3.3. Results

#### 3.3.1. Participants and clinical measures

Fifty-six participants were recruited for the study, including 12 non-frail (age=76.92±7.32 years), 40 pre-frail (age=80.53±8.12 years), and four frail individuals (age=88.25±4.43 years). Of note, due to the small number of frail participants (n=4), frail and pre-frail groups were merged for the statistical analysis. A summary of demographics is presented in Table 3.1. There was no significant difference in demographic parameter between the frailty groups ( $p > 0.10$ ). Among clinical measures, CCI comorbidity and PHQ-9 depression scores were significantly different between frailty groups ( $p < 0.03$ , Table 3.1).

#### 3.3.2. CCM analysis

Significant effects of frailty on CCM correlation values were observed for interconnections in both directions, i.e., predicting HR time series based on motor function (motor to HR) and predicting motor function based on HR (HR to motor) as reported in Table 3.2, Figure 3.2 and 3.3. Pre-frail/frail older adults showed smaller correlations in CCM for both directions, compared to non-frail older adults. There was also a significant effect of frailty on NRMSE values ( $p < 0.05$ ); for both motor and HR CCM predictions, NRMSE values were significantly smaller among non-frail compared to pre-frail/frail ( $p < 0.05$ ).

**Table 3.1.** Demographic information and clinical measures of participants.

Variables	Non-frail (n=12)	Pre-frail/Frail (n=44)	<i>p</i> -value (effect size)
Female, n (% of the group)	7 (42%)	34 (77%)	0.20
Age, year (SD)	76.92 (7.32)	81.23 (8.14)	0.10 (0.54)
Height, cm (SD)	164.36 (9.13)	164.23 (10.27)	0.97 (0.01)
Weight, kg (SD)	66.58 (14.69)	75.53 (19.56)	0.15 (0.48)
Body mass index, kg/m <sup>2</sup> (SD)	24.67 (5.55)	27.74 (5.71)	0.10 (0.54)
MMSE score, 0-30 (SD)	29.67 (0.65)	29.14 (1.34)	0.19 (0.53)
MoCA score, 0-30 (SD)	26.25 (3.08)	24.88 (2.80)	0.15 (0.48)
CCI score, 0-29 (SD)	1.42 (1.78)	3.86 (2.89)	<0.01* (0.91)
PHQ-9 score, 0-30 (SD)	0.42 (0.51)	2.35 (2.89)	0.03* (0.75)
<b>Fried criteria, n (% of the group)</b>			
Weight loss	0	1 (2%)	
Weakness	0	18 (41%)	
Slowness	0	34 (77%)	
Exhaustion	0	7 (16%)	
Low energy	0	8 (18%)	

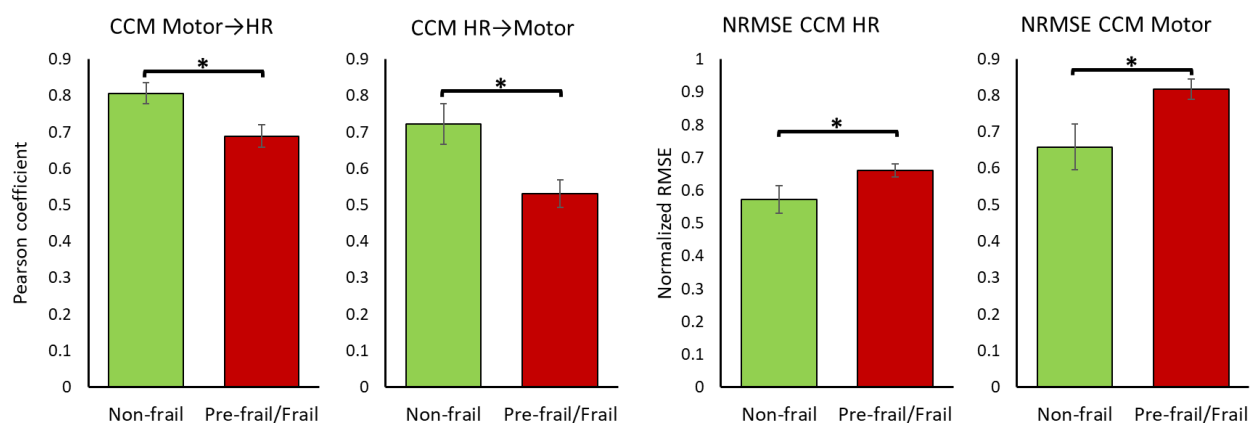


**Figure 3.2.** CCM parameters and NRMSE across frailty groups. A significant between group difference is identified by the asterisk ( $p < 0.05$ ).

Within the stepwise regression analysis, UEF score, HR percent increase, and CCM Motor-to-HR parameters were selected as independent predictors of frailty categories (non-frail vs. pre-frail/frail). Using these three parameters, pre-frailty/frailty was predicted with an AUC, sensitivity, and specificity of 0.91, 0.89, and 0.83 (Table 3.3, Figure 3.4), which had a 7% higher AUC than models that included only individual motor or HR parameters as predictors.

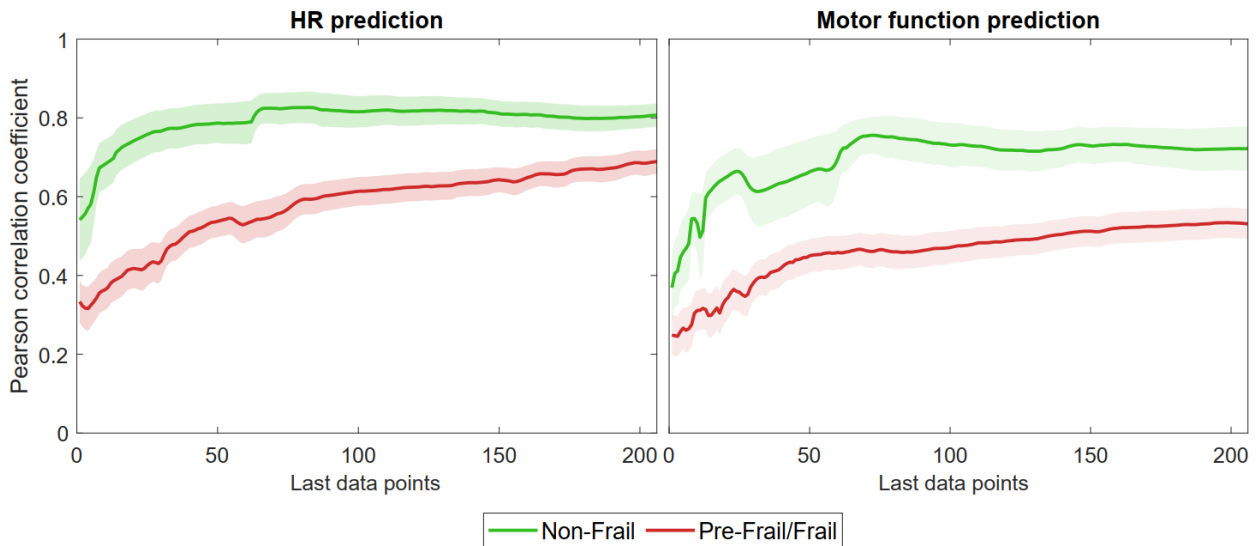


**Figure 3.3.** Convergence curves distribution for CCM predictions. Solid lines represent the average across each group at each library length and shaded regions show the standard error.

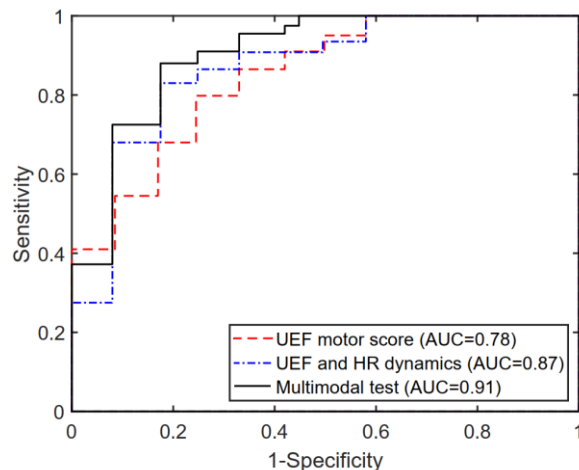


**Figure 3.4.** The area under the receiver operator characteristics (ROC) curve for the UEF score, the previous multimodal test (HR + UEF score), and the current model incorporating the CCM parameter.

**Table 3.2.** Differences in UEF, HRV, and CCM features across frailty groups. A significant association is represented by the asterisk.

Parameters	Non-frail (n=12)	Pre-frail/Frail (n=44)	P-value (Effect size)
<b>UEF motor score</b>			
UEF motor score, 0-1 (SD)	0.32 (0.18)	0.53 (0.23)	0.01* (0.90)
<b>HR dynamics parameters</b>			
HR mean, bpm (SD)	71.52 (11.38)	77.59 (15.97)	0.23 (0.43)
Time to peak HR, seconds (SD)	16.84 (6.46)	16.12 (5.62)	0.43 (0.28)
HR recovery time, seconds (SD)	13.71 (6.22)	14.04 (5.76)	1.00 (0.001)
HR percent increase, % (SD)	19.28 (7.55)	10.29 (4.79)	<0.01*(1.49)
HR percent decrease, % (SD)	15.24 (7.65)	8.13 (3.97)	<0.01*(1.25)
<b>CCM parameters</b>			
Correlation Motor→HR (SD)	0.81 (0.10)	0.69 (0.21)	0.03*(0.77)
Correlation HR→Motor (SD)	0.72 (0.19)	0.53 (0.26)	0.01*(0.89)
NRMSE HR, % (SD)	57.28 (14.47)	66.10 (13.26)	0.02*(0.86)
NRMSE Motor, % (SD)	65.82 (21.67)	81.68 (19.00)	0.04*(0.73)

*UEF: upper extremity function; SD: standard deviation; HR: heart rate; bpm: beats per minute; CCM: convergent cross-mapping; NRMSE: normalized root mean square error.*

## 3.4. Discussion

### 3.4.1. Effect of frailty on system interconnections

As hypothesized, a significantly weaker interconnection between motor and cardiac systems was observed among pre-frail and frail older adults compared to non-frail individuals (Table 3.2 and Figure 3.2). Indeed, these results are consistent with expected changes due to aging-related physiological dysregulation. Autonomic nervous system (ANS) regulates heart activity during exercise by signals from the central nervous system (139) and feedback mechanisms from the exercise pressor reflex (group III and IV muscle afferents) (140) and the arterial baroreflex, which controls blood pressure and consequently cardiac

output (141). Previous studies have shown that exercise pressor reflex is impacted by aging (142–145), which would potentially alter the interconnection between the motor and cardiac systems. Nevertheless, the effect is still controversial and further research is needed to fully understand this interconnection pathway. One potential explanation is that frailty leads to an altered control of motor to cardiac system by affecting exercise pressor reflex. Nevertheless, this hypothesis should be investigated in future research.

In addition to exercise pressor reflex, the observed weaker CCM values among pre-frail and frail older adults may be explained by the general concepts of homeostatic physiological dysregulation and heightened inflammatory state (106,146). In this regard, aging and more specifically frailty can be caused by breakdowns of key regulatory processes and excessive increase of immune factors, leading to the loss of homeostasis and functional impairment (102,104–106,108). Different methods have been used previously to identify physiological dysregulation, such as Mahalanobis multivariate statistical distance and principal component analysis. Mahalanobis multivariate statistical distance is a multivariate model built to assess dysregulation within relevant blood-based biomarkers for frailty, such as red blood cell count, IL-6, CRP, calcium, and hemoglobin (147). This method showed that the increase in the multivariate distance is accelerated with age, which represents the loss of integration of the system physiology. Similarly, the principal component analysis approach considered the variability of blood-based biomarkers, and consequently was showed to be an independent frailty predictor (148). Both methods included information from multiple systems to assess frailty, analogously to how CCM parameters were computed from HR and motor time-series, and how they were associated with physiological dysregulation and frailty status.

**Table 3.3.** Logistic models for predicting frailty using UEF motor score, HR dynamics, and CCM parameters. A significant association is represented by the asterisk.

Independent variable	Parameter estimate	Standard error	Chi-square ( $\chi^2$ )	p-value (95% CI)
<b>Model 1 – UEF motor score</b> (AUC=0.78; AICc=53.94; Sensitivity=0.75; Specificity=0.75)				
Intercept	0.61	0.73	0.70	0.4 (-0.81:2.12)
UEF motor score	-0.05	0.02	6.85	<0.01 (-0.08:-0.01)*
<b>Model 2 – HR dynamics</b> (AUC=0.84; AICc=44.25; Sensitivity=0.80; Specificity=0.75)				
Intercept	-4.91	1.27	14.97	<0.001(-7.92:-2.81)*
HR percent increase	0.25	0.08	10.38	<0.001 (0.12:0.44)*
<b>Model 3 – CCM</b> (AUC=0.74; AICc=55.60; Sensitivity=0.75; Specificity=0.25)				
Intercept	4.21	1.52	7.72	<0.01 (1.77:7.86)*
CCM HR→M	-4.53	2.11	4.59	0.03 (-9.45:-0.98)*
<b>Model 4 – Combined UEF &amp; HR dynamics</b> (AUC=0.87; AICc=76.67; Sensitivity=0.82; Specificity=0.83)				
Intercept	-3.21	1.55	4.28	0.04 (-6.68:-0.45)*
HR percent increase	0.23	0.08	7.73	<0.01 (0.09:0.42)*
UEF motor score	-0.03	0.02	2.67	0.10 (-0.07:0.01)
<b>Model 5 – Combined UEF, HR dynamics &amp; CCM</b> (AUC=0.91; AICc=42.80; Sensitivity=0.89; Specificity=0.83)				
Intercept	6.26	2.83	4.88	0.03 (1.69:13.14)*
HR percent increase	0.22	0.08	7.38	<0.01 (-0.42:-0.08)*
UEF motor score	-0.03	0.02	2.69	0.10 (-0.00:0.08)
CCM HR→M	4.54	2.90	2.45	0.12 (-11.27:0.51)

*HR heart rate; UEF upper-extremity function; CCM convergent cross-mapping; AUC area under curve; CI confidence interval; AICc Akaike's information criterion with correction for small sample size.*

### 3.4.2. Frailty identification using multimodal models

Current findings confirmed that assessing two physiological systems of motor and cardiac autonomic control, and especially the dynamic interaction between them, can improve frailty identification compared to models that focus on individual physiological systems in isolation. These two physiological systems were selected in this study as they are strongly associated with frailty. Muscle loss and weakness (sarcopenia and dynapenia) are the main symptoms of frailty, caused by inflammatory, metabolic, and hormonal derangements (101–109). Motor deficits and muscle weakness are commonly assessed using walking speed or grip strength tests (Fried phenotype) or counting deficits/disorders (Rockwood deficit index) (38,149). Nevertheless, performing walking tests in the clinical setting is cumbersome, and many frail older adults have walking disabilities. Grip strength, on the other hand, only measures muscle strength and cannot reveal other aspects of motor deficits. We have previously validated the sensor based UEF motor task to accurately detect systematic decrements in motor function associated with frailty, including slowness, weakness, inflexibility, fatigue, and motor variability (130,150).

In addition to the motor system, the implemented method included cardiac autonomic control. Previous research showed an association between frailty and an impaired ANS because of alterations in electrical conduction and action potential morphology (151,152). The presence of a compromised neurohormonal homeostasis associated with ANS dysfunction is, in turn, associated with health complications (153,154). HRV (i.e., variability in RR intervals within QRS-waves) during resting have been used for assessing ANS dysfunction, and has been proposed as a “vital sign” (40,155,156). However, between-subject and diurnal variability exists in resting HRV (e.g., due to breathing regulation and environmental factors (41–43)). Here, a novel measure of *HR dynamics* (HR response to physical activity) was introduced as a direct measure of sympathetic (during activity) and parasympathetic (during recovery) performance. The advantages of HR dynamics over HRV are twofold: 1) by normalizing the HR response to the resting condition, we will reduce between-subject and diurnal variability (112); and 2) we directly assess ANS performance and cardiac physiological reserve in response to a controlled stressor (physical task), to establish a stress-response model that can be further used for assessing interconnection measures.

As the last component, within the current study, we investigated the interconnection between physiological systems in response to stress caused by the physical task. The concept of stress-response

testing for quantifying frailty has become the subject of recent research. Evidence suggests that differences in physiological reserve between non-frails and frails are subtle under the basal condition (157). Implementing provocative testing accentuates frailty-related alterations in measurable dynamics of physiological systems in response to stimuli. The provocative UEF test is designed to be hard enough to stress motor and cardiac systems, and not too demanding, so they can be incorporated in a routine clinical setting for frail older adults, especially those with walking disabilities. Simultaneous assessment of motor and heart function in this manner allows us to accurately quantify the dysregulation of interconnection between these systems. Further, the motion artifacts are minimum with the proposed testing, with HR measurement acquiring from the left side while the participant perform the physical task on the right side.

### 3.4.3. Limitations and further work

Despite the promising findings of the current study, there are some limitations related to the recruited sample. First, the sample of community dwelling older adult selected for this study was small. Second, there was a limited number of frail participants, and therefore, pre-frail and frail groups were merged. Third, participants with arrhythmia and those who require  $\beta$ -blockers and pacemakers were excluded from the study. Also, test-retest reliability of CCM parameters were not investigated here. Therefore, the interconnection analysis should be confirmed in larger studies incorporating test-retest reliability measures. Additionally, we used time-series library lengths that may not provide accurate results for some participants, since some HR data may have a higher level of short-term complexity, leading to less dense attractor shadow manifolds and consequently a non-completely developed convergence of CCM parameters. Possible solutions would be to perform longer arm tests; however, this will lead to more physical demand on frail older adults.

### 3.4.4. Conclusions and clinical implications

In the present work a novel quantification of interconnection between motor and cardiac autonomic systems was implemented for frailty assessment. We demonstrated that CCM parameters showed weaker interconnection between motor and cardiac systems among pre-frail/frail older adults compared to non-frails. The new CCM parameters also showed promising results in improving frailty prediction within

logistic models. The simplicity of the investigated UEF test permits performing it even for hospitalized bed-bound patients, for predicting therapy complications, in-hospital outcomes, and rehabilitation strategies. We expect to present this multimodal test as an alternative to accurate but impractical frailty assessment tools such the Fried phenotype, when patients are not able to walk. Further, commercialized wearable devices are now allow accurate assessment of HR and motion. Showing the proof of concept in the current study, in our future investigation, we will develop an easy-to-use app for Smart Watch for identifying frailty using simultaneous measures of motor and cardiac functions.

### 3.5. Acknowledgements

This project was supported by two awards from the National Institute of Aging (NIA/NIH - Phase 2B Arizona Frailty and Falls Cohort 2R42AG032748-04 and NIA/NIH - 1R21AG059202-01A1). The views represented in this work are solely the responsibility of the authors and do not represent the views of NIH. We want to thank Ben Carpenter and Kayleigh Ruberto for their contribution to data collection and analysis.

## 4. FRAILTY ASSESSMENT IN AORTIC STENOSIS BASED ON DYNAMIC INTERCONNECTION BETWEEN CARDIAC AND MOTOR SYSTEMS

### 4.1. Introduction

Frailty is a geriatric syndrome associated with loss of physiological reservoir and, in consequence, augmented risk of hospitalization, negative therapy outcomes, disability and mortality (35). Muscle loss and weakness (sarcopenia and dynapenia) are the main symptoms of frailty (101), caused by inflammatory (elevated interleukin 6 (IL-6), C-reactive protein (CRP), and tumor necrosis factor alpha (TNF $\alpha$ )), metabolic (deficiencies of various mitochondrial subunits), and hormonal derangements (cortisol and testosterone) that shift homeostasis from an anabolic to a catabolic state (102–108). Notably, similar muscle dysfunction has been observed in cardiac frailty with the same inflammatory, metabolic, and hormonal contributors, further exacerbated by lack of cardiovascular reserve and a compromised autonomic nervous system (158–163). All these factors can move frail individuals with heart diseases to a more imbalance (less homeostatic) and already stressed state, causing an inability to respond to additional stress, such as therapy burden. Consequently, assessing frailty would be useful for cardiologists as an associated risk score, improving selection of candidates for invasive therapies, by identifying individuals with progressed frailty that may develop therapy complications, as well as those that can reverse their frailty.

Heart diseases are frequent and mortal with nearly 523 million cases worldwide (50). Remarkably, aortic stenosis (AS) is the most common acquired valvar disease, shows a high frailty prevalence of 9.4 million patients in 2019, and more than 1% in older adults beyond 75 years old (50). Although much progress has been made in treatment of patients with AS, morbidity, mortality, and the economic burden remain unacceptably high (51–53). For instance, average aggregate 6-month inpatient costs are above \$60,000 and mortality is as high as 50% for severe AS, with a predicted doubling AS cases in the next 50 years (164). Like other types of heart disease, AS is a disease of aging and associated with risk for frailty, and is becoming more frequent as the population average age increases (54–57). Frailty assessment is, however, not common in cardiology, especially for AS patients, because current assessment tools are impractical to implement in busy clinical environments (58). While frailty assessments such as Fried frailty phenotype or

Rockwood deficit index show promising results in predicting AS therapy outcomes, they are arduous, fully or partially subjective, require trained clinical staff to perform, or require walking for physical assessment (59,60). More importantly, no disease-specific tool is available to identify heart disease-related frailty that can be implemented for AS patients.

We have previously developed a methodology for assessing frailty that incorporates an upper-extremity function (UEF), the corresponding heart rate (HR) response, and the cardiac-motor interconnection (165). The UEF test consists of repetitive and rapid elbow flexion and extension (111), during which several kinematics features representing dynapenia are measured using motion sensors (35). Since UEF involves upper-extremity motion, it is feasible to perform for bedbound patients and when walking tests are difficult for frail older adults. In addition, we showed that HR dynamics, direct measure of sympathetic (HR behavior during activity) and parasympathetic (HR behavior during recovery) health, were significantly associated with frailty (112). Finally, we validated the cardiac-motor interconnection parameters, generated using convergent cross-mapping between motor function and HR dynamics, as independent predictors for frailty (165). Combining UEF motor, cardiac functions, and their interconnection, we were able to establish a multimodal frailty assessment tool with higher accuracy compared to models including each of the motor or HR dynamics parameters separately (113).

The goal of the current study was to first investigate frailty symptoms in AS patients (motor and cardiac performance) in comparison with non-AS older adults, and second, determine outcome predictive of frailty status regardless of heart disease condition. Our first hypothesis was that both frailty and AS condition would influence motor and HR dynamics parameters in similar ways. Based on our previous research, our second hypothesis was that due to frailty, a weaker interconnection would exist between motor and HR performance that independent of AS condition would be associated with frailty status. Current findings will pave the way to develop a heart disease-specific tool for identifying frailty.

## 4.2. Methods

### 4.2.1. Participants

Two groups of older adult participants were recruited. Non-aortic stenosis (NAS) older adults ( $\geq 55$  years) were enrolled between October 2016 and March 2018 from primary, secondary, and tertiary health care settings such as primary and community care providers, assisted living facilities, retirement homes, and aging service organizations. Also, advanced AS-diagnosed older adults ( $\geq 55$  years) were recruited from the Banner University Cardiovascular program – Advanced Heart Failure and TAVR clinics between September 2021 and October 2022.

The inclusion criteria for the NAS group were: 1) being 55 years or older; 2) the ability to walk a minimum distance of 4.57 m (15 ft) for frailty assessment; and 3) the ability to read and sign an informed consent. For the AS group, an additional inclusion criterion was being diagnosed for aortic stenosis. The exclusion criteria for both groups were: 1) severe motor disorders (Parkinson's disease, multiple sclerosis, or recent stroke); 2) severe upper-extremity disorders (e.g., bilateral elbow fractures or rheumatoid arthritis); 3) cognitive impairment identified by a Mini Mental State Examination (MMSE) score  $\leq 23$  (123); 4) terminal illness; 5) diseases/treatments that could bias the HR measurements (including arrhythmia and use of pacemaker); and 6) usage of  $\beta$ -blockers or similar medications that can influence HR. Written informed consent was obtained from all participants. The study was approved by the University of Arizona Institutional Review Board. All research was performed in accordance with the relevant guidelines and regulations, according to the principles expressed in the Declaration of Helsinki (124).

### 4.2.2. Frailty assessment and clinical measures

Frailty assessment was executed using the five-component Fried phenotype (35), which involves the following five criteria: 1) unintentional weight loss of 4.54 kg (10 pounds) or more in the previous year; 2) grip strength weakness (adjusted with body mass index (BMI) and sex); 3) slowness based on the required time to walk 4.57 m (15 ft) (adjusted with height and sex); 4) self-reported exhaustion based on a short two-question version of Center for Epidemiological Studies Depression (CES-D); and 5) self-reported low energy expenditure based on a short version of Minnesota Leisure Time Activity Questionnaire (125).

Participants were categorized into three frailty groups, which were non-frail if they met none of the criteria, pre-frail if they met one or two criteria, and frail if they met three or more criteria. Collected clinical measures included: 1) MMSE and Montreal Cognitive Assessment (MoCA) for cognition (123,126); 2) comorbidity based on Charlson Comorbidity Score (CCI) (127); 3) depression using Patient Health Questionnaire (PHQ-9) (128); and for AS patients 4) The Kansas City Cardiomyopathy Questionnaire (KCCQ) to measure the quality of life (QoL) (166). Clinical measures with significant association with frailty were considered for both groups as adjusting variables in the statistical analysis because they could potentially influence physical activity and the cardiovascular system performance.

#### 4.2.3. Upper extremity function (UEF) motor test

After completing questionnaires, participants were asked to sit on a chair and rest for two minutes to regain normal resting status. Participants then performed the UEF task of elbow flexion-extension as quickly as possible for 20 seconds with the right arm. In a separate study, we showed that UEF results are similar on both left and right hands (129). After the UEF task, participants rested on the chair for another two minutes. Before the test, participants practiced the UEF test with their non-dominant arm to become familiar with the protocol. The protocol was explained to participants and using the exact same verbal instruction they were encouraged only once, before elbow flexion, to do the task as fast as possible. Wearable motion sensors (triaxial gyroscope sensors, BioSensics LLC, Cambridge, MA, sampling frequency=100 Hz; Figure 4.1A) were used to measure forearm and upper arm motion, and ultimately the elbow angular velocity. Angular velocity data from gyroscopes were filtered using a first-order high pass Butterworth filter with a cutoff of 2.5 Hz. Maximums and minimums of the angular velocity signal were detected, and subsequently, elbow flexion cycles were identified. Motor performance was assessed to represent: 1) slowness based on speed of elbow flexion; 2) flexibility based on range of motion, 3) weakness based on strength of upper-extremity muscles; 4) speed variability and motor accuracy; 5) fatigue based on reduction in speed during the 20-second task, and 6) number of flexion cycles. A sub-score was assigned for each of those features, determined previously based on multivariable ordinal logistic models, with the Fried frailty categories as the dependent variable and UEF parameters plus demographic information as independent variables (112). The normalized UEF motor score from zero (resiliency) to one (extreme frailty) was computed as the sum of sub-scores corresponding to performance

results and demographic information (i.e., BMI) (111). More details about UEF validation, repeatability, and the normalized score are explained in previous research (111,129,130).

#### 4.2.4. Heart rate (HR) outcomes

HR was recorded using a wearable ECG device with two electrodes and one built-in accelerometer (360° eMotion Faros, Mega Electronics, Kuopio, Finland; ECG sampling frequency=1000 Hz and accelerometer sampling frequency=100 Hz; Figure 4.1A). One ECG electrode was placed on the upper mid-thorax and the other one inferior to the left rib cage. The placement of the electrodes on the left chest would minimize the movement artifacts due to UEF test with the right arm. ECG data was analyzed for 20 seconds of baseline, 20-second UEF, and 30 seconds of recovery. RR intervals (successive R peaks of the QRS signal) were computed using the Pan-Tompkins algorithm (131). The automated peak detection process was manually inspected by two researchers (PA and NT). Two types of HR parameters were extracted, one representing baseline HR and HR variability (HRV), and one representing HR dynamics (changes in HR during UEF and HR recovery after the task) (44,112,167). HR dynamics included time to reach maximum peak and recovery HR, as well as percent increase and decrease in HR during activity and recovery periods, respectively. In addition, HR distribution per groups were represented using linear interpolation to provide equidistant HR time series across samples.

#### 4.2.5. Convergent cross mapping (CCM) analysis

We quantified the directional nonlinear interconnections between HR and motor data using CCM. An overview of CCM is summarized in Figure 4.1. This method uses a historical trace of HR for predicting motor performance (or inversely, a historical trace of motor performance for predicting HR). Firstly, we created evenly sampled data of synchronized HR and motor function with a sampling frequency of 10Hz, using spline interpolation (Figure 4.1B). Each HR data point represents average HR values over 0.1 seconds. Corresponding motor data represent the angular displacement travelled during each 0.1 second of UEF. For calculating motor performance, motor function  $M_f$  was defined by:

$$M_{f_i} = \int_{t_i}^{t_i+0.1} \omega_e dt, \quad (1)$$

where  $\omega_e$  represents the rectified angular velocity of the elbow.

Takens's embedding theorem was used here, which guarantees that the information of a chaotic dynamic system could be represented from a single-observed time series  $X$  as an  $E$ -dimensional manifold (132). The shadow manifold  $M_X$  consists of an  $E$ -dimensional data with lagged coordinates ( $\tau$ ) of the variable:

$$M_X = \langle X(t), X(t - \tau), X(t - 2\tau) \dots X(t - (E - 1)\tau) \rangle. \quad (2)$$

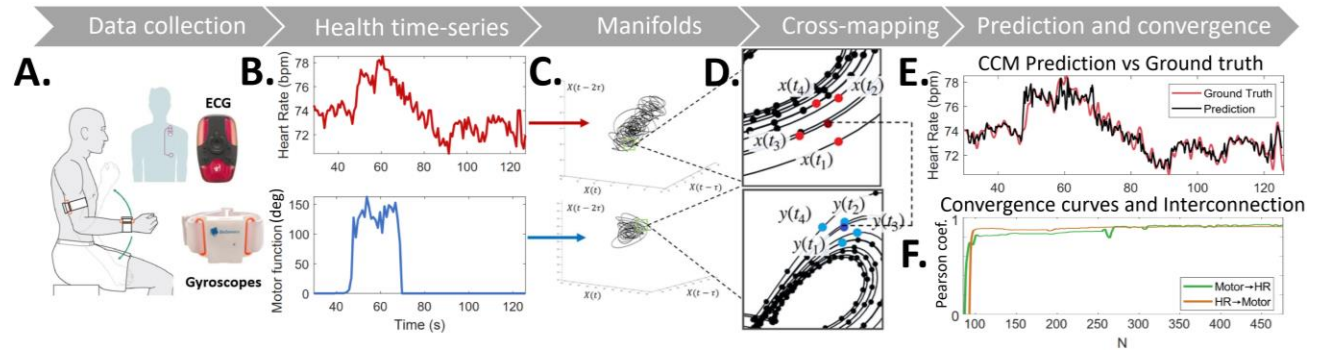


**Figure 4.1:** Overview of the CCM method to assess interconnection between motor and HR data: **A.** wearable devices (gyroscopes) to obtain angular velocity and ECG during the UEF physical task; **B.** motor performance and HR extraction; **C.** CCM shadow attractor manifolds on time-lagged coordinate systems; **D.** prediction of HR from motor function and vice-versa in a time point (dark red and dark blue dots, respectively) using a distance-based weighted average of neighbors (bright red and bright blue dots); **E.** comparison between predicted HR data and ground truth, also applicable to motor function; and **F.** convergence curves of Pearson correlation coefficient between predicted and ground truth as a function of library length (data points used for developing manifolds).

We built  $E$ -dimensional manifolds from each of these two time series (132) (Figure 4.1C). Dimension ( $E$ ) of four was selected based on the average false nearest neighbor approach (133). A time lag ( $\tau$ ) of one

second was used for analysis based on the delayed mutual information method (134). We predicted one time series (e.g., HR) by historical records of the other signal (e.g., shadow manifold of motor function) using a k-nearest neighbor technique. For a dimension  $E$ , we determined  $E + 1$  nearest neighbors and identified indices of each data points in manifolds ( $M_X$ ). Using these indices for one manifold (e.g., HR  $X(t)$ ), we found corresponding neighbors in the second manifold (e.g., motor function data  $Y(t)$ ) (Figure 4.1D), and then predicted  $X(t)$  to  $\hat{Y}(t)$  as the weighted mean of  $E + 1$  points in the second manifold (135):

$$\hat{Y}(t) = \sum_{i=1}^{E+1} w_i Y(t_i), \quad (3)$$

where  $w_i$  weights are calculated based on the Euclidean distances between  $M_Y$  and its  $i^{th}$  nearest neighbor on  $X(t)$ . The Pearson correlation coefficient between the predicted and original time series was calculated to assess the strength of interconnections between motor and HR data (Figure 4.1E). As documented in previous studies, the correlation coefficient is expected to increase with increasing the time-series length (i.e., library length, Figure 4.1F). We selected as the so-called CCM parameters to the correlation values at the maximum library length.

#### 4.2.6. Statistical analysis

We used Analysis of variance (ANOVA) models to determine the differences in demographic information between frailty groups, except for sex. Instead, the chi-square ( $\chi^2$ ) test was used to assess the difference in sex categories between frailty groups. UEF, HR dynamics, and CCM parameters were compared between frailty groups and NAS/AS conditions using multivariable ANOVA models; age, sex, and BMI were considered as adjusting variables since they have been previously associated with motor and cardiac performance and frailty (111,136–138). Cohen's effect size ( $d$ ) was estimated. ANOVA analyses for comparing motor, cardiac, and CCM parameters across frailty groups and NAS/AS conditions were repeated with clinical measures with significant association with frailty as covariates. The statistical analysis was performed using JMP® Pro 16.1.

## 4.3. Results

### 4.3.1. Participants and clinical measures

Fifty-six non-aortic stenosis (NAS) older participants were recruited for the study, including 12 non-frail (age=76.92±7.32 years), 40 pre-frail (age=80.53±8.12 years), and four frail individuals (age=88.25±4.43 years). On the other hand, 30 aortic stenosis (AS) participants were enrolled, including 10 non-frail (age=69.00±3.61 years), 17 pre-frail (age=72.71±2.77 years), and 3 frail individuals (age=75.67±6.60 years). Of note, due to the small number of frail participants (n=7), frail and pre-frail groups were merged for the statistical analysis. A summary of demographics is presented in Table 4.1. There were significant differences in age and height between AS and NAS groups, and therefore all statistical analyses were adjusted for these two variables.

### 4.3.2. Effect of frailty

There are no significant differences in frail population between AS and NAS groups. Significant effects of frailty on UEF motor score, resting HR baseline, HR percentage increase and decrease, and CCM values were observed across the participants, as reported in Table 2 and Figures 4.2.A, 4.2.C, 4.2.E, 4.2.G, 4.2.I and 4.3.A. Pre-frail/frail older adults showed higher UEF motor score, higher baseline HR (in rest), lower changes in HR due by physical task and smaller correlations in CCM for both directions, compared to non-frail older adults ( $p<0.05$ , Figure 4.4.A).

### 4.3.3. Effect of AS condition

Significant effect of AS condition (AS vs. NAS) on UEF motor score and HR percentage increase and decrease were observed ( $p<0.01$ , Figures 4.2.B, 4.2.D and 4.2.F), as well as time to peak and HR recovery time ( $p<0.0001$ , Figures 4.2.L and 4.2.N), as reported in Table 4.2. AS individuals showed worse UEF motor score and larger (in percentage) but slower HR changes due to the physical task. In contrast to UEF motor score and HR dynamics results, which showed significant differences between both frailty groups and the

AS condition, CCM parameters were only significantly different across frailty groups ( $p=0.04$  and  $<0.01$ , Figure 4.2.G and 4.2.I), and not the AS condition ( $p>0.62$ , Figure 4.2.H and 4.2.J, and Table 4.2).

**Table 4.1.** Demographic information and clinical measures of participants.

Variables	Non-frail (n=22)	Pre-frail/Frail (n=64)	p-value (effect size)	Non-aortic stenosis (n=55)	Aortic stenosis (n=31)	P-value (effect size)
Female, n (% of the group)	12 (54.55)	42 (65.63)	-	40 (72.73)	14 (27.27)	-
Age, year (SD)	73.31 (9.17)	78.70 (10.12)	0.06 (0.48)	80.09 (8.02)	72.42 (11.63)	0.001* (0.77)
Height, cm (SD)	166.31 (11.17)	166.21 (10.25)	0.81 (0.06)	164.24 (10.05)	169.77 (10.29)	0.017* (0.55)
Weight, kg (SD)	72.30 (16.85)	77.02 (20.95)	0.26 (0.28)	73.59 (19.04)	79.75 (21.34)	0.14 (0.34)
Body mass index, kg/m <sup>2</sup> (SD)	26.12 (5.63)	27.59 (5.85)	0.29 (0.27)	27.08 (5.82)	27.46 (5.83)	0.68 (0.09)
CCI score, 0-29 (SD)	4.45 (1.84)	5.80 (2.39)	0.008* (0.68)	5.09 (2.12)	6.10 (2.56)	0.022* (0.53)
<b>Fried criteria, n (% of the group)</b>						
Non-frail subjects	-	-	-	12 (22%)	10 (32%)	0.29 (-)
Weight loss	0	3 (5%)	-	1 (2%)	2 (6%)	-
Weakness	0	27 (42%)	-	17 (31%)	10 (32%)	-
Slowness	0	41 (%)	-	34 (62%)	7 (23%)	-
Exhaustion	0	18 (%)	-	7 (13%)	11 (35%)	-
Low energy	0	13 (%)	-	8 (15%)	5 (16%)	-

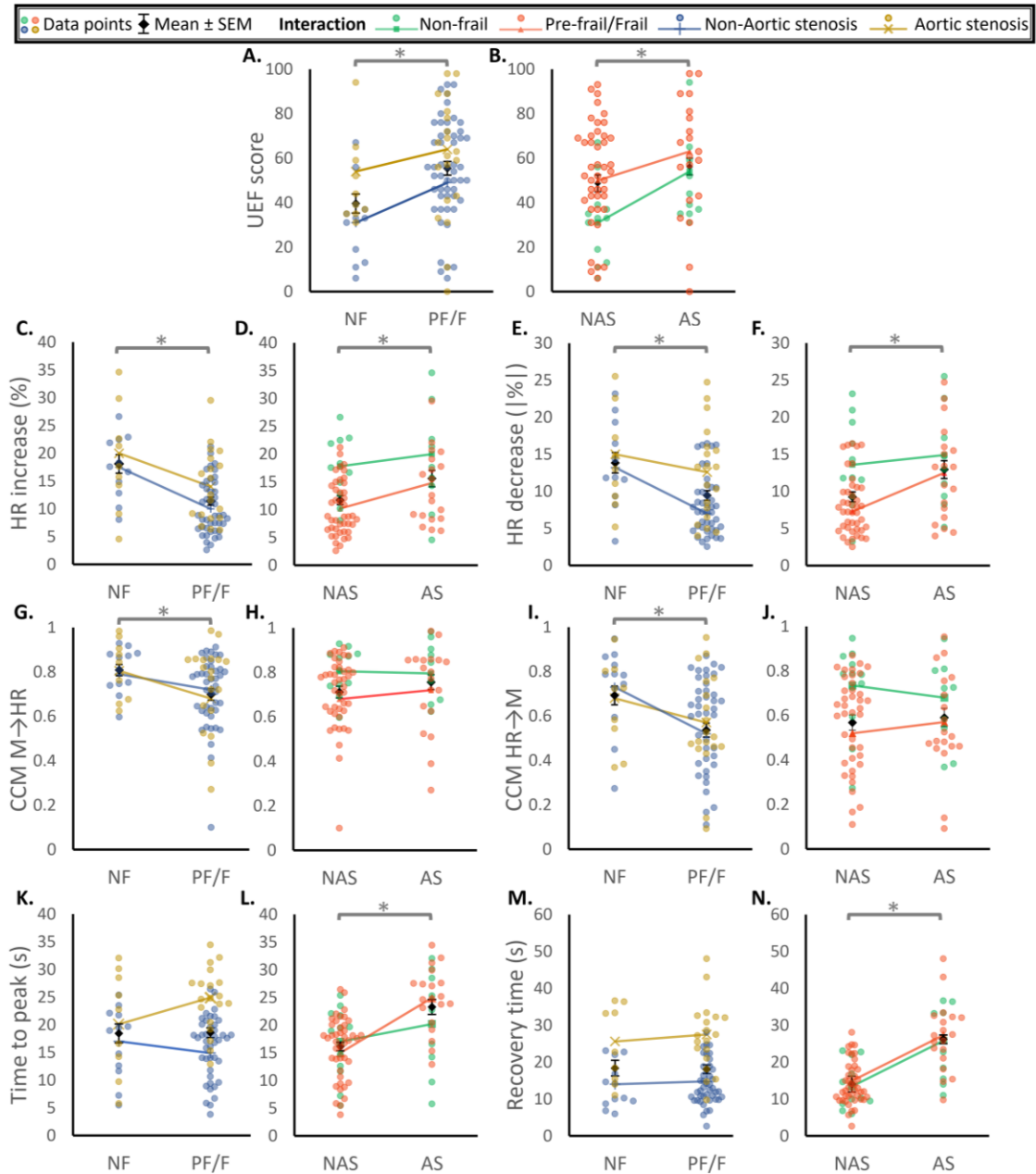


**Figure 4.2.** UEF score (A. and B.), HR percentage changes (C. to F.), CCM parameters (G. to J.), time to HR peak from rest (K. and L.) and time to recover HR baseline (M. and N.) for frailty and aortic stenosis categories. Each data point corresponds to an individual. Interaction profiles are incorporated to show the cross-effects between different subgroups. A significant between group difference is identified by the asterisk ( $p < 0.05$ ).

**Table 4.2.** Differences in UEF, HR dynamics, and CCM features across frailty groups. A significant association is represented by the asterisk.

Parameters	Non-frail (n=22)	Pre-frail/Frail (n=63)	P-value (Effect size)	Non-aortic stenosis (n=55)	Aortic stenosis (n=30)	P-value (Effect size)
<b>UEF motor score</b>						
UEF motor score, 0-100 (SD)	39.59 (20.20)	55.46 (24.12)	0.01* (0.66)	48.69 (23.43)	56.23 (24.92)	<0.01* (0.70)
<b>HR dynamics parameters</b>						
HR rest mean, bpm (SD)	68.21 (10.46)	76.31 (15.99)	0.01* (0.66)	76.20 (15.34)	70.45 (14.27)	0.24 (0.30)
Time to peak HR, seconds (SD)	18.43 (7.86)	18.57 (6.85)	0.71 (0.10)	16.12 (5.69)	23.28 (7.19)	<0.0001* (1.28)
Recovery time, seconds (SD)	18.36 (9.71)	18.07 (9.19)	0.53 (0.17)	14.04 (5.83)	26.20 (9.54)	<0.0001* (1.73)
HR percent increase, % (SD)	18.10 (7.47)	11.40 (5.63)	0.0001* (1.10)	11.71 (5.78)	15.59 (7.75)	0.01* (0.62)
HR percent decrease, % (SD)	-13.85 (6.12)	-9.45 (5.17)	<0.01* (0.77)	-9.26 (4.95)	-12.96 (6.35)	0.01* (0.67)
HR absolute increase, bpm (SD)	12.65 (4.05)	10.42 (8.06)	0.44 (0.21)	11.11 (7.44)	10.70 (7.24)	0.66 (0.11)
HR absolute decrease, bpm (SD)	-10.64 (4.88)	-7.79 (4.34)	0.056 (0.53)	-7.67 (4.03)	-10.04 (5.31)	0.06 (0.49)
<b>CCM parameters</b>						
Correlation Motor→HR (SD)	0.81 (0.11)	0.70 (0.20)	0.04* (0.55)	0.71 (0.19)	0.76 (0.18)	0.62 (0.13)
Correlation HR→Motor (SD)	0.69 (0.19)	0.54 (0.25)	<0.01* (0.72)	0.57 (0.26)	0.59 (0.22)	0.72 (0.09)

*UEF: upper extremity function; SD: standard deviation; HR: heart rate; bpm: beats per minute; CCM: convergent cross-mapping.*

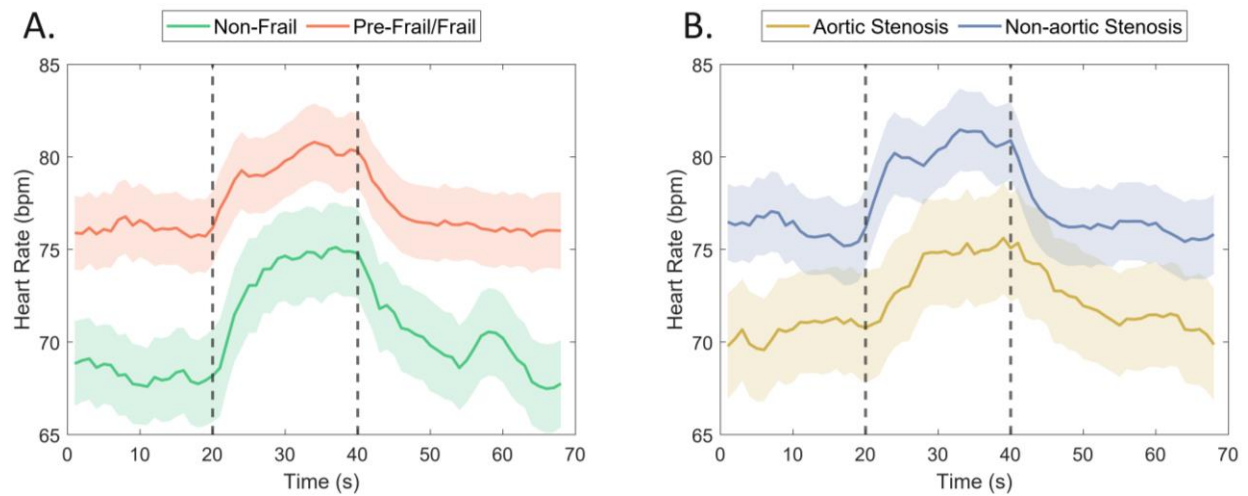


**Figure 4.3.** Heart rate distributions for frailty (A) and aortic stenosis (B) groups. Means and standard error are represented by solid lines and shaded regions, respectively. Physical task 20-seconds arm test starting and ending points are indicated with vertical lines. Linear interpolation was used to provide equidistant HR time series across samples.

## 4.4. Discussion

### 4.4.1. Effect of frailty on HR dynamics and motor performance

In confirmation of previous work (44), there were significant associations between frailty level and HR changes during physical activity and the consecutive recovery period. During activity there is an increase in sympathetic outflow, and consequently an increase in HR and stroke volume to satisfy circulatory requirements (168). Afterwards in the recovery period, the parasympathetic activity is enhanced to reduce HR to the baseline level (169–171). An impaired ANS performance is represented by an absence of resilience in changing HR, and previous studies have shown the effect of frailty on ANS outflow, such as the study by Weiss et. al, which HR was monitored during a seated step test (172), or the one by Romero-Ortuno et. al, which monitored HR during and after 3 minutes of a lying to standing orthostatic test (173). In confirmation of these findings, we observed significant lower HR changes on pre-frail/frail population in comparison to non-frail individuals (Figure 4.2.C and 2.E, Table 4.2). Our findings suggest, unlike the

amount of change, the timing of HR changes (i.e., HR rest-to-peak and recovery times) was not associated with frailty ( $p > 0.53$  and  $0.71$ , respectively, for HR increase and recovery times).

Motor performance is impacted by frailty through sarcopenia and dynapenia (diminished muscle mass and performance), leading to poorer physical activity (35). Dynapenia is typically quantified by walking speed or grip strength tests. Nevertheless, performing walking tests in clinical settings is challenging, and many frail older adults, especially those with AS may have walking disabilities. Grip strength, on the other hand, only measures muscle strength and cannot reveal other aspects of motor deficits, such as flexibility. We have previously validated the sensor based UEF motor task to detect with an accuracy of 0.7 (111) systematic decrements in motor function associated with frailty, including slowness, weakness, inflexibility, fatigue, and motor variability (130,150). Here, we found significant increases in the UEF motor score for pre-frail/frail participants compared to non-frails (Figure 4.2.A, Table 4.2), confirming previous findings. In addition, we observed that frail participants with additional burden of AS showed even higher UEF motor score than AS non-frail or NAS frail subjects, revealing the accentuated deficits in motor function due to doubling effects of heart disease and frailty. These findings demonstrate the importance of frailty assessment in AS patients who have less physiological reservoirs and an impaired ANS performance, and consequently higher risk of poorer outcomes after invasive therapies such as open-chest surgeries.

#### 4.4.2. Effect of AS on HR dynamics and motor performance

According to literature, AS impacts cardiac and motor performances. Historically, HR variability (HRV) has been used for assessing ANS dysfunction and proposed as a vital sign (174). However, a low correlation has been found between several time and frequency-domain HRV parameters and AS severity (175). In the current work we have found several HR dynamics parameters that could potentially be used for assessing cardiac autonomic dysfunction due to aortic stenosis, such as significantly higher HR changes during and post non-demanding physical tasks, together with a significant slower HR response to the physical task. A previous study in which HR was monitored before and after one minute of supine bicycle exercise showed that HR increase on AS patients were slightly greater than NAS (176). Here, we observed that monitoring HR in real time gives similar trends. Consistent with other reports (177,178), myocardial

work, which is a measure of oxygen demand defined by the product between the myocardial wall stress and wall stress rate, was also greater in AS than controls, pointing to a relative supply/demand imbalance, which would make these patients more vulnerable to myocardial ischemia (176). In our study we found that AS subjects had significantly higher changes in HR, during both physical activity and rest than NAS participants (Table 4.2, Figure 4.2.D and 4.2.F). We attributed the higher HR change by exercise among AS to the ANS response to a higher myocardial oxygen need, a consequence of myocardial hypertrophy AS-associated (179). This fact is supported by other studies which the rapid rise of HR in AS patients is a compensatory mechanism to maintain cardiac output (180). The aforementioned myocardial ischemia risk and the impaired perfusion to myocytes usually lead to AS patients gradually decrease their physical activity to accommodate their condition (181). This fact is supported by our results since the motor performance in AS individuals was significantly worse than NAS participants, showing higher UEF scoring (Table 4.2, Figure 4.2.B) and consequently an increased muscular frailty such as weakness, slowness, exhaustion, and flexibility (111). Noteworthy, we observed significant differences in HR percentage changes, but is not the case for the absolute changes. We attributed this fact to the influence on the differences between AS and NAS in HR magnitude distributions observed on Figure 4.3.B, so HR percentage changes cover both changes in HR and HR magnitudes, making them significant parameters to the subjects AS status.

#### 4.4.3. CCM parameters for identifying frailty

We previously proved that CCM was an independent predictor for frailty on a community dwelling population, finding a significantly weaker interconnection between motor and cardiac systems for pre-frail and frail participants compared to non-frails (165). We attributed those results to aging-related physiological dysregulation in the motor cortex - reflexes feedback system (139–145), and loss of homeostasis and heightened inflammatory state (102,104–106,108,146). In the current study, CCM parameters showed significant differences across frailty groups for the combined sample of AS and NAS (Figure 4.2.G and 4.2.I, Table 4.2), while similar magnitudes were calculated for NAS vs AS samples for CCM  $M \rightarrow HR$  ( $p=0.62$ ) and CCM  $HR \rightarrow M$  ( $p=0.72$ ). These results indicate that CCM parameters are mostly not affected by the AS condition, as indicated in Figure 4.2.G and Figure 4.2.I. This observation support the importance of extracting parameters associated with physiological networks for a proper and accurate

frailty assessment, regardless of comorbid condition (45–47). CCM parameters are promising parameters in order to develop an accurate tool for AS-related frailty assessment.

#### 4.4.4. Limitations and further work

Despite the promising findings of the current study, there are some limitations related to the recruited sample. First, there was a limited number of frail participants, and therefore, pre-frail and frail groups were merged. Second, if there are no significant differences in frail population between AS and NAS groups (Table 4.1,  $p=0.29$ ), equally distributed frail subjects on AS and NAS groups should validate our results. Third, we found that age and height was significant different between our AS and NAS populations, however we adjusted age, sex, and BMI for all our statistical analysis. Nevertheless, current findings should be further validated in age matched AS and NAS samples. Fourth, participants with arrhythmia and those who require  $\beta$ -blockers and pacemakers were excluded from the study. Also, test-retest reliability of CCM parameters were not investigated here. Therefore, the interconnection analysis should be confirmed in larger studies incorporating test-retest reliability measures. Additionally, we used time-series library lengths that may not provide accurate results for some participants, since some HR data may have a higher level of short-term complexity, leading to less dense attractor shadow manifolds and consequently a non-completely developed convergence of CCM parameters. Possible solutions would be to perform longer arm tests; however, this will lead to more physical demand on frail and those with aortic stenosis.

#### 4.4.5. Conclusions and clinical implications

In the present work a novel quantification of interconnection between motor and cardiac autonomic systems was implemented for frailty assessment. We demonstrated that CCM parameters showed weaker interconnection between motor and cardiac systems among pre-frail/frail older adults compared to non-frails, regardless of AS condition. The simplicity of the investigated UEF test permits performing it even for hospitalized bed-bound patients with heart disease, for predicting therapy complications, in-hospital outcomes, and rehabilitation strategies. We expect to develop a heart disease-specific tool for frailty assessment using the CCM parameters, contributing to early assessment and better therapy strategies for

AS patients. Further, commercialized wearable devices are now allow accurate assessment of HR and motion. Showing the proof of concept in the current study, in our future investigation, we will develop an easy-to-use app for Smart Watch for identifying frailty using simultaneous measures of motor and cardiac functions.

#### 4.5. Acknowledgements

This project was supported by three awards from the National Institute of Aging (NIA/NIH - Phase 2B Arizona Frailty and Falls Cohort 2R42AG032748-04, NIA/NIH - 1R21AG059202-01A1, and NIH/NIA - 1R01AG076774-01A1). The views represented in this work are solely the responsibility of the authors and do not represent the views of NIH. We want to thank Allison Klatt and Sarver Heart Center for data collection.

## 5. CONCLUDING REMARKS

The accelerated development of wearable technology and wearable health monitoring instruments has influenced the medical industry with promising devices that offer compactivity, comfort, user-friendliness, and accuracy. However, the data acquired by wearable sensors require a translation to medical terms, for diagnosis of certain diseases or syndromes. The current work was a an effort to contribute to the a “translation”, in which we built a data-driven emulator for feeding machine learning algorithms to improve brain injury prediction and characterize head impact kinematics, and an assessment tool based on the network physiology principle that states that accurate frailty assessment requires a collection of information across multiple physiological systems. Considering the interconnection between the cardiac and the motor autonomic systems, we developed a novel approach for frailty assessment that measures frailty regardless of comorbidities such as heart diseases. The research presented in this dissertation encompasses three major studies, summarized in the subsequent sections.

### 5.1. Low-rank representation of head impact kinematics: A data-driven emulator

Head impact kinematics are useful metrics for determining brain injury, but there is no large available data set for this purpose. We developed an approach for reducing the dimensionality of an initial dataset of head impact kinematics in sports using principal component analysis. We showed that our simplification was superior to other biphasic impulses, contrasting them in several injury metrics. In general, our approximation based on 15 modes was nearly indistinguishable from the ground truth data. Consequently, we developed a data-driven emulator capable of emulating head impact data sets with any given number of cases without needing access to the ground truth measurements. Noteworthy, we characterized the head impact kinematics by observing higher linear accelerations in the anterior-posterior direction, and higher angular accelerations in the sagittal direction, attributing this to the type and direction of loading in a specific sport (e.g. direction of tackling in football). Furthermore, we observed in the frequency domain analysis that there is a dominant low-frequency response from 10 to 40 Hz, expressing over 74% of the total angular velocity response for all directions. These findings ensure their utility for designing

better safety devices like helmets, as well as presenting a simplification of head impact kinematics useful for generating new kinematic data, which could be provided to train modern machine learning algorithms.

## 5.2. Associating frailty and dynamic dysregulation between motor and cardiac autonomic systems limitations

In this work, we demonstrated that the interconnection between cardiac and motor systems provides additional and relevant information for evaluating the frailty status of older adults. We found a significantly weaker interconnection in frail adults compared to non-frail individuals. Previously Toosizadeh et al. (44) developed a combined motor and cardiac multimodal test for frailty assessment. We tested an improved version of frailty assessment tool considering interconnection parameters, which increased the accuracy of the model from 0.87 to 0.91 AUC of the ROC curve for the same sample. Thus, the new CCM parameters showed promising results in improving frailty prediction and we expect to present this multimodal test as an alternative to accurate but impractical frailty assessment tools such as the Fried phenotype when patients are not able to walk.

## 5.3. Frailty assessment in aortic stenosis based on dynamic interconnection between cardiac and motor systems

We investigated the interconnection effects between aortic stenosis and frailty. We confirmed the results of previous work where significant associations were observed between frailty level and HR changes, as well as motor performance. Importantly, frail participants with the additional burden of AS showed even worse motor performance than AS non-frail or NAS frail participants, revealing the accentuated deficits in motor function due to the doubling effects of heart disease and frailty. These findings demonstrate the importance of frailty assessment in AS patients who have less physiological reservoirs and impaired ANS performance, and consequently higher risk of poorer outcomes after invasive therapies such as open-chest surgeries.

We found that AS impacted motor performance and HR. HRV has been used for assessing ANS dysfunction, and a low correlation has been found between several HRV parameters and AS. Using HR dynamics we

observed significant associations between AS and HR magnitudes and percentile changes, showing the potential of using wearable sensors to measure HR dynamics for AS diagnosis, and potentially other heart diseases. Motor performance was significantly impacted by AS presumably because myocardial ischemia risk and the impaired perfusion to myocytes that usually lead to AS patients gradually decreasing their physical activity to accommodate their condition.

Cardiac-motor interconnection was a parameter we extensively studied in this work. Similarly to the findings shown in chapter 3, we found significant differences in the interconnection between frailty groups, confirming its predictive power. Nevertheless, we explored the effects of AS on this parameter, finding nearly no differences between AS and NAS subjects ( $p>0.62$ ). These results indicate that CCM parameters are mostly not affected by the AS condition. This observation supports the importance of extracting parameters associated with physiological networks for a proper and accurate frailty assessment, regardless of comorbid conditions. Overall, CCM parameters are promising parameters to develop an accurate tool for heart disease-related frailty assessment.

## 5.4. Limitations

There are several limitations in this study, as mentioned in each chapter. For the data-driven emulator and characterization of head impacts in sports, certain sports like soccer or cycling would not be represented in our emulator, since the location and behavior of the impact usually are inherent to the sport, as well as other kinds of impacts like falls, or even TBI cases in which their causes are inertial changes instead of impacts. Further work considering ground truth kinematics of real head impacts and/or inertial changes would increase the representativity of the emulator. In addition, the core method used in that study, principal component analysis (PCA), assumes a linear relationship between features, and for some kinematics, we could lose information regarding non-linear interactions.

The novel proposed assessment tool for frailty, incorporating interconnection, has limitations too. We need to validate the assessment tool in an increased sample of older adults, which equally represent frailty groups, demographics, and comorbidity indexes. For both studies of chapters 3 and 4, participants with arrhythmia and those who require  $\beta$ -blockers and pacemakers were excluded from the study. Also, the test-retest reliability of CCM parameters was not investigated. Therefore, the interconnection analysis

should be confirmed in larger and more diverse comorbidity status studies, incorporating test-retest reliability measures. An interesting aspect to further study is the effect of other diseases on the physiological interconnection, in contrast to how frailty impacts it. Additionally, we used time-series library lengths that may not provide accurate results for some participants, since some HR data may have a higher level of short-term complexity, leading to less dense attractor shadow manifolds and consequently a non-completely developed convergence of CCM parameters. Possible solutions would be to perform longer arm tests; however, this will lead to more physical demand on frail older adults and those with comorbidities such as aortic stenosis.

## 5.5. Further directions

The development of the proposed data-driven emulator is a starting point for generating an effective and accurate brain injury prediction tool. As was mentioned before, this emulator will provide the required amount of kinematics data for training advanced deep learning techniques such as convolutional neural networks. Next steps towards an informative and precise brain dynamic behavior during impacts, in addition to brain damage quantification, is the development of a brain injury probability atlas which could show the regions of the brain most susceptible to injury in sports. In order to reach that objective, we will associate brain zones that reach strain thresholds obtained by finite element head models (feed by kinematic data), with damage within the brain. Damaged regions are defined from a population mapping of microhemorrhage obtained by segmentation of clinical MRI patient scans that have at least one traumatic axon injury (TAI) or diffuse axonal injury (DAI). If the association between TBI head impact kinematics and subsequent damage within the brain can be accurately captured, then predictive mapping could improve clinical diagnosis, prognosis, prevention, and treatment following TBI.

In the present work we showed that we can accurately assess frailty through a simple, fast, and accurate UEF test. Further work will be related to a longitudinal study for validating the multimodal frailty risk score and to establish cutoffs for predicting adverse outcomes and reversible frailty in a sample undergoing invasive therapy for aortic stenosis, such as ventricular assist device (VAD) or transcatheter aortic valve replacement (TAVR). We will define dichotomous clinical therapy outcome (favorable vs unfavorable) from the arm test taken before the therapy. An additional objective will be to identify reversible frailty, studying the differences in the test before and after the therapy. This following work paves the way for direct clinical

implications of the UEF test, helping in reducing the cost of therapy, and the expansion of this test in other fields and comorbid conditions.

## 5.6. Conclusions

While an increase in people suffering from one or more comorbidities is expected (given the increase in life expectancy), these persons will have a high motivation to stay in their familiar home environment and not in an institutional care facility. The combination of wearable sensor technology and assessment tools will open options for healthcare at home. Currently, commercial wearable devices meet the technical capabilities of measuring health time series such as kinematics or heart rate. We showed in this work that with real-time information, it is possible to detect injuries and to deduce frailty status and even morbidities. We are almost getting to the point in which easy-to-use apps for Fitbit or smartwatch devices, or maybe other wearables, will allow early diagnosis and consequently increase possibilities of early interventions not only in our golden ages but in our entire life.

## APPENDIX A – SUPPLEMENTARY MATERIALS (CHAPTER 2)

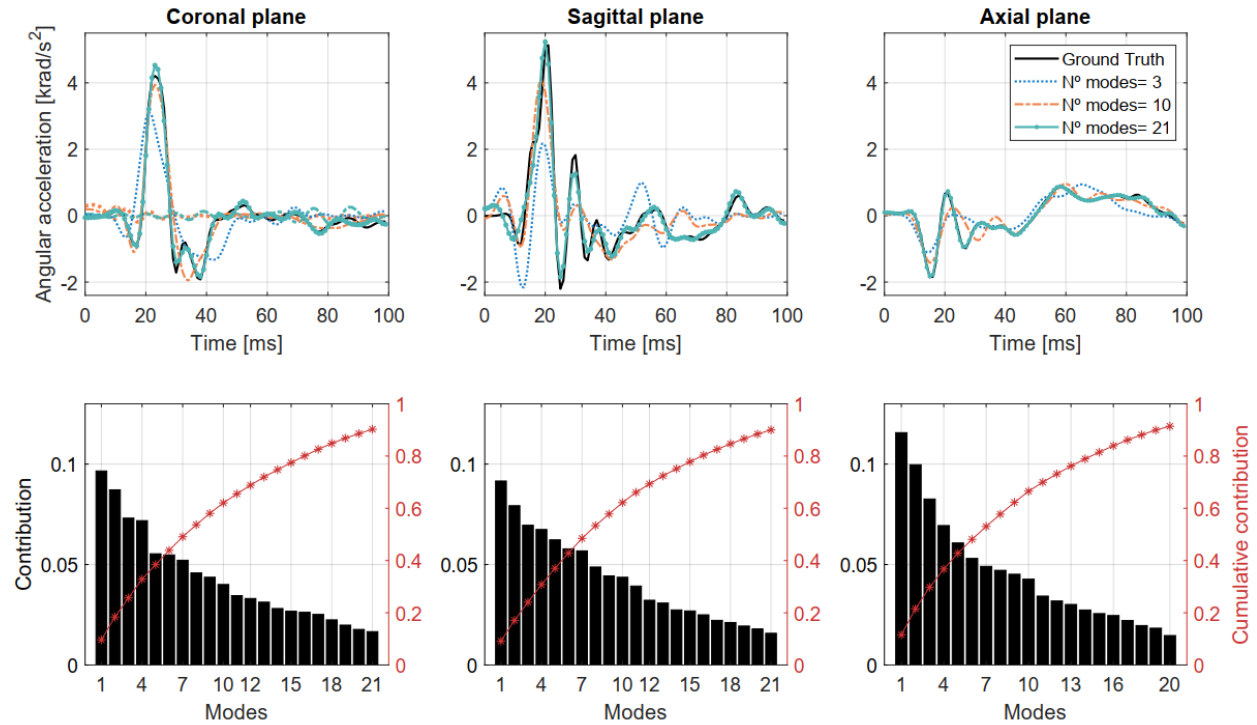


**Figure SM.1:** *Top:* Representative reconstruction of the linear acceleration data for a single head impact. *Bottom:* Individual and cumulative contribution of the temporal modes derived through PCA for angular velocity in each anatomical direction, constituting over 90% of the ground truth measurements.

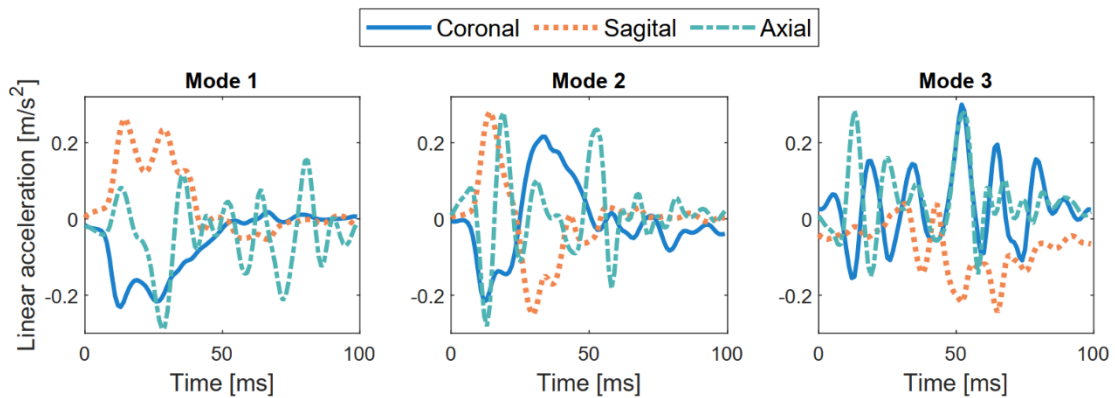


**Figure SM.2:** The three most relevant temporal modes for linear acceleration for the entire dataset.

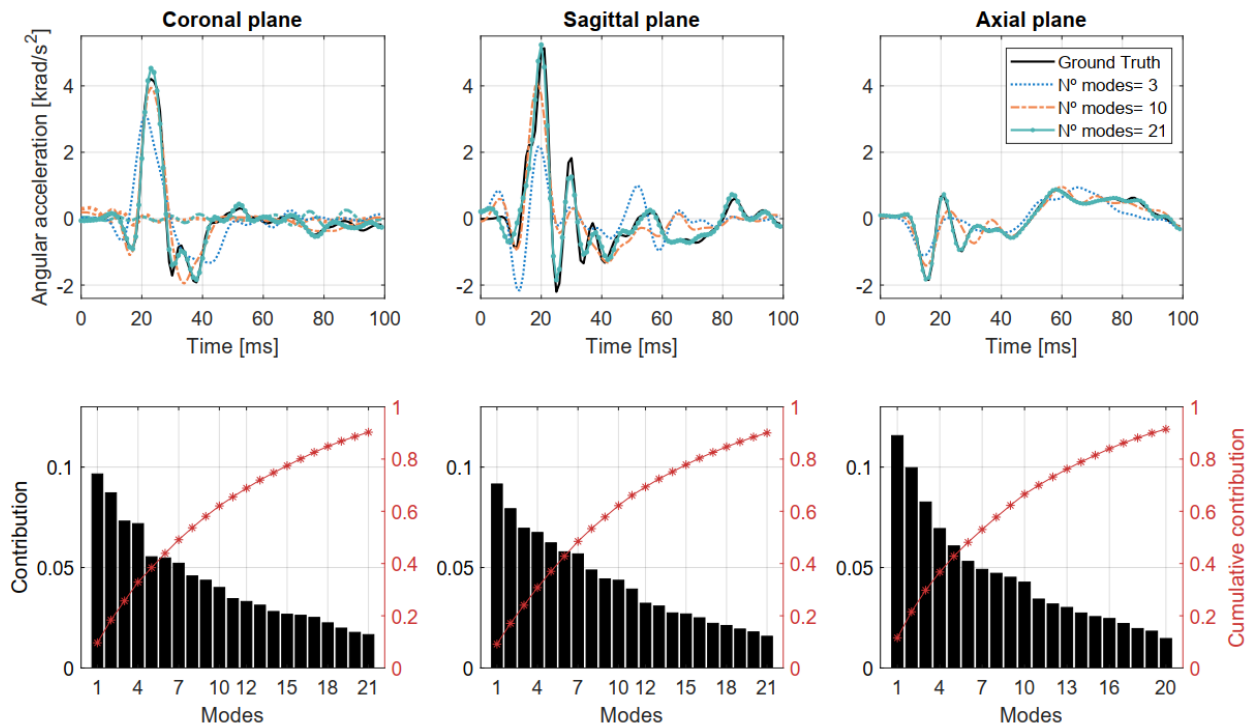


**Figure SM.3:** *Top:* Representative reconstruction of the angular acceleration data for a single head impact. *Bottom:* Individual and cumulative contribution of the temporal modes derived through PCA for angular velocity in each anatomical direction, constituting over 90% of the ground truth measurements.

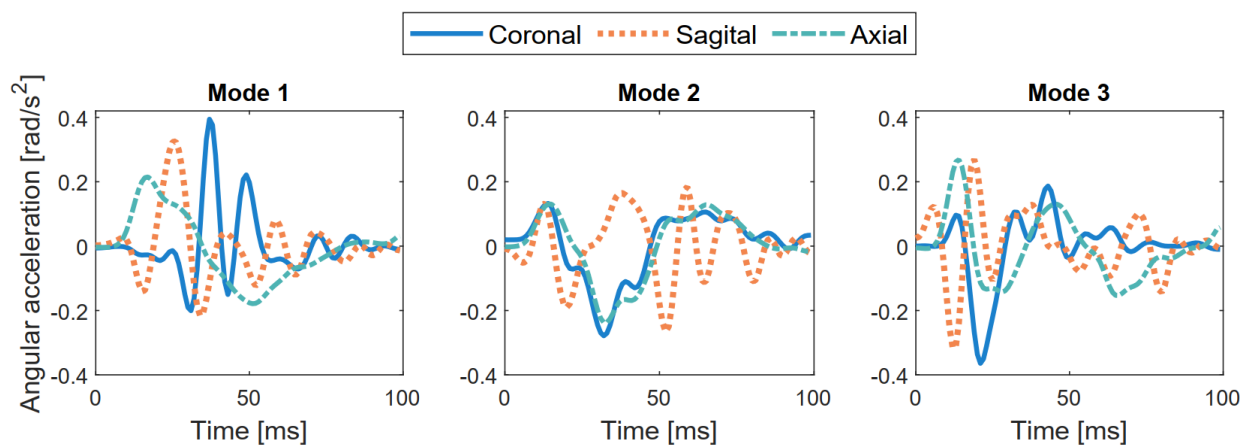


**Figure SM.4:** The three most relevant temporal modes for linear acceleration for the entire dataset.

**Table SM.1:** p- values for the significant differences with respect the ground truth for all the studied injury metrics.

Parameter	PCA	Tri.	H.S
$HIC_{15}$	0.7919	< 0.001	< 0.001
$RIC_{36}$	0.1478	< 0.001	< 0.001
$BrIC$	0.636	0.380	0.311
Coronal BAM	0.955	< 0.001	< 0.001
Sagittal BAM	0.917	0.007	0.001
Axial BAM	0.846	< 0.001	< 0.001
MPS WB	0.731	0.001	< 0.001
MPS CC	0.780	< 0.001	< 0.001
FS CC	0.807	< 0.001	< 0.001

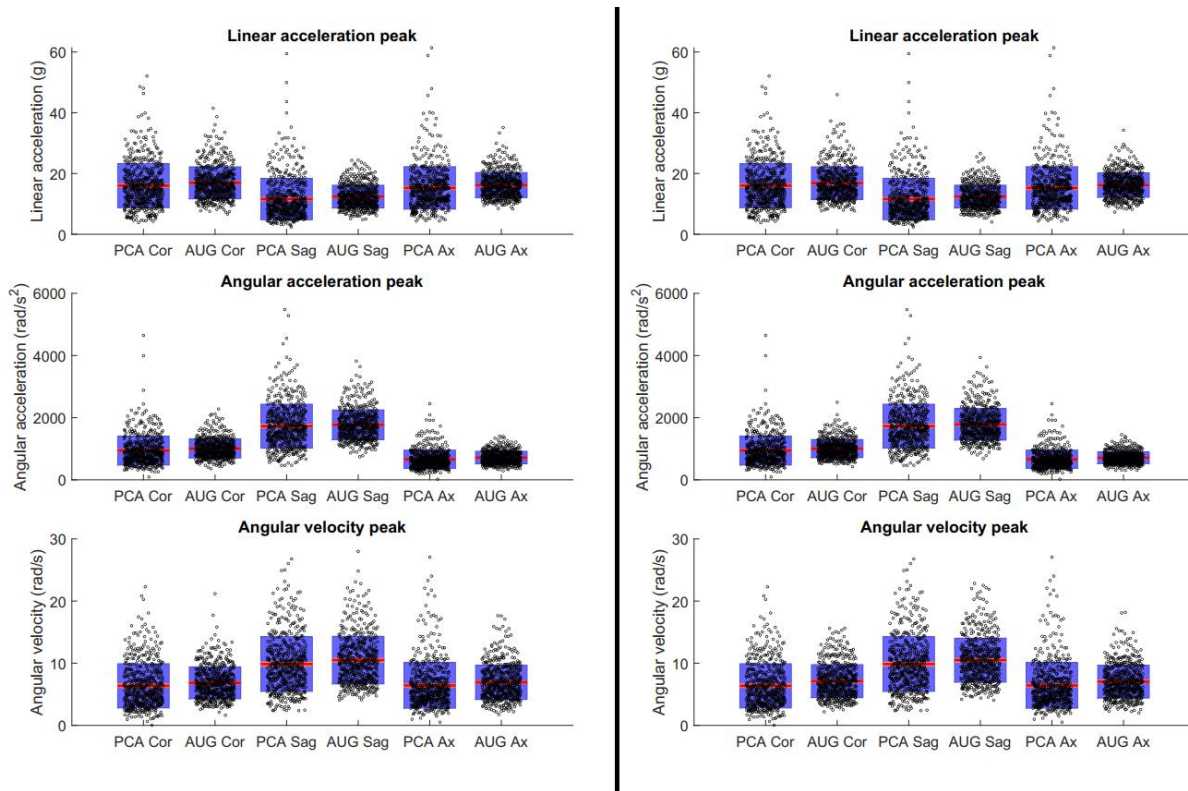


**Figure SM.5:** Peak distribution comparison between augmented data (two tests) and ground truth data.

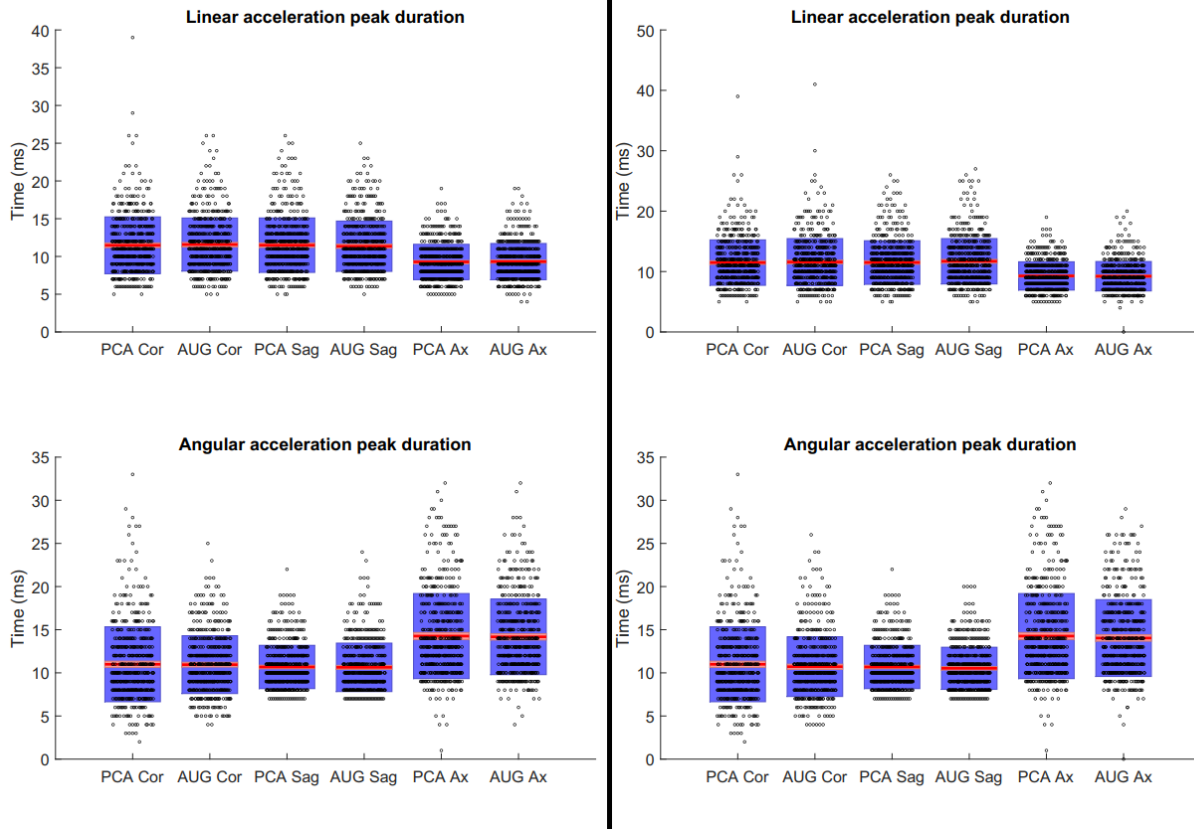


**Figure SM.6:** Peak duration distribution comparison between augmented data (two tests) and ground truth data.

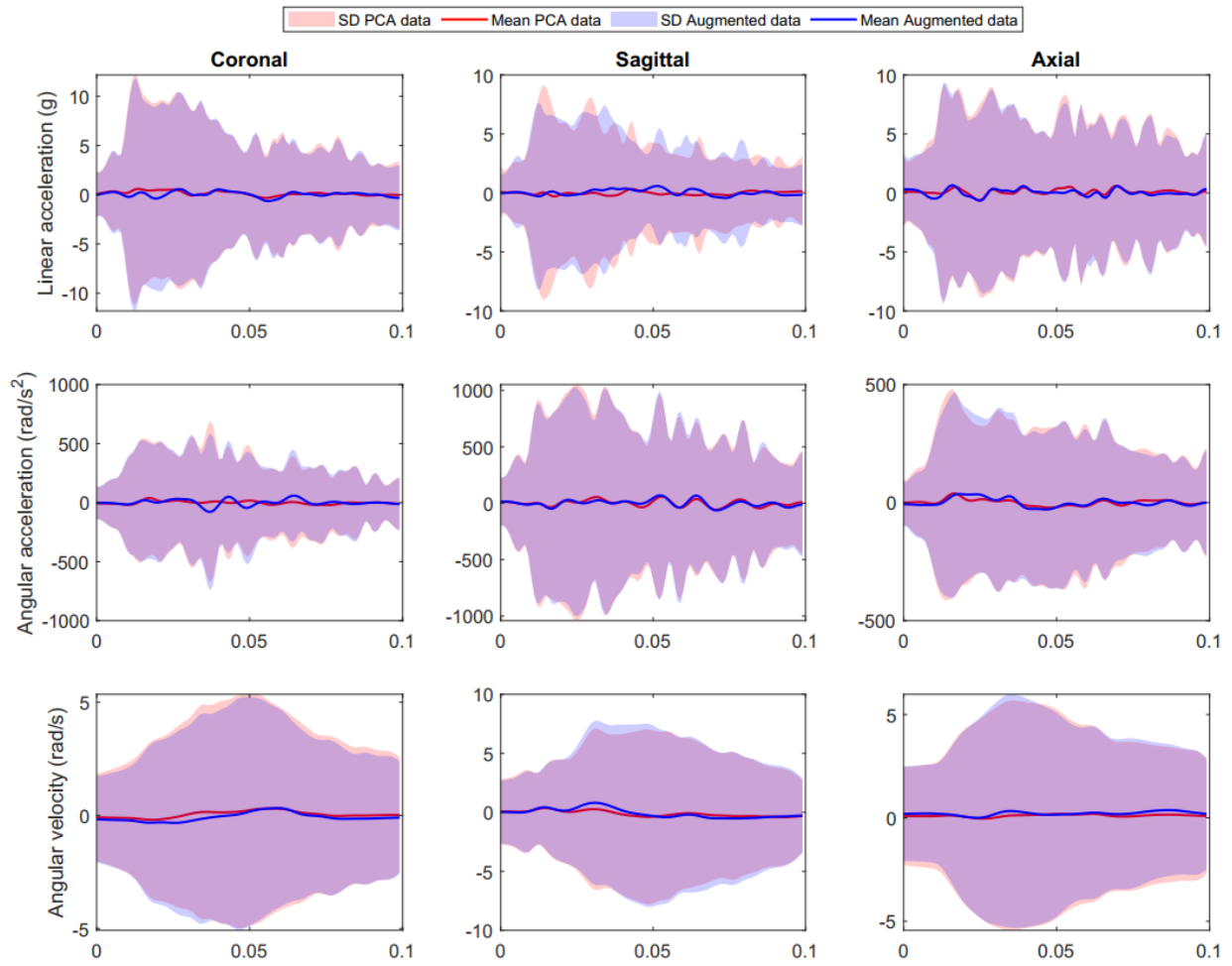


**Figure SM.7:** Statistical parameters per time point for ground truth and an augmented dataset.

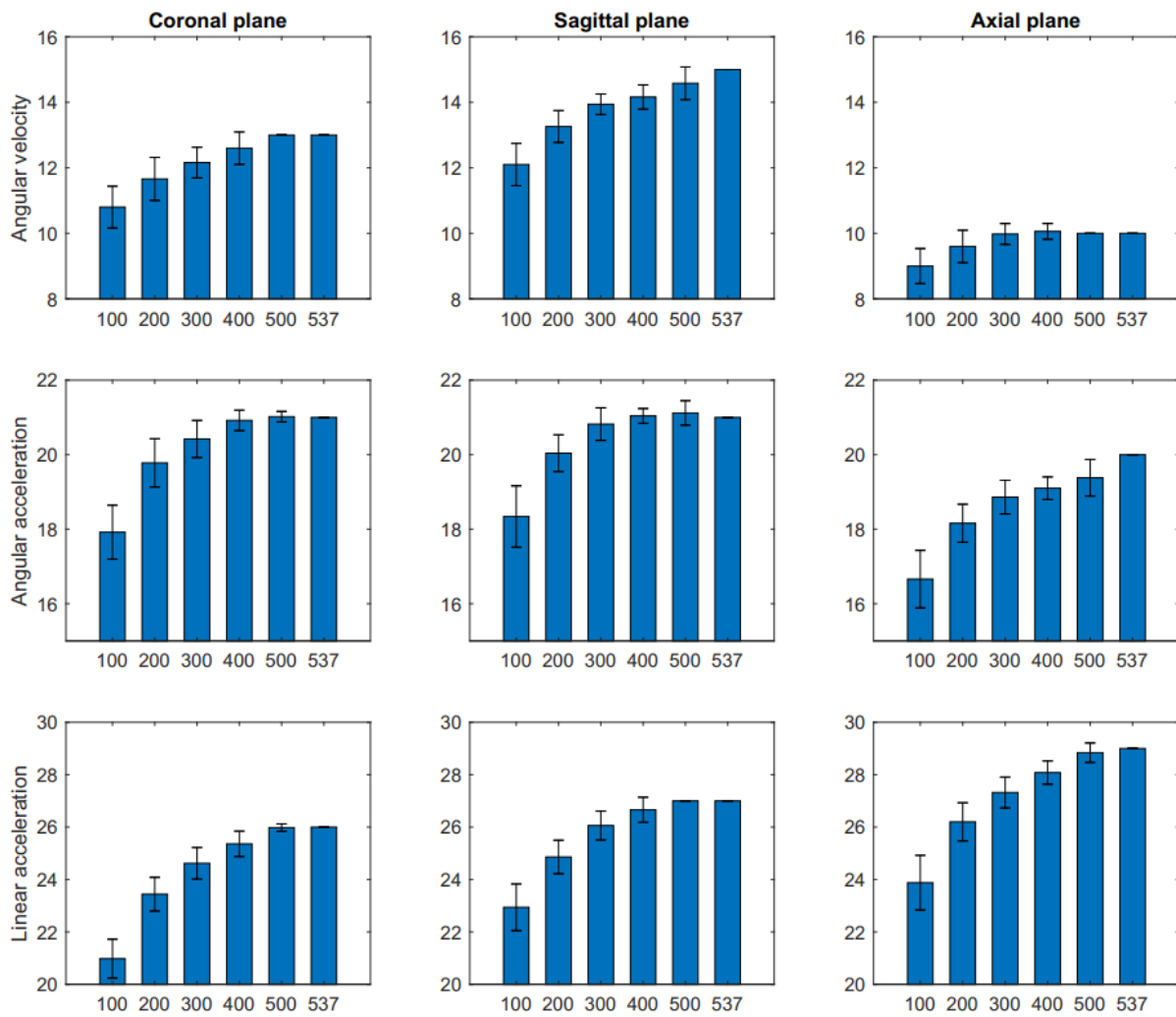


**Figure SM.8:** Convergence analysis for required number of modes to satisfy Equation 2.1 for random subsets of different size, showing convergence to the values obtained with the entire dataset (537).

## 6.1. REFERENCES

1. Nations U. World Population Ageing : 1950-2050. UNITED NATIONS PUBLICATIONS. UNITED NATIONS PUBLICATIONS; 2001. 2001–2003 p.
2. Steinhagen-Thiessen E, Borchelt M. Morbidity, medication, and functional limitations in very old age. In: *The Berlin Aging Study: Aging from 70 to 100*. New York, NY, US: Cambridge University Press; 1999. p. 131–66.
3. Sanderson WC, Scherbov S. Remeasuring Aging. *Science (80- )* [Internet]. 2010 Sep 10;329(5997):1287–8. Available from: <https://doi.org/10.1126/science.1193647>
4. Montani S, Bellazzi R, Portinale L, Stefanelli M. A multi-modal reasoning methodology for managing IDDM patients. *Int J Med Inform*. 2000;58–59:243–56.
5. Taylor CA, Bell JM, Breiding MJ, Xu L. Traumatic brain injury-related emergency department visits, hospitalizations, and deaths - United States, 2007 and 2013. *MMWR Surveill Summ*. 2017;
6. Lingsma HF, Roozenbeek B, Steyerberg EW, Murray GD, Maas AI. Early prognosis in traumatic brain injury: from prophecies to predictions. *Lancet Neurol* [Internet]. 2010;9(5):543–54. Available from: [http://dx.doi.org/10.1016/S1474-4422\(10\)70065-X](http://dx.doi.org/10.1016/S1474-4422(10)70065-X)
7. Christodoulou E, Ma J, Collins GS, Steyerberg EW, Verbakel JY, Van Calster B. A systematic review shows no performance benefit of machine learning over logistic regression for clinical prediction models. *J Clin Epidemiol* [Internet]. 2019;110:12–22. Available from: <https://doi.org/10.1016/j.jclinepi.2019.02.004>
8. Matsuo K, Aihara H, Nakai T, Morishita A, Tohma Y, Kohmura E. Machine learning to predict in-hospital morbidity and mortality after traumatic brain injury. *J Neurotrauma*. 2020;37(1):202–10.
9. Rau CS, Kuo PJ, Chien PC, Huang CY, Hsieh HY, Hsieh CH. Mortality prediction in patients with isolated moderate and severe traumatic brain injury using machine learning models. *PLoS One*. 2018;13(11):1–12.

10. Wu S, Zhao W, Ghazi K, Ji S. Convolutional neural network for efficient estimation of regional brain strains. *Sci Rep.* 2019;
11. Linka K, Kuhl E. A new family of Constitutive Artificial Neural Networks towards automated model discovery. *Comput Methods Appl Mech Eng.* 2023;403:1–31.
12. Wu T, Rifkin JA, Rayfield AC, Anderson ED, Panzer MB, Meaney DF. Concussion Prone Scenarios: A Multi-Dimensional Exploration in Impact Directions, Brain Morphology, and Network Architectures Using Computational Models. *Ann Biomed Eng.* 2022;50(11):1423–36.
13. Zhao W, Choate B, Ji S. Material properties of the brain in injury-relevant conditions – Experiments and computational modeling. *J Mech Behav Biomed Mater [Internet].* 2018;80(February):222–34. Available from: <https://doi.org/10.1016/j.jmbbm.2018.02.005>
14. NHTSA. National Highway Traffic Safety Administration . 1972;
15. Kimpara H, Iwamoto M. Mild traumatic brain injury predictors based on angular accelerations during impacts. *Ann Biomed Eng.* 2012;
16. Takhounts EG, Craig MJ, Moorhouse K, McFadden J, Hasija V. Development of brain injury criteria (BrIC). *Stapp Car Crash J.* 2013;
17. Laituri TR, Henry S, Pline K, Li G, Frankstein M, Weerappuli P. New Risk Curves for NHTSA’s Brain Injury Criterion (BrIC): Derivations and Assessments. *Stapp Car Crash J.* 2016;
18. National Operating Committee on Standards for Athletic. Standard performance specification for newly manufactured football helmets NOCSAE doc (ND) 002-11m12. 2012;
19. Hernandez F, Wu LC, Yip MC, Laksari K, Hoffman AR, Lopez JR, et al. Six Degree of Freedom Measurements of Human Mild Traumatic Brain Injury. *Ann Biomed Eng [Internet].* 2014 Dec; Available from: <http://www.ncbi.nlm.nih.gov/pubmed/25533767>
20. Laksari K, Fanton M, Wu LC, Nguyen TH, Kurt M, Giordano C, et al. Multi-directional dynamic model for traumatic brain injury detection. *arXiv Prepr arXiv181207731.* 2018;
21. Miller LE, Kuo C, Wu LC, Urban JE, Camarillo DB, Stitzel JD. Validation of a Custom Instrumented

- Retainer Form Factor for Measuring Linear and Angular Head Impact Kinematics. *J Biomech Eng.* 2018;140(5):1–6.
22. Wu LC, Kuo C, Loza J, Kurt M, Laksari K, Yanez LZ, et al. Detection of American Football Head Impacts Using Biomechanical Features and Support Vector Machine Classification. *Sci Rep* [Internet]. 2018;8(1):1–14. Available from: <http://dx.doi.org/10.1038/s41598-017-17864-3>
  23. Theadom A, Mahon S, Hume P, Starkey N, Barker-Collo S, Jones K, et al. Incidence of Sports-Related Traumatic Brain Injury of All Severities: A Systematic Review. *Neuroepidemiology.* 2020;54(2):192–9.
  24. Yoganandan N, Li J, Zhang J, Pintar FA, Gennarelli TA. Influence of angular acceleration-deceleration pulse shapes on regional brain strains. *J Biomech.* 2008;
  25. Ji S, Zhao W, Ford JC, Beckwith JG, Bolander RP, Greenwald RM, et al. Group-wise evaluation and comparison of white matter fiber strain and maximum principal strain in sports-related concussion. *J Neurotrauma* [Internet]. 2014;14(603):1–43. Available from: <http://www.ncbi.nlm.nih.gov/pubmed/24735430>
  26. Abderezaei J, Zhao W, Grijalva CL, Fabris G, Ji S, Laksari K, et al. Nonlinear Dynamical Behavior of the Deep White Matter during Head Impact. *Phys Rev Appl.* 2019;
  27. Kleiven S. Predictors for traumatic brain injuries evaluated through accident reconstructions. *Stapp Car Crash J.* 2007;
  28. Willinger R, Baumgartner D. Human head tolerance limits to specific injury mechanisms. *Int J Crashworthiness.* 2003;8(6):605–17.
  29. King AI, Yang KH, Zhang L, Hardy W, Viano DC. Is head injury caused by linear or angular acceleration. In: IRCOBI conference. Lisbon, Portugal; 2003.
  30. Ho J, Kleiven S. Dynamic response of the brain with vasculature: a three-dimensional computational study. *J Biomech* [Internet]. 2007 Jan [cited 2013 Nov 18];40(13):3006–12. Available from: <http://www.ncbi.nlm.nih.gov/pubmed/17433331>
  31. Takhounts EG, Ridella SA, Hasija V, Tannous RE, Campbell JQ, Malone D, et al. Investigation of

- Traumatic Brain Injuries Using the Next Generation of Simulated Injury Monitor (SIMon) Finite Element Head Model. SAE Tech Pap. 2008;2008-Novem(November).
32. Van Der Ploeg T, Austin PC, Steyerberg EW. Modern modelling techniques are data hungry: A simulation study for predicting dichotomous endpoints. *BMC Med Res Methodol*. 2014;14(1):1–13.
  33. Horak FB, Shupert CL, Mirka A. Components of postural dyscontrol in the elderly: A review. *Neurobiol Aging*. 1989;10(6):727–38.
  34. Mitnitski A, Howlett SE, Rockwood K. Heterogeneity of Human Aging and Its Assessment. *Journals Gerontol - Ser A Biol Sci Med Sci*. 2017;72(7):877–84.
  35. Fried LP, Tangen CM, Walston J, Newman AB, Hirsch C, Gottdiener J, et al. Frailty in older adults: Evidence for a phenotype. *Journals Gerontol - Ser A Biol Sci Med Sci*. 2001;56(3):146–57.
  36. Walters S, Chan S, Goh L, Ong T, Sahota O. The Prevalence of Frailty in Patients Admitted to Hospital with Vertebral Fragility Fractures [Internet]. Vol. 12, *Current Rheumatology Reviews*. 2016. p. 244–7. Available from: <http://www.eurekaselect.com/article/76669>
  37. McRae PJ, Walker PJ, Peel NM, Hobson D, Parsonson F, Donovan P, et al. Frailty and Geriatric Syndromes in Vascular Surgical Ward Patients. *Ann Vasc Surg* [Internet]. 2016;35(May 2016):9–18. Available from: <http://dx.doi.org/10.1016/j.avsg.2016.01.033>
  38. Rockwood K, Song X, Macknight C, Bergman H, Hogan DB, McDowell I, et al. A global clinical measure of fitness and frailty in elderly people. *CMAJ*. 2005;173 (5)(Appendix 1):489–95.
  39. HOLTER NJ. New method for heart studies. *Science*. 1961 Oct;134(3486):1214–20.
  40. Muller JE, Tofler GH, Stone PH. Circadian variation and triggers of onset of acute cardiovascular disease. *Circulation*. 1989;79(4):733–43.
  41. Cipryan L, Litschmannova M. Intra-day and inter-day reliability of heart rate variability measurement. *J Sports Sci*. 2013;31(2):150–8.
  42. Taelman J, Vandeput S, Spaepen A, Van Huffel S. Influence of mental stress on heart rate and

- heart rate variability. *IFMBE Proc.* 2008;22:1366–9.
43. Valencia JF, Porta A, Vallverdú M, Clarià F, Baranowski R, Orłowska-Baranowska E, et al. Multiscale sample entropy in heart rate variability of aortic stenosis patients. *Proc 30th Annu Int Conf IEEE Eng Med Biol Soc EMBS'08 - "Personalized Healthc through Technol.* 2008;2000–3.
  44. Toosizadeh N, Eskandari M, Ehsani H, Parvaneh S, Asghari M, Sweitzer N. Frailty assessment using a novel approach based on combined motor and cardiac functions: a pilot study. *BMC Geriatr* [Internet]. 2022;22(1):1–10. Available from: <https://doi.org/10.1186/s12877-022-02849-3>
  45. Bartsch RP, Liu KKL, Bashan A, Ivanov PC. Network physiology: How organ systems dynamically interact. *PLoS One* [Internet]. 2015;10(11):1–36. Available from: <http://dx.doi.org/10.1371/journal.pone.0142143>
  46. Bashan A, Bartsch RP, Kantelhardt JW, Havlin S, Ivanov PC. Network physiology reveals relations between network topology and physiological function. *Nat Commun* [Internet]. 2012;3:702–9. Available from: <http://dx.doi.org/10.1038/ncomms1705>
  47. Romero-Ortuño R, Martínez-Velilla N, Sutton R, Ungar A, Fedorowski A, Galvin R, et al. Network Physiology in Aging and Frailty: The Grand Challenge of Physiological Reserve in Older Adults. *Front Netw Physiol.* 2021;1(July):1–6.
  48. Ivanov PC, Wang JWJL, Zhang X, Chen B. The New Frontier of Network Physiology: Emerging Physiologic States in Health and Disease from Integrated Organ Network Interactions. 2021;237–54.
  49. Global Burden of Disease Collaborative Network. *Global Burden of Disease Study 2019 (GBD 2019).* 2020.
  50. Roth GA, Mensah GA, Johnson CO, Addolorato G, Ammirati E, Baddour LM, et al. Global Burden of Cardiovascular Diseases and Risk Factors, 1990-2019: Update From the GBD 2019 Study. *J Am Coll Cardiol.* 2020;76(25):2982–3021.
  51. Ambrosy AP, Fonarow GC, Butler J, Chioncel O, Greene SJ, Vaduganathan M, et al. The global health and economic burden of hospitalizations for heart failure: Lessons learned from

- hospitalized heart failure registries. *J Am Coll Cardiol* [Internet]. 2014;63(12):1123–33. Available from: <http://dx.doi.org/10.1016/j.jacc.2013.11.053>
52. Kazi DS, Mark DB. The Economics of Heart Failure. *Heart Fail Clin* [Internet]. 2013;9(1):93–106. Available from: <http://dx.doi.org/10.1016/j.hfc.2012.09.005>
  53. Shafie AA, Tan YP, Ng CH. Systematic review of economic burden of heart failure. *Heart Fail Rev*. 2018;23(1):131–45.
  54. Faggiano P, Antonini-Canterin F, Baldessin F, Lorusso R, D’Aloia A, Dei Cas L. Epidemiology and cardiovascular risk factors of aortic stenosis. *Cardiovasc Ultrasound*. 2006;4:1–5.
  55. Mendez GF, Cowie MR. The epidemiological features of heart failure in developing countries: A review of the literature. *Int J Cardiol*. 2001;80(2–3):213–9.
  56. Osnabrugge RLJ, Mylotte D, Head SJ, Van Mieghem NM, Nkomo VT, Lereun CM, et al. Aortic stenosis in the elderly: Disease prevalence and number of candidates for transcatheter aortic valve replacement: A meta-analysis and modeling study. *J Am Coll Cardiol*. 2013;62(11):1002–12.
  57. Roger VL, Go AS, Lloyd-Jones DM, Benjamin EJ, Berry JD, Borden WB, et al. Heart disease and stroke statistics-2012 update: A report from the American heart association. *Circulation*. 2012;125(1):2–220.
  58. Purser JL, Kuchibhatla MN, Fillenbaum GG, Harding T, Peterson ED, Alexander KP. Identifying frailty in hospitalized older adults with significant coronary artery disease. *J Am Geriatr Soc*. 2006;54(11):1674–81.
  59. Dunlay SM, Park SJ, Joyce LD, Daly RC, Stulak JM, McNallan SM, et al. Frailty and outcomes after implantation of left ventricular assist device as destination therapy. *J Hear Lung Transplant* [Internet]. 2014;33(4):359–65. Available from: <http://dx.doi.org/10.1016/j.healun.2013.12.014>
  60. McNallan SM, Chamberlain AM, Gerber Y, Singh M, Kane RL, Weston SA, et al. Measuring frailty in heart failure: A community perspective. *Am Heart J* [Internet]. 2013;166(4):768–74. Available from: <http://dx.doi.org/10.1016/j.ahj.2013.07.008>
  61. Defense and Veterans Brain Injury Center. DoD Worldwide Numbers for TBI | DVBIC. Department

- of Defense. 2018.
62. Selassie AW, Wilson D a., Pickelsimer EE, Voronca DC, Williams NR, Edwards JC. Incidence of sport-related traumatic brain injury and risk factors of severity: a population-based epidemiologic study. *Ann Epidemiol* [Internet]. 2013 Sep; Available from: <http://linkinghub.elsevier.com/retrieve/pii/S1047279713003189>
  63. Dekosky ST, Blennow K, Ikonovic MD, Gandy S. Acute and chronic traumatic encephalopathies: Pathogenesis and biomarkers. *Nature Reviews Neurology*. 2013.
  64. Kuo C, Wu LC, Ye PP, Laksari K, Camarillo DB, Kuhl E. Pilot Findings of Brain Displacements and Deformations During Roller Coaster Rides. *J Neurotrauma* [Internet]. 2017;In Press(July). Available from: <http://online.liebertpub.com/doi/10.1089/neu.2016.4893>
  65. Kurt M, Laksari K, Kuo C, Grant GA, Camarillo DB. Modeling and Optimization of Airbag Helmets for Preventing Head Injuries in Bicycling. *Ann Biomed Eng*. 2017;45(4):1148–60.
  66. Siegkas P, Sharp DJ, Ghajari M. The traumatic brain injury mitigation effects of a new viscoelastic add-on liner. *Sci Rep* [Internet]. 2019;9(1):3471. Available from: <http://www.nature.com/articles/s41598-019-39953-1>
  67. Manoogian S, McNeely D, Duma S, Brolinson G, Greenwald R. Head acceleration is less than 10 percent of helmet acceleration in football impacts. In: *Biomedical Sciences Instrumentation*. 2006.
  68. Wu LC, Zarnescu L, Nangia V, Cam B, Camarillo DB. A Head Impact Detection System Using SVM Classification and Proximity Sensing in an Instrumented Mouthguard. *IEEE Trans Biomed Eng* [Internet]. 2014 Nov;61(11):2659–68. Available from: <http://www.ncbi.nlm.nih.gov/pubmed/24800918>
  69. Pershing AJ, Alexander MA, Hernandez CM, Kerr LA, et al. Slow adaptation in the face of rapid warming leads to collapse of the Gulf of Maine cod fishery. *Science* (80- ) [Internet]. 2015;350(6262):809. Available from: <http://science.sciencemag.org/content/350/6262/809.abstract>

70. Laksari K, Wu LC, Kurt M, Kuo C, Camarillo DC. Resonance of human brain under head acceleration. *J R Soc Interface*. 2015;12:20150331.
71. Gabler LF, Joodaki H, Crandall JR, Panzer MB. Development of a Single-Degree-of-Freedom Mechanical Model for Predicting Strain-Based Brain Injury Responses. *J Biomech Eng*. 2018;
72. Kleiven S. Why most traumatic brain injuries are not caused by linear acceleration but skull fractures are. *Front Bioeng Biotechnol*. 2013;1:15.
73. Zhao W, Ford JC, Flashman LA, McAllister TW, Ji S. White Matter Injury Susceptibility via Fiber Strain Evaluation Using Whole-Brain Tractography. *J Neurotrauma* [Internet]. 2016;33(20):1834–47. Available from: <http://online.liebertpub.com/doi/10.1089/neu.2015.4239>
74. Laksari K, Fanton M, Wu L, Nguyen T, Kurt M, Giordano C, et al. Multi-directional dynamic model for traumatic brain injury detection. *J Neurotrauma*. 2019;(ja).
75. Wu S, Zhao W, Rowson B, Rowson S, Ji S. A network-based response feature matrix as a brain injury metric. *Biomech Model Mechanobiol* [Internet]. 2019;(0123456789). Available from: <http://link.springer.com/10.1007/s10237-019-01261-y>
76. Laksari K, Kurt M, Babae H, Kleiven S, Camarillo D. Mechanistic Insights into Human Brain Impact Dynamics through Modal Analysis. *Phys Rev Lett* [Internet]. 2018;120(13):138101. Available from: <https://link.aps.org/doi/10.1103/PhysRevLett.120.138101>
77. Miller LE, Pinkerton EK, Fabian KC, Wu LC, Espeland MA, Lamond LC, et al. Characterizing head impact exposure in youth female soccer with a custom-instrumented mouthpiece. *Res Sport Med* [Internet]. 2019;0(0):1–17. Available from: <https://doi.org/10.1080/15438627.2019.1590833>
78. Ji S, Zhao W. A pre-computed model responses atlas for instantaneous brain strain estimation in contact sports. *Ann Biomed Eng*. 2014;
79. Cai Y, Zhao W, Li Z, Ji S. Concussion classification via deep learning using whole-brain white matter fiber strains. 2016;under review.
80. Sapsis TP, Lermusiaux PFJ. Dynamically orthogonal field equations for continuous stochastic dynamical systems. *Phys D Nonlinear Phenom*. 2009;238(23–24):2347–60.

81. Babae H, Sapsis TP. A minimization principle for the description of modes associated with finite-time instabilities. *Proc R Soc London A Math Phys Eng Sci* [Internet]. 2016;472(2186). Available from: <http://dx.doi.org/10.1098/rspa.2015.0779>
82. Babae H, Choi M, Sapsis TP, Karniadakis GE. A robust bi-orthogonal/dynamically-orthogonal method using the covariance pseudo-inverse with application to stochastic flow problems. *J Comput Phys* [Internet]. 2017;344:303–19. Available from: <http://www.sciencedirect.com/science/article/pii/S0021999117303364>
83. Babae H. An observation-driven time-dependent basis for a reduced description of transient stochastic systems. *Proc R Soc A Math Phys Eng Sci* [Internet]. 2019;475(2231):20190506. Available from: <https://doi.org/10.1098/rspa.2019.0506>
84. Patil P, Babae H. Real-time reduced-order modeling of stochastic partial differential equations via time-dependent subspaces. *J Comput Phys* [Internet]. 2020;415:109511. Available from: <http://www.sciencedirect.com/science/article/pii/S0021999120302850>
85. Newman JA, Shewchenko N. A Proposed New Biomechanical Head Injury Assessment Function - The Maximum Power Index. In: *SAE Technical Papers*. 2000.
86. Marjoux D, Baumgartner D, Deck C, Willinger R. Head injury prediction capability of the HIC, HIP, SIMon and ULP criteria. *Accid Anal Prev*. 2008;
87. Zhang F, Wu Y, Norton I, Rigolo L, Rathi Y, Makris N, et al. An anatomically curated fiber clustering white matter atlas for consistent white matter tract parcellation across the lifespan. *Neuroimage*. 2018;
88. Kornhauser M. Prediction and evaluation of sensitivity to transient accelerations. *J Appl Mech*. 1954;
89. Low T, Stalnaker R. A lumped parameter approach to simulate the rotational head motion. *Int Res Counc Biokinetics Impacts*. 1987;
90. Sullivan S, Eucker SA, Gabrieli D, Bradfield C, Coats B, Maltese MR, et al. White matter tract-oriented deformation predicts traumatic axonal brain injury and reveals rotational direction-

- specific vulnerabilities. *Biomech Model Mechanobiol.* 2015;
91. Ji S, Zhao W, Ford JC, Beckwith JG, Bolander RP, Greenwald RM, et al. Group-wise evaluation and comparison of white matter fiber strain and maximum principal strain in sports-related concussion. *J Neurotrauma* [Internet]. 2014;14(603):1–43. Available from: <http://www.ncbi.nlm.nih.gov/pubmed/24735430>
  92. Zhao W, Cai Y, Li Z, Ji S. Injury prediction and vulnerability assessment using strain and susceptibility measures of the deep white matter. *Biomech Model Mechanobiol.* 2017;16(5):1–19.
  93. Daniel WW. *Applied Nonparametric Statistics* [Internet]. PWS-KENT Pub.; 1990. (Duxbury advanced series in statistics and decision sciences). Available from: <https://books.google.com/books?id=0hPvAAAAMAAJ>
  94. Patton DA, McIntosh AS, Kleiven S, Fréchède B. Injury data from unhelmeted football head impacts evaluated against critical strain tolerance curves. In: *Proceedings of the Institution of Mechanical Engineers, Part P: Journal of Sports Engineering and Technology.* 2012.
  95. Giordano C, Kleiven S. Evaluation of Axonal Strain as a Predictor for Mild Traumatic Brain Injuries Using Finite Element Modeling. *Stapp Car Crash J.* 2014;
  96. Arrué P. Data-driven head impacts emulator. Laksari's lab. [\ \ \href{https://uweb.engr.arizona.edu/~klaksari/Resources.html}{\(https://uweb.engr.arizona.edu/\\$~\\$klaksari/Resources.html\)}](https://uweb.engr.arizona.edu/~klaksari/Resources.html). Laksari's Lab. 2020;
  97. Giordano C, Cloots RJH, van Dommelen JAW, Kleiven S. The influence of anisotropy on brain injury prediction. *J Biomech.* 2014;
  98. Zhao W, Ji S. White Matter Anisotropy for Impact Simulation and Response Sampling in Traumatic Brain Injury. *J Neurotrauma.* 2019;36(2):250–63.
  99. Eckersley CP, Nightingale RW, Luck JF, Bass CR. Effect of neck musculature on head kinematic response following blunt impact. In: *Conference proceedings International Research Council on the Biomechanics of Injury, IRCOBI.* 2017.

100. Wu LC, Nangia V, Bui K, Hammoor B, Kurt M, Hernandez F, et al. In Vivo Evaluation of Wearable Head Impact Sensors. *Ann Biomed Eng* [Internet]. 2016 Aug;44(4):1234–45. Available from: <http://www.ncbi.nlm.nih.gov/pubmed/26289941>
101. Clark BC, Manini TM. What is dynapenia? *Tissue Eng*. 2012;28(5):495–503.
102. Serviddio G, Romano AD, Greco A, Rollo T, Bellanti F, Altomare E, et al. Frailty syndrome is associated with altered circulating redox balance and increased markers of oxidative stress. *Int J Immunopathol Pharmacol*. 2009;22(3):819–27.
103. Johar H, Emeny RT, Bidlingmaier M, Reincke M, Thorand B, Peters A, et al. Blunted diurnal cortisol pattern is associated with frailty: A cross-sectional study of 745 participants aged 65 to 90 years. *J Clin Endocrinol Metab*. 2014;99(3):464–8.
104. O’Connell MDL, Tajar A, Roberts SA, Wu FCW. Do androgens play any role in the physical frailty of ageing men? *Int J Androl*. 2011;34(3):195–211.
105. López-Armada MJ, Riveiro-Naveira RR, Vaamonde-García C, Valcárcel-Ares MN. Mitochondrial dysfunction and the inflammatory response. *Mitochondrion*. 2013;13(2):106–18.
106. Yao X, Li H, Leng SX. Inflammation and Immune System Alterations in Frailty. *Clin Geriatr Med*. 2011;27(1):79–87.
107. Schaap LA, Pluijm SMF, Deeg DJH, Visser M. Inflammatory Markers and Loss of Muscle Mass (Sarcopenia) and Strength. *Am J Med*. 2006;119(6).
108. Visser M, Pahor M, Taaffe DR, Goodpaster BH, Simonsick EM, Newman AB, et al. Relationship of interleukin-6 and tumor necrosis factor- $\alpha$  with muscle mass and muscle strength in elderly men and women: The health ABC study. *Journals Gerontol - Ser A Biol Sci Med Sci*. 2002;57(5):326–32.
109. Manini TM, Clark BC. Dynapenia and aging: An update. *Journals Gerontol - Ser A Biol Sci Med Sci*. 2012;67 A(1):28–40.
110. Katayama PL, Dias DPM, Silva LEV, Virtuoso-Junior JS, Marocolo M. Cardiac autonomic modulation in non-frail, pre-frail and frail elderly women: a pilot study. *Aging Clin Exp Res*. 2015;27(5):621–9.

111. Toosizadeh N, Wendel C, Hsu CH, Zamrini E, Mohler J. Frailty assessment in older adults using upper-extremity function: index development. *BMC Geriatr*. 2017;17(1):1–7.
112. Toosizadeh N, Ehsani H, Parthasarathy S, Carpenter B, Ruberto K, Mohler J, et al. Frailty and heart response to physical activity. *Arch Gerontol Geriatr* [Internet]. 2021;93(November 2020):104323. Available from: <https://doi.org/10.1016/j.archger.2020.104323>
113. Toosizadeh N, Sweitzer N. Frailty Assessment Using a Novel Approach Based on Combined Motor and Cardiac Functions : A Pilot Study. *BMC Geriatr* [Internet]. 2021;1–14. Available from: <https://doi.org/10.1186/s12877-022-02849-3>
114. Schiecke K, Schumann A, Benninger F, Feucht M, Baer KJ, Schlattmann P. Brain-heart interactions considering complex physiological data: Processing schemes for time-variant, frequency-dependent, topographical and statistical examination of directed interactions by convergent cross mapping. *Physiol Meas*. 2019;40(11).
115. Schiecke K, Schumann A, Baer KJ. Influence of Individual Heart Rate on Nonlinear Brain-Heart Interactions Estimated by Convergent Cross Mapping in Schizophrenic Patients and Healthy Controls. *Proc Annu Int Conf IEEE Eng Med Biol Soc EMBS*. 2020;2020-July:549–52.
116. Heskamp L, Abeelen ASSM den, Lagro J, Claassen JAHR. CCM a new non-linear method for the quantification of cerebral autorregulation.pdf. *Int J Clin Neurosci Ment Heal*. 2015;
117. Verma AK, Garg A, Xu D, Bruner M, Fazel-Rezai R, Blaber AP, et al. Skeletal Muscle Pump Drives Control of Cardiovascular and Postural Systems. *Sci Rep*. 2017;7(March):1–8.
118. Schiecke K, Pester B, Piper D, Benninger F, Feucht M, Leistriz L, et al. Nonlinear Directed Interactions between HRV and EEG Activity in Children with TLE. *IEEE Trans Biomed Eng*. 2016;63(12):2497–504.
119. Heskamp L, Abeelen ASSM den, Lagro J, Claassen JAHR. Convergent cross mapping: a promising technique for cerebral autoregulation estimation. *Int J Clin Neurosci Ment Heal*. 2014;1(1(Suppl. 1)):S20.
120. Granger CJW. Investigating Causal Relations by Econometric Models and Cross-spectral Methods

Authors ( s ): C . W . J . Granger Published by : The Econometric Society Stable URL :  
<http://www.jstor.org/stable/1912791> Accessed : 25-03-2016 19 : 26 UTC Your use of the JS.  
Econometrica. 1969;37(3):424–38.

121. Sugihara G, May R, Ye H, Hsieh CH, Deyle E, Fogarty M, et al. Detecting causality in complex ecosystems. *Science* (80- ). 2012;338(6106):496–500.
122. Tsonis AA. *Advances in Nonlinear Geosciences*. Advances in Nonlinear Geosciences. 2018.
123. Folstein M, Folstein S, Mchugh P. “Mini-Mental State” A Practical Method For Grading The Cognitive State Of Patients For The Clinical. *J psychist*. 1975;12:189–98.
124. Association WM. World Medical Association Declaration of Helsinki: ethical principles for medical research involving human subjects. *JAMA*. 2013;310(20):2197–2194.
125. Fieo R, Mortensen E, Rantanen T, Avlund K. Improving a Measure of Mobility-Related Fatigue (The Mobility- Tiredness Scale) by Establishing Item Intensity. *J Am Geriatr Soc*. 2013;61(3):429–33.
126. Nasreddine ZS, Phillips NA, Bédirian V, Charbonneau S, Whitehead V, Collin I, et al. The Montreal Cognitive Assessment, MoCA: A brief screening tool for mild cognitive impairment. *J Am Geriatr Soc*. 2005;53(4):695–9.
127. Charlson ME. a New Method of Classifying Prognostic in Longitudinal Studies : Development. *J Chronic Dis* [Internet]. 1987;40(5):373–83. Available from:  
<http://www.sciencedirect.com/science/article/pii/0021968187901718>
128. Kroenke K, Spitzer RL, Williams JBW. The PHQ-9. 46202:606–13.
129. Toosizadeh N, Mohler J, Najafi B. Assessing upper extremity motion: An innovative method to identify frailty. *J Am Geriatr Soc*. 2015;63(6):1181–6.
130. Toosizadeh N, Joseph B, FACS, Heusser M, Orouji Jokar T, Mohler J, et al. Assessing Upper-Extremity Motion: An Innovative, Objective Method to Identify Frailty in Older Bed-Bound Trauma Patients. *J Am Coll Surg*. 2016;223(2):240–8.
131. Pan J, Tompkins WJ. A Real-Time QRS Detection Algorithm. *IEEE Trans Biomed Eng*. 1985;BME-

- 32(3):230–6.
132. Takens F. Detecting strange attractors in turbulence *Dynamical Systems and Turbulence*, Warwick 1980. *Dyn Syst Turbul* [Internet]. 1981;898:366–81. Available from: <http://dx.doi.org/10.1007/bfb0091924>
  133. Cao L. Practical method for determining the minimum embedding dimension of a scalar time series. *Phys D Nonlinear Phenom*. 1997;110(1–2):43–50.
  134. Leng S, Ma H, Kurths J, Lai YC, Lin W, Aihara K, et al. Partial cross mapping eliminates indirect causal influences. *Nat Commun* [Internet]. 2020;11(1):1–9. Available from: <http://dx.doi.org/10.1038/s41467-020-16238-0>
  135. Tsonis AA, Deyle E, Ye H, Sugihara G. *Advances in Nonlinear Geosciences. Advances in Nonlinear Geosciences - Convergent Cross Mapping: Theory and an Example*. Springer, Cham; 2018. 587–600 p.
  136. Anderson R, Jönsson P, Sandsten M. Effects of Age, BMI, anxiety and stress on the parameters of a stochastic model for heart rate variability including respiratory information. *BIOSIGNALS 2018 - 11th Int Conf Bio-Inspired Syst Signal Process Proceedings; Part 11th Int Jt Conf Biomed Eng Syst Technol BIOSTEC 2018*. 2018;4(Biostec):17–25.
  137. Gordon EH, Peel NM, Samanta M, Theou O, Howlett SE, Hubbard RE. Sex differences in frailty: A systematic review and meta-analysis. *Exp Gerontol* [Internet]. 2017;89:30–40. Available from: <http://dx.doi.org/10.1016/j.exger.2016.12.021>
  138. Hubbard RE, Lang IA, Llewellyn DJ, Rockwood K. Frailty, body mass index, and abdominal obesity in older people. *Journals Gerontol - Ser A Biol Sci Med Sci*. 2010;65 A(4):377–81.
  139. Williamson JW, Fadel PJ, Mitchell JH. New insights into central cardiovascular control during exercise in humans: A central command update. *Exp Physiol*. 2006;91(1):51–8.
  140. Kaufman MP, Hayes SG. The exercise pressor reflex. *Clin Auton Res*. 2002;12(6):429–39.
  141. Charkoudian N, Joyner MJ, Johnson CP, Eisenach JH, Dietz NM, Wallin BG. Balance between cardiac output and sympathetic nerve activity in resting humans: Role in arterial pressure

- regulation. *J Physiol*. 2005;568(1):315–21.
142. Trinity JD, Layec G, Hart CR, Richardson RS. Sex-specific impact of aging on the blood pressure response to exercise. *Am J Physiol - Hear Circ Physiol*. 2018;314(1):H95–104.
143. Hasegawa D, Hori A, Okamura Y, Baba R, Suijo K, Mizuno M, et al. Aging exaggerates blood pressure response to ischemic rhythmic handgrip exercise in humans. *Physiol Rep*. 2021;9(22):1–15.
144. Caron G, Decherchi P, Marqueste T. Alteration of Metabosensitive Afferent Response With Aging: Exercised versus Non-exercised Rats. *Front Aging Neurosci*. 2018;10(November):1–8.
145. Teixeira AL, Vianna LC. The exercise pressor reflex: An update. *Clin Auton Res [Internet]*. 2022;32(4):271–90. Available from: <https://doi.org/10.1007/s10286-022-00872-3>
146. Milot E, Morissette-Thomas V, Li Q, Fried LP, Ferrucci L, Cohen AA. Trajectories of physiological dysregulation predicts mortality and health outcomes in a consistent manner across three populations. *Mech Ageing Dev*. 2014;0(1):56–63.
147. Cohen AA, Milot E, Yong J, Seplaki CL, Fülöp T, Bandeen-Roche K, et al. A novel statistical approach shows evidence for multi-system physiological dysregulation during aging. *Mech Ageing Dev*. 2013;134(3–4):110–7.
148. Nakazato Y, Sugiyama T, Ohno R, Shimoyama H, Leung DL, Cohen AA, et al. Estimation of homeostatic dysregulation and frailty using biomarker variability: a principal component analysis of hemodialysis patients. *Sci Rep [Internet]*. 2020;10(1):1–12. Available from: <http://dx.doi.org/10.1038/s41598-020-66861-6>
149. Rockwood K, Mitnitski A. Frailty in relation to the accumulation of deficits. *Journals Gerontol - Ser A Biol Sci Med Sci*. 2007;62(7):722–7.
150. Ehsani H, Mohler MJ, Golden T, Toosizadeh N. Upper-extremity function prospectively predicts adverse discharge and all-cause COPD readmissions: A pilot study. *Int J COPD*. 2019;14:39–49.
151. Varadhan R, Chaves PHM, Lipsitz LA, Stein PK, Tian J, Windham BG, et al. Frailty and impaired cardiac autonomic control: New insights from principal components aggregation of traditional

- heart rate variability indices. *Journals Gerontol - Ser A Biol Sci Med Sci*. 2009;64(6):682–7.
152. Moghtadaei M, Jansen HJ, Mackasey M, Rafferty SA, Bogachev O, Sapp JL, et al. The impacts of age and frailty on heart rate and sinoatrial node function. *J Physiol*. 2016;594(23):7105–26.
  153. Arslan U, Özdemir M, Kocaman SA, Balcioglu S, Cemri M, Çengel A. Heart rate variability and heart rate turbulence in mild-to-moderate aortic stenosis. *Europace*. 2008;10(12):1434–41.
  154. Zebrowski J, Kowalik I, Orłowska-Baranowska E, Andrzejewska M, Baranowski R, Gieraltowski J. On the risk of aortic valve replacement surgery assessed by HRV parameters.pdf. IOP Publishing; 2015. p. 163–75.
  155. Morris JA, Norris PR. Role of reduced heart rate volatility in predicting death in trauma patients. *Adv Surg*. 2005;39:77–96.
  156. Kleiger RE, Miller JP, Bigger JT, Moss AJ. Decreased heart rate variability and its association with increased mortality after acute myocardial infarction. *Am J Cardiol*. 1987;59(4):256–62.
  157. Varadhan R, Seplaki CL, Xue QL, Bandeen-Roche K, Fried LP. Stimulus-response paradigm for characterizing the loss of resilience in homeostatic regulation associated with frailty. *Mech Ageing Dev*. 2008;129(11):666–70.
  158. Díez-Villanueva P, Salamanca J, Rojas A, Alfonso F. Importance of frailty and comorbidity in elderly patients with severe aortic stenosis. *J Geriatr Cardiol*. 2017;14(6):379–82.
  159. Anker SD, Ponikowski PP, Clark AL, Leyva F, Rauchhaus M, Kemp M, et al. Cytokines and neurohormones relating to body composition alterations in the wasting syndrome of chronic heart failure. *Eur Heart J*. 1999;20(9):683–93.
  160. Anker SD, Clark AL, Kemp M, Salsbury C, Teixeira MM, Hellewell PG, et al. Tumor necrosis factor and steroid metabolism in chronic heart failure: Possible relation to muscle wasting. *J Am Coll Cardiol [Internet]*. 1997;30(4):997–1001. Available from: [http://dx.doi.org/10.1016/S0735-1097\(97\)00262-3](http://dx.doi.org/10.1016/S0735-1097(97)00262-3)
  161. McMurray J, Abdullah I, Dargie HJ, Shapiro D. Increased concentrations of tumour necrosis factor in “cachectic” patients with severe chronic heart failure. *Br Heart J*. 1991;66(5):356–8.

162. von Haehling S, Doehner W, Anker SD. Nutrition, metabolism, and the complex pathophysiology of cachexia in chronic heart failure. *Cardiovasc Res*. 2007;73(2):298–309.
163. Uchmanowicz I, Łoboz-Rudnicka M, Szelaąg P, Jankowska-Polańska B, Łoboz-Grudzień K. Frailty in heart failure. *Curr Heart Fail Rep*. 2014;11(3):266–73.
164. Goldsweig AM, Tak HJ, Chen LW, Aronow HD, Shah B, Kolte D, et al. Relative Costs of Surgical and Transcatheter Aortic Valve Replacement and Medical Therapy. *Circ Cardiovasc Interv*. 2020;13(5):1–9.
165. Arrué P, Laksari K, Toosizadeh N. Associating Frailty and Dynamic Dysregulation between Motor and Cardiac Autonomic Systems. *Quant Methods Q-bioQM ArXiv*. 2023;
166. Green CP, Porter CB, Bresnahan DR, Spertus JA. Development and evaluation of the Kansas City cardiomyopathy questionnaire: A new health status measure for heart failure. *J Am Coll Cardiol* [Internet]. 2000;35(5):1245–55. Available from: [http://dx.doi.org/10.1016/S0735-1097\(00\)00531-3](http://dx.doi.org/10.1016/S0735-1097(00)00531-3)
167. Eskandari M, Parvaneh S, Ehsani H, Fain M, Toosizadeh N. Frailty Identification Using Heart Rate Dynamics: A Deep Learning Approach. *IEEE J Biomed Heal Informatics*. 2022;26(7):3409–17.
168. Evrengul H, Tanriverdi H, Kose S, Amasyali B, Kilic A, Celik T, et al. The relationship between heart rate recovery and heart rate variability in coronary artery disease. *Ann Noninvasive Electrocardiol*. 2006;11(2):154–62.
169. Carter R, Watenpaugh DE, Wasmund WL, Wasmund SL, Smith ML. Muscle pump and central command during recovery from exercise in humans. *J Appl Physiol*. 1999;87(4):1463–9.
170. Nishime EO, Cole CR, Blackstone EH, Pashkow FJ, Lauer MS. Heart rate recovery and treadmill exercise score as predictors of mortality in patients referred for exercise ECG. *Jama*. 2000;284(11):1392–8.
171. Savin WM, Davidson DM, Haskell WL. Autonomic contribution to heart rate recovery from exercise in humans. *J Appl Physiol Respir Environ Exerc Physiol*. 1982;53(6):1572–5.
172. Weiss CO, Hoenig HH, Varadhan R, Simonsick EM, Fried LP. Relationships of cardiac, pulmonary,

- and muscle reserves and frailty to exercise capacity in older women. *Journals Gerontol - Ser A Biol Sci Med Sci*. 2010;65 A(3):287–94.
173. Romero-Ortuno R, Cogan L, O’shea D, Lawlor BA, Kenny RA. Orthostatic haemodynamics may be impaired in frailty. *Age Ageing*. 2011;40(5):576–83.
  174. Parvaneh S, Howe C, Toosizadeh N, Honarvar B, Slepian MJ, Fain M, et al. Regulation of Cardiac Autonomic Nervous System Control across Frailty Status: A Systematic Review. *Gerontology*. 2015;62(1):3–15.
  175. Shokouhmand A, Aranoff ND, Driggin E, Green P, Tavassolian N. Efficient detection of aortic stenosis using morphological characteristics of cardiomechanical signals and heart rate variability parameters. *Sci Rep [Internet]*. 2021;11(1):1–14. Available from: <https://doi.org/10.1038/s41598-021-03441-2>
  176. Lumley M, Williams R, Asrress KN, Arri S, Briceno N, Ellis H, et al. Coronary Physiology During Exercise and Vasodilation in the Healthy Heart and in Severe Aortic Stenosis. *J Am Coll Cardiol*. 2016;68(7):688–97.
  177. Fukui S, Kawakami M, Otaka Y, Ishikawa A, Mizuno K, Tsuji T, et al. Physical frailty in older people with severe aortic stenosis. *Aging Clin Exp Res*. 2016;28(6):1081–7.
  178. Okoh AK, Chauhan D, Kang N, Haik N, Merlo A, Cohen M, et al. The impact of frailty status on clinical and functional outcomes after transcatheter aortic valve replacement in nonagenarians with severe aortic stenosis. *Catheter Cardiovasc Interv*. 2017;90(6):1000–6.
  179. Grimard BH, Larson JANM, Clinic M, Augustine S. Aortic Stenosis: Diagnosis and Treatment.
  180. Chambers JB, Rajani R, Parkin D, Saeed S. Rapid early rise in heart rate on treadmill exercise in patients with asymptomatic moderate or severe aortic stenosis: A new prognostic marker? *Open Hear*. 2019;6(1).
  181. Joseph J, Naqvi SY, Giri J, Goldberg S. Aortic Stenosis: Pathophysiology, Diagnosis, and Therapy. *Am J Med [Internet]*. 2017;130(3):253–63. Available from: <http://dx.doi.org/10.1016/j.amjmed.2016.10.005>